UTS UNIVERSITY OF TECHNOLOGY SYDNEY

Optical properties of quantum emitters in hexagonal boron nitride in cryogenic thermal shock

by Thi Ngoc Anh Mai

Thesis submitted in fulfilment of the requirements for the degree of

Doctor of Philosophy

under the supervision of

- Dr. Trong Toan Tran (Principal supervisor)
- Dr. Helen Xu (Co-supervisor)

University of Technology Sydney
Faculty of Engineering and Information Technology

February 2025

Certificate of Original Authorship

I, Thi Ngoc Anh Mai declare that this thesis, is submitted in fulfillment of the requirements for the award of Doctor of Philosophy, in the School of Electrical and Data Engineering, Faculty of Engineering and Information Technology, at the University of Technology Sydney.

This thesis is wholly my own work unless otherwise referenced or acknowledged. In addition, I certify that all information sources and literature used are indicated in the thesis.

This document has not been submitted for qualifications at any other academic institution.

This research is supported by the Australian Government Research Training Program.

Signature: Production Note: Signature removed prior to publication.

Date: 18/02/2025

Copyright notice

Acknowledgment

My doctorate journey would not have been possible without the help from people I mentioned in this acknowledgement section.

First, I would like to express my utmost gratitude to my principal supervisor—Dr. Trong Toan Tran who gave me another chance to not give up my dream of pursuing this degree. It has been my truly fortunate to have had the opportunity to learn from Dr. Tran whose knowledge in physics, material science and chemical engineering are incomparable. He has taught me, a fresh Ph.D. student with little experience, the fundamental principles of all kinds of physics to chemistry. More importantly, he patiently guides me step by step on doing experiment in photonics and quantum optics laboratory. His insightful discussion and invaluable feedback have made significant impacts on my work. He tirelessly explains and repeats through individual concepts and theory in quantum optics and modern physics to me until I can understand them. He gives me plenty of lectures and courses from experts in the field in top universities in the world to learn more. Outside working in the lab, he is a kind-hearted senior that mentally supports, encourages me throughout the challenging of thesis writing and other obstacles of my life in Australia. He has not only enhanced my research skills but also inspired me to face

and overcome all the hardships to become a better version of myself. Thank you for your understanding and continuous support which has been a cornerstone of my success. I look forward to carrying forward the lessons learned under your guidance in my future endeavors.

Secondly, my gratitude goes to my co-supervisor, Dr. Helen Xu, for her unwavering support and guidance throughout my research journey. Her assistance in chemical experiments, XRD and TEM measurements and data analysis has been invaluable. She has been dedicated to helping me find information about scholarships and encouraging me to apply. Additionally, she motivated me to join the Women in STEM Research (WiSR) Mentoring Program, which has been a transformative experience during my studies in Australia. Her continuous encouragement and belief in my abilities have been a source of great motivation.

I would also like to thank Associate Professor Hoang Dinh and Dr. Mehran Kianinia for being chair and expert in all my three candidature stage assessments. They have provided me with critical feedback and encouragement, helping me to move forward and make progress on my candidature.

The technical staff – Dr. Blake Regan, Mr. Herbert Yuan, Dr. James Bishop in Microstructural Analysis Unit (MAU) and Mr. Kevin Cook, Mr. Michael Lee in Tech Lab – also play a critical role in my Ph.D. journey.

They have been teaching me work with the Lindberg Blue Mini-mite tube furnace, atomic force microscopy, reactive ion etching machine and liquid nitrogen. Without these dedicated staff, I could not have been able to finish the experiments promptly.

This journey would have been much lonelier without daily morning coffees and lunchtime chats with my lab mates, internship students, and Vietnamese friends in Techlab. I would, therefore, like to thank Dr. Chaohao Chen, Dr. Lei Ding, Shakhawath Hossain, Nhat Minh Nguyen, Dr. Quang Dieu Nguyen, Dr. Huyen Tran Vu, Mrs. Hang Luong and others.

I would like to thank the Graduate Research School at the University of Technology Sydney for giving me the opportunity to pursue my Ph.D. at one of the world's top universities. I am grateful for the financial support from the University of Technology Sydney, Faculty of Engineering and Information Technology, which provided me with a tuition fee waiver and living stipend scholarships for the duration of my Ph.D. through the Joint Technology and Innovation Research Center between UTS and VNU. Thank you to the School of Electrical and Data Engineering and the Administration team for offering HDR students various networking activities and for assisting me with all the paperwork during my candidature. I also extend my gratitude to the UTS Tech Lab and

Operations team for providing extensive facilities, from general areas to Photonics Laboratory.

It has been my great pleasure to have the chance to meet Professor Diep N. Nguyen (UTS), Professor Xuan Tu Tran (VNU), A/ Prof Linh Trung Nguyen (VNU), Dr. Tran Hiep Dinh (VNU), Dr. Thi Hong Nhung Nguyen, Dr. Viet Khoa Tran. Your unconditional help make significant impact on my journey. I would like to thank all of my Vietnamese friends in Australia, especially Mrs. Bich Thuy and Mr. Chi Cuong Nguyen family and others for supporting to my family in Australia. I would also like to thank Dr. Hien Nguyen, Dr. Tu An Nguyen and the rest of Vietnamese PhD mums group for their understanding and guidance throughout all the stages of the challenging yet rewarding journey of being a mom and pursuing my PhD simultaneously.

From the bottom of my heart, I would like to express my heartfelt gratitude to my husband, Mr. Manh Dat Nguyen for all he did. My Ph.D. journey would have been impossible without him. He has always been by my side and been my companion through all the ups and downs of this incredible journey. He not only makes me smile even on days when my experiments fail but also has taken care of our son when I had to leave early and came home late for experiments and thesis writing, on both

sunny and rainy days, and during weekends. His unwavering support has been invaluable.

My Ph.D. journey would have missed most of its meaning without having my 3-year-old son, Mai Nhat Son Nguyen. He made me giggle and laugh, comforted me with “It’s ok, mommy” when I needed it, and asked me to sing him Cocomelon songs and read him the cute, sweet, funny stories to help me get through tough times. His hugs, cuddles, and gentle pats have been a source of immense comfort and joy.

Lastly, I would like to thank my parents and my extended family for their endless support and understanding during my Ph.D. journey. Without them I could not finish this challenging adventure.

This thesis is dedicated to my husband, Mr. Manh Dat Nguyen,

and my son, Mai Nhat Son Nguyen.

Declaration of thesis by compilation

This is a thesis compilation of my published works.

Chapter 2 in this thesis is compiled from one review paper which was published in Advanced Functional Materials—a peer-reviewed journal. **Thi Ngoc Anh Mai,** Md Shakhawath Hossain, Nhat Minh Nguyen, Yongliang Chen, Chaohao Chen, Xiaoxue Xu, Quang Thang Trinh, Toan Dinh, Toan Trong Tran, "Quantum Emitters in Hexagonal Boron Nitride: Principles, Engineering and Applications". *Advanced Functional Materials*, **2025**, 2500714.

Chapter 3 and 4 in this thesis are compiled from one published paper in ACS Applied Materials & Interfaces—a peer-reviewed journal. **Thi Ngoc Anh Mai**, Sajid Ali, Md Shakhawath Hossain, Chaohao Chen, Lei Ding, Yongliang Chen, Alexander S. Solntsev, Hongwei Mou, Xiaoxue Xu, Nikhil Medhekar, and Toan Trong Tran, "Cryogenic Thermal Shock Effects on Optical Properties of Quantum Emitters in Hexagonal Boron Nitride", *ACS Applied Materials and Interfaces*, **2024**, 16, 19340.

The extent of the contribution to the research and all the authors in these papers have been truthfully stated, and signatures from all authors have been obtained as permission to include the published material in this thesis.

List of publications:

Thesis works:

1. **Thi Ngoc Anh Mai**, Sajid Ali, Md Shakhawath Hossain, Chaohao Chen, Lei Ding, Yongliang Chen, Alexander S. Solntsev, Hongwei Mou, Xiaoxue Xu, Nikhil Medhekar, and Toan Trong Tran, "Cryogenic Thermal Shock Effects on Optical Properties of Quantum Emitters in Hexagonal Boron Nitride", *ACS Applied Materials and Interfaces*, **2024**, 16, 19340.
2. **Thi Ngoc Anh Mai,** Md Shakhawath Hossain, Nhat Minh Nguyen, Yongliang Chen, Chaohao Chen, Xiaoxue Xu, Quang Thang Trinh, Toan Dinh, Toan Trong Tran, "Quantum Emitters in Hexagonal Boron Nitride: Principles, Engineering and Applications", *Advanced Functional Materials*, **2025**, 2500714.

Non-thesis and contributed work:

1. Md Shakhawath Hossain, Miguel Bacaoco, **Thi Ngoc Anh Mai**, Guillaume Ponchon, Chaohao Chen, Lei Ding, Yongliang Chen, Evgeny Ekimov, Xiaoxue Xu, Alexander S. Solntsev, and Toan Trong Tran, "Fiber-Based Ratiometric Optical Thermometry with Silicon Vacancy in Microdiamonds", *ACS Applied Optical Materials*, **2024**, 2, 97.

Declaration specifies the contribution of authors

Title: **Cryogenic Thermal Shock Effects on Optical Properties of Quantum Emitters in Hexagonal Boron Nitride**

Authorship: Thi Ngoc Anh Mai, Sajid Ali, Md Shakhawath Hossain, Chaohao Chen, Lei Ding, Yongliang Chen, Alexander S. Solntsev, Hongwei Mou, Xiaoxue Xu, Nikhil Medhekar, and Toan Trong Tran

Publication outlet: ACS Applied Materials and Interfaces

Status: In press

My Contribution: Experiments (**90%**), Manuscript (**60%**)

Contribution: Thi Ngoc Anh Mai and Toan Trong Tran conceived the idea of the project. Thi Ngoc Anh Mai and Toan Trong Tran built the optical system and its software. Thi Ngoc Anh Mai fabricated the quantum emitters in hBN and performed all the optical characterization. Xiaoxue Xu and Hongwei Mou conducted the TEM, SAED and XRD experiments and analyzed the data. Sajid Ali and Nikhil Medhekar carried out the DFT calculations for strain effect on hBN quantum emitters. Toan Trong Tran

supervised the project. All authors discussed the results and commented on the manuscript.

Signatures:

Name of Author	Signature of Author	Date
Thi Ngoc Anh Mai	Production Note: Signature removed prior to publication.	23/01/2025
Sajid Ali	Production Note: Signature removed prior to publication.	24/01/2025
Md Shakhawath Hossain	Production Note: Signature removed prior to publication.	26/01/2025
Chaohao Chen	Production Note: Signature removed prior to publication.	23/01/2025
Lei Ding	Production Note: Signature removed prior to publication.	23/01/2025
Yongliang Chen	Production Note: Signature removed prior to publication.	25/01/2025
Alexander S. Solntsev	Production Note: Signature removed prior to publication.	24/01/2025
Hongwei Mou	Production Note: Signature removed prior to publication.	24/01/2025
Xiaoxue Xu	Production Note: Signature removed prior to publication.	23/01/2025
Nikhil Medhekar	Production Note: Signature removed prior to publication.	29/01/2025
Toan Trong Tran	Production Note: Signature removed prior to publication.	23/01/2025

Title: **Quantum Emitters in Hexagonal Boron Nitride: Principles, Engineering and Applications**

Authorship: Thi Ngoc Anh Mai, Md Shakhawath Hossain, Nhat Minh Nguyen, Yongliang Chen, Chaohao Chen, Xiaoxue Xu, Quang Thang Trinh, Toan Dinh and Toan Trong Tran

Publication outlet: Advanced Functional Materials

Status: In press

My Contribution: Manuscript (**60%**)

Contribution: Thi Ngoc Anh Mai and Toan Trong Tran conceived the idea of the project. Thi Ngoc Anh Mai and Toan Trong Tran outlined the structure of the manuscript. Thi Ngoc Anh Mai conducted the literature research and compiled the initial draft of the manuscript. Thi Ngoc Anh Mai, Chaohao Chen and Nhat Minh Nguyen edited the figures and ensured their accuracy and clarity. Quang Thang Trinh focused on the theoretical background and contributed to the discussion of future directions. Yongliang Chen, Xiaoxue Xu and Toan Dinh reviewed and provided critical comments. Toan Trong Tran supervised the project. All authors discussed the results and commented on the manuscript.

Signatures:

Name of Author	Signature of Author	Date
Thi Ngoc Anh Mai	Production Note: Signature removed prior to publication.	23/01/2025
Md Shakhawath Hossain	Production Note: Signature removed prior to publication.	26/01/2025
Nhat Minh Nguyen	Production Note: Signature removed prior to publication.	24/01/2025
Yongliang Chen	Production Note: Signature removed prior to publication.	25/01/2025
Chaohao Chen	Production Note: Signature removed prior to publication.	23/01/2025
Xiaoxue Xu	Production Note: Signature removed prior to publication.	23/01/2025
Quang Thang Trinh	Production Note: Signature removed prior to publication.	28/01/2025
Toan Dinh	Production Note: Signature removed prior to publication.	23/01/2025
Toan Trong Tran	Production Note: Signature removed prior to publication.	23/01/2025

Table of Contents

List of illustrations

Abstract

Quantum information science promises to usher in a new era of analyzing, processing, and transferring information in manners unimaginable decades ago. At the heart of these protocols is quantum hardware known as quantum emitters—molecular-sized entities emitting a single photon at a time. Compared to their gas-phase counterparts, quantum emitters in solids have gained tremendous traction owing to their unique suite of properties, such as room-temperature operation, high photostability, and ease of usage. One of the front-runners in this category is quantum emitters in hexagonal boron nitride (hBN) since they offer incredibly high brightness, high single-photon purity, chemical inertness, and low fabrication cost. The quantum emitters have been, therefore, recently considered for space-related communication applications such as satellite-ground quantum key distribution. To enable this task, the quantum emitters must be tested against thermal shocks—similar to those encountered in space. Such a study has, however, remained elusive to date. This thesis presented a statistical test on hBN quantum emitters under different temperature drop protocols. The optical properties including photoluminescence spectra, zero phonon line peak, full width at half maximum, photostability, single-photon emission rate and lifetime,

of quantum emitters in hBN flakes are studied in detail. By using a combination of different structural characterizations such as atomic force microscopy, transmission electron microscopy, X-ray diffraction, and density functional calculations, it was confirmed that the observed spectral shifts and photo-bleaching of hBN quantum emitters are attributed to lattice strain caused by cryogenic temperature shock. Furthermore, a slow-cooling process is shown to alleviate such detrimental changes. This work provides insights into the stability of the quantum emitters under harsh conditions resembling those faced in outer space. It also proposes a more thorough testing method for quantum emitters in future space-based quantum applications.

Chapter 1

Introduction

1.1. Motivation

Nowadays, technology makes our lives more convenient than several decades ago as we can shop, study and work online, or video call to see our family and friends from far distance. Along with these benefits, there are also downsides. People might lose their money or accounts just by clicking on the wrong links, emails, text messages, answering suspicious phone calls and following the steps. When we send emails, shop online, use banking applications or chat with loved ones through different platforms, our personal accounts are generally protected by encryption. Encryption is like a secret code that only us—the right person with the correct "key" can unlock. Most of the current encryption methods use very difficult math problems that are nearly impossible to solve but still sometimes be hackable.[1] A very active research field to achieve completely secure information called quantum cryptography or quantum key distribution (QKD) has emerged. Quantum key distribution has

[1] https://www.qld.gov.au/community/your-home-community/cyber-security/cyber-security-for-queenslanders/case-studies/medibank-private-cyber-incident

advantages that using an unconventional technique—the polarization states of single photons to encrypt the secret information and is protected by quantum physics laws. One of the earliest and most famous QKD methods is called **BB84**, invented in 1984 by scientists Charles Bennett and Gilles Brassard.[1-2] In a BB84 experiment, a person (named A) will encode the single photons by randomly selecting one of the four polarization states then send them to a person (named B) through a channel. At the end of the channel, B receives the photons one by one and randomly chooses a polarizer filter to measure the polarization states of received photons. Then, B lets A know in public the type of filters was used without telling the results of each measurement. Afterwards, A comments on which filter's orientation is correct. The incorrect measurements of polarization states of photon are discarded, left only exact photons defined with filters upon their associated orientations are used to decode the secret key A wants to let B know. Both A and B know this key precisely regardless of the random nature of the key generation process. If there is an eavesdropper, named E, want to get to know the secret key by steal the photons and decoded them. The receiver person B will know immediately because there are no photons received (the single photons source that A used just produce one photon at a time in sequence). Hence, E must intercept the photons and duplicate another photon to send

back to B to avoid B's conscious. However, in quantum physics, the no-cloning theorem stated that E cannot exactly duplicate an unknown quantum system.[3] Thanks to this unique quantum nature of the no-cloning theory, quantum communication with quantum key distribution guarantees absolute secured for information.[2] Although there are still challenges of photons getting lost or being distorted during transmission channel, through air, optical fibres or over long distances, QKD have already been tested in real-life situation as Liao and his colleagues have successfully sent secure messages in free space using satellites performed by the **Micius satellite in 2017**.[5] The experiment proves that QKD is not just a theory—it works in practice.

At the heart of every quantum key distribution setup is quantum emitter—the object can generate a single photon at a time. Among the various quantum emitter platforms, hBN stands out thanks to its unique properties. Hexagonal boron nitride is an atomically thin, wide bandgap material that hosts robust, optically active luminescent point defects. These defects act as stable single-photon sources at room temperature, making hBN a promising candidate for scalable quantum photonic applications.

[2] An interactive simulation of an optical implementation of the BB84 quantum key distribution protocol in the Virtual Lab by Quantum Flytrap for easier visualization and understanding can be found at https://lab.quantumflytrap.com/lab/bb84?mode=waves.[4] P. Migdał, K. Jankiewicz, P. Grabarz, C. Decaroli, P. Cochin, Visualizing quantum mechanics in an interactive simulation – Virtual Lab by Quantum Flytrap, *Optical Engineering* **2022**, *61*, 081808.

Integrating hBN with existing photonic and electronic platforms further enhances its potential for practical quantum technologies. These emitters have been employed in the proposal as the first quantum light sources for satellite-based quantum communication and testing extended physical theory in space. Unlike conditions on Earth, the extraterrestrial counterparts are extreme and detrimental to many common materials. Even though there has been research on the stability of hBN quantum structures under different aggressive gas conditions, high temperatures up to 500ºC, and gamma ray irradiation, but still a lack of research on the optical properties of hBN quantum emitters under cryogenic thermal shock and several repeated cycles. In this thesis, we report the up-to-date review on hBN quantum emitters and focus on first studying the behavior of hBN quantum emitters in different shock cooling schemes and deep characterization of mechanisms and structures of hBN before and after each route.

1.2. Thesis organization

The structure of this thesis is organized as follows:

Chapter 1: Introduction presents the motivation of this thesis along with its structure and background of quantum emitters definition and properties.

Chapter 2: Literature review goes through basics principles of quantum emitters in hexagonal boron nitride, excitation mechanisms, and quantum emission measurement. The statistics, global scientific research on hBN quantum emitters, and theoretical and experimental investigations on the origin of various defect families are provided. The overview of fabrication of hBN lattice structure and defect engineering was expressed. The roadmap of integration of hBN quantum emitters into photonics structures and up-to-date applications of hBN quantum emitters in quantum sensing, quantum cryptography, and quantum communications. The robustness of hBN quantum emitters makes it the first and most promising platform for future satellite-based quantum communication and testing fundamental physics theory. Significant portions of this chapter are copied verbatim from a peer-reviewed article "*Quantum Emitters in Hexagonal Boron Nitride: Principles, Engineering and Applications*" **Thi Ngoc Anh Mai,** Md Shakhawath Hossain, Nhat Minh Nguyen, Yongliang Chen, Chaohao

Chen, Xiaoxue Xu, Quang Thang Trinh, Toan Dinh and Toan Trong Tran, *Advanced Functional Materials* **2025**, 2500714.[6]

Chapter 3: Research methodology presents the fabrication method, experiment processes, measurement techniques and simulation information I used in this thesis. A significant portion of this chapter is copied and compiled by adding more figures and details information from the **Methods** section of the peer-reviewed article "*Cryogenic Thermal Shock Effects on Optical Properties of Quantum Emitters in Hexagonal Boron Nitride"* **Thi Ngoc Anh Mai**, Sajid Ali, Md Shakhawath Hossain, Chaohao Chen, Lei Ding, Yongliang Chen, Alexander S. Solntsev, Hongwei Mou, Xiaoxue Xu, Nikhil Medhakar, and Toan Trong Tran, *ACS Applied Materials & Interfaces* **2024**, 16, 19340.[7]

Chapter 4: Results and discussion of cryogenic thermal shock effects on optical properties of quantum emitters in hexagonal boron nitride investigate the impact of cryogenic temperature shock on spectral, photostability, quantum emission and structure of hexagonal boron nitride flakes. A significant portion of this chapter is copied verbatim from the peer-reviewed article "*Cryogenic Thermal Shock Effects on Optical Properties of Quantum Emitters in Hexagonal Boron Nitride*" **Thi Ngoc Anh Mai,** Sajid Ali, Md Shakhawath Hossain, Chaohao Chen, Yongliang Chen, Alexander S. Solntsev, Hongwei Mou, Xiaoxue Xu, Nikhil

Medhakar, and Toan Trong Tran, *ACS Appl. Mater. Interfaces* **2024**, 16, 19340.[7]

Chapter 5: Conclusions summarizes thesis contents and recommendations for future works.

1.3. Background of quantum emitters

Quantum emitter is the core research object of this thesis. This section presents the definition and fundamental characteristics of quantum emitters in general.

As mentioned in **Section 1.1.** quantum emitters or quantum light sources or single photon sources or single photon emitters are defined as systems that can generate a single photon at a time, on demand.[8] Quantum emitters have unique and distinct properties that cannot be explained by classical theories.[9] In this section, I provide some basic characteristics to quantify quantum emitters that are important for this thesis. More detail can be found in quantum optics books.[10-12]

1.3.1. Quantum emission and correlation measurements

The first and foremost important characteristic of a quantum emitter is the quantum emission. This is characterized by using the second-order autocorrelation measurement with the Hanbury Brown and Twiss (HBT) experiment. Here, I present a general theory of the second-order correlation function and in **Section 2.2** the HBT experiment setup will be introduced in practice.

The first- and second-order correlation functions are defined as below respectively:

$$g^{(1)}(\tau) = \frac{\langle \hat{a}^\dagger(t)\hat{a}(t+\tau)\rangle}{\langle \hat{a}^\dagger(t)\hat{a}(t)\rangle} \tag{1.1}$$

$$g^{(2)}(\tau) = \frac{\langle \hat{a}^\dagger(t)\hat{a}^\dagger(t+\tau)\hat{a}(t+\tau)\hat{a}(t)\rangle}{\langle \hat{a}^\dagger(t)\hat{a}(t)\rangle^2} \tag{1.2}$$

Where t is the arrival time of the first photon, $t+\tau$ is the arrival time of the second photon; $\hat{a}^\dagger$ and $\hat{a}$ are creation and annihilation operators for the photons.

The first-order correlation function is calculated on the average photon number $\langle n\rangle = \langle \hat{a}^\dagger\hat{a}\rangle$ only. Such an expression means that any light sources that have the same average photon number lead to the same first-order results. In fact, thermal light and coherent light sources when spectrally-filtered with the same $\langle n\rangle$ have the same first-order results.

Then, the meaning of having the second-order correlation function is showing the difference between these two sources.

For a number state $|n\rangle$ of light,

$$g^{(2)}(0) = \frac{\langle n|\hat{a}^\dagger \hat{a}^\dagger \hat{a}\hat{a}|n\rangle}{\langle n|\hat{a}^\dagger(t)\hat{a}(t)|n\rangle^2} = 1 - \frac{1}{n} \tag{1.3}$$

A thermal light source:

$$g^{(2)}(0) = 1 + \frac{(\Delta n)^2 - \langle n\rangle}{\langle n\rangle^2} = 2 \tag{1.4}$$

A coherent light source (e.g. laser light):

$$g^{(2)}(0) = \frac{\langle \alpha|\hat{a}^\dagger \hat{a}^\dagger \hat{a}\hat{a}|\alpha\rangle}{\langle \alpha|\hat{a}^\dagger(t)\hat{a}(t)|\alpha\rangle^2} = 1 \tag{1.5}$$

With clearly different results as above, the second-order correlation function can be used to differentiate the thermal, coherent and other light sources. A source with $g^{(2)}(0) < 1$ is entirely non-classical, qualified as a quantum emitter and proved its quantum emission.[9, 13]

As definition, a true quantum emitter is the one generate single photon at a time, it means that in **Equation 1.3** $n = 1$ and we have:

$$g^{(2)}(0) = \frac{\langle n|\hat{a}^{\dagger}\hat{a}^{\dagger}\hat{a}\hat{a}|n\rangle}{\langle n|\hat{a}^{\dagger}(t)\hat{a}(t)|n\rangle^2} = 1 - \frac{1}{n} = 1 - \frac{1}{1} = 0 \qquad (1.6)$$

In practice, it is hard to reach this absolute zero value.

When substitute n = 2 into **Equation 1.3** we have

$$g^{(2)}(0) = \frac{\langle n|\hat{a}^{\dagger}\hat{a}^{\dagger}\hat{a}\hat{a}|n\rangle}{\langle n|\hat{a}^{\dagger}(t)\hat{a}(t)|n\rangle^2} = 1 - \frac{1}{n} = 1 - \frac{1}{2} = \frac{1}{2} \qquad (1.7)$$

When substitute n = 3 into **Equation 1.3** we have

$$g^{(2)}(0) = \frac{\langle n|\hat{a}^{\dagger}\hat{a}^{\dagger}\hat{a}\hat{a}|n\rangle}{\langle n|\hat{a}^{\dagger}(t)\hat{a}(t)|n\rangle^2} = 1 - \frac{1}{n} = 1 - \frac{1}{3} = \frac{2}{3} \qquad (1.8)$$

And so on, we can conclude that when $n \geq 2$ the $g^{(2)}(0) \geq \frac{1}{2}$. Therefore, a value of $g^{(2)}(0) < 0.5$ is started to be accepted as a single photon emitter. Results of second-order correlation function measurement on hBN quantum emitters will be presented later in **Chapter 4**: Results and Discussion.

1.3.2. Emission rate and emission lifetime of quantum emitter

Another essential characteristic of a quantum emitter is the emission rate and corresponding emission lifetime.

Emission lifetime is determined by the **Equation 1.9** below:

$$\tau_f = \frac{1}{\Gamma_0} \tag{1.9}$$

With Γ_0 is the spontaneous emission rate of the emitter.

A quantum emitter in an uniform medium with refractive index n, the spontaneous emission rate is entirely dependent on two factors: 1-the transition frequency-ω and 2-the transition dipole moment-μ_{eg} between ground and excited states[13] as in the **Equation 1.10** below:

$$\Gamma_0 = \frac{4}{3n}\frac{\mu_{eg}^2}{4\pi\epsilon_0\hbar}\left(\frac{\omega}{c}\right)^3 \tag{1.10}$$

With $\epsilon_0, \hbar, c$ are vacuum permittivity, reduced Planck constant and the speed of light, respectively.

The transition frequency refers to the frequency of light associated with the transition between two energy levels in a material. It is given by the energy difference between the ground and excited states divided by Planck's constant. The transition dipole moment is a vector quantity that

describes the strength and orientation of the interaction between the electromagnetic field and the material during a transition between two states.

The emission rate will define how bright the quantum source is. The **Equation 1.9** shows that the emission rate and lifetime are inversely proportional. The higher emission rate and shorter emission lifetime are desired to get a high data rate for quantum information processing. The typical emission rate of hBN quantum emitters is around a few million counts per second and emission lifetime of 3 nanoseconds.[14]

1.3.3. Indistinguishability photons

The utmost characteristic of a quantum emitter is the capacity to produce indistinguishable photons—the emitted photons are all in the same mode, or in other words, they have to be identical, exactly/absolutely same in all characteristics such as frequency (or energy), momentum and polarization. The solid-state quantum emitters usually have problems of losing the indistinguishability property because of the dephasing and spectral diffusion process. The property of producing indistinguishable photons of a quantum light source is determined by the Hong-Ou-Mandel (HOM) experiment. This was named after three physicists first

demonstrated this experiment in 1987 at the University of Rochester. One experiment measurement of Hong-Ou-Mandel effect with hBN quantum emitters was realized and presented in **Section 2.10 Chapter 2**.

Chapter 2

Literature Review

Preamble

In this chapter, I go through the different aspects of quantum emitters in hexagonal boron nitride. **Section 2.2** explains in detail three excitation mechanisms (resonant, Stokes and anti-Stokes), and typical quantum emission measurement (the second-order autocorrelation). **Section 2.3** summarizes and highlights the sharp growth of this research topic based on the collected data from Web of Science (Clarivate Analytics). **Section 2.4** reviews the contentious question about the atomic structures of the defects from the beginning. The recent achievement with enriching simulations/ calculations platforms including the explosion of artificial intelligence and machine learning was discussed. The pioneer experimental results revealed the defect configuration also was reported. **Section 2.5** demonstrates the material aspects from different fabrication methods to various engineering techniques. **Section 2.6 and 2.7** compare several quantum photonic integrations from research groups in the world. Meanwhile, other reviews are out of date or focused on very specific applications, in **section 2.8, 2.9, 2.10** of this review, different applications

of different classes of hBN quantum emitters are updated. I proved that quantum emitters in hBN are one of the most promising platforms for quantum technologies.

Significant portion of this chapter is copied verbatim from the peer-reviewed article "*Quantum Emitters in Hexagonal Boron Nitride: Principles, Engineering and Applications*" **Thi Ngoc Anh Mai**, Md Shakhawath Hossain, Nhat Minh Nguyen, Yongliang Chen, Chaohao Chen, Xiaoxue Xu, Quang Thang Trinh, Toan Dinh and Toan Trong Tran, *Advanced Functional Materials*, **2025**, 2500714.[6]

All graphics have been recreated to match the style of this thesis.

Quantum Emitters in Hexagonal Boron Nitride: Principles, Engineering and Applications

*Thi Ngoc Anh Mai, Md Shakhawath Hossain, Nhat Minh Nguyen, Yongliang Chen, Chaohao Chen, Xiaoxue Xu, Quang Thang Trinh, Toan Dinh, Toan Trong Tran**

Thi Ngoc Anh Mai, Md Shakhawath Hossain, Nhat Minh Nguyen, Toan Trong Tran

School of Electrical and Data Engineering, University of Technology Sydney, Ultimo, NSW, 2007, Australia

Email: trongtoan.tran@uts.edu.au

Yongliang Chen

Department of Physics, The University of Hong Kong, Pokfulam, Hong Kong 999077, China

Chaohao Chen

Department of Electronic Materials Engineering, Research School of Physics, The Australian National University, Canberra, Australian Capital Territory 2601, Australia

Chaohao Chen

ARC Centre of Excellence for Transformative Meta-Optical Systems (TMOS), Research School of Physics, The Australian National University, Canberra, Australian Capital Territory 2601, Australia

Xiaoxue Xu

School of Biomedical Engineering, University of Technology Sydney, Ultimo, NSW, 2007, Australia

Quang Thang Trinh

Queensland Micro, and Nanotechnology Centre, Griffith University, 170 Kessel Road, Nathan, QLD 4111, Australia

Toan Dinh

School of Engineering, University of Southern Queensland, Toowoomba, Queensland 4350, Australia

Toan Dinh

Centre for Future Materials, University of Southern Queensland, Toowoomba, Queensland 4350, Australia

Keywords: hexagonal boron nitride, quantum emitters, single photon emitters, defect centers, quantum technologies

Abstract:

Solid-state quantum emitters, molecular-sized complexes releasing a single photon at a time, have garnered much attention owing to their use as a key building block in various quantum technologies. Among these, quantum emitters in hexagonal boron nitride have emerged as front runners with superior attributes compared to other competing platforms. These attributes are attainable thanks to the robust, two-dimensional

lattice of the material formed by the extremely strong B-N bonds. This review discusses the fundamental properties of quantum emitters in hBN and highlights recent progress in the field. The focus is on the fabrication and engineering of these quantum emitters facilitated by state-of-the-art equipment. Strategies to integrate the quantum emitters with dielectric and plasmonic cavities to enhance their optical properties are summarized. The latest developments in new classes of spin-active defects, their predicted structural configurations, and the proposed suitable quantum applications are examined. Despite the current challenges, quantum emitters in hBN have steadily become a promising platform for applications in quantum information science.

2.1. Introduction

Quantum information science—a branch of study that seamlessly blends information theory and quantum mechanics—promises to revolutionize how we live, from ultra-secure transactions and parallel computing to the teleportation of information over distances.[15-18] At the heart of such technologies are quantum hardware called quantum emitters that can release a single photon at a time, on demand.[9, 19-20] Traditionally, gas-phase platforms such as single atoms or single trapped ions were

employed to generate single photons thanks to their superior optical properties.[21] These platforms, however, suffer from drawbacks, including high cost, bulkiness, and complicated operations.[8] Unlike these systems, most solid-state quantum emitters can operate at room temperature under ambient conditions and at a comparatively lower cost.[13, 22-24] Therefore, the past few decades have witnessed an explosion in research studies focused on exploring and utilizing new solid-state quantum emitters. To date, a wide variety of solid-state quantum emitters exist, from single molecules, colloidal and epitaxial quantum dots, to defect centers in diamond,[25-26] silicon carbide,[27-28] gallium nitride,[29-30] carbon nanotubes,[31-32] transition metal dichalcogenides (TMDs)[33-34] and hexagonal boron nitride,[14, 35] as shown in **Figure 2.1a**.

Among these, quantum emitters in hBN have attracted significant research attention owing to their excellent optical properties and the unique hosting lattice. Hexagonal boron nitride has a honeycomb lattice structure similar to that of graphite. However, the hBN lattice is formed by the B-N bond that is both covalent and ionic, thanks to the relatively large differences in electron affinities of boron and nitrogen atoms. As a result, hBN is an indirect, wide bandgap material (~6 eV) that can host a variety of optically active defect centers. Such a wide bandgap value is critical for a host material since it can accommodate quantum emitters with various optical

transition energies within its bandgap. In addition, hBN is a two-dimensional (2D) material that can be exfoliated layer-by-layer into single-atom-thick sheets of material, owing to the weak interplane van der Waals forces.[36] This property allows for efficient extraction of the emission from the quantum emitters and excellent coupling to external photonic architectures, which will be discussed later in the text. Another advantage of hBN as a host stems from its extremely strong B-N bond that provides excellent chemical and physical protection for the embedded emitters. In the past decade, there have been several review articles about hBN quantum emitters. However, some discuss hBN quantum emitters as part of single-photon sources in 2D materials, while others only give a brief summary of the quantum emitters.[37-38] Some other articles do give a detailed literature review on hBN quantum emitters.[39-40] These, nevertheless, need to be updated due to the fast-evolving nature of the topic. In this review, we curate the latest advancements in the fabrication and integration of hBN quantum emitters and provide in-depth perspectives and opinions based on our years of experience working with the material system. We also give an update on the rapid growth of the research topic based on our statistical bibliographic data.

The current review is arranged as follows. First, we introduce the fundamental properties of quantum emitters in hBN, including their

excitation and detection schemes. We then discuss the current status of research on quantum emitters, followed by an overview of theoretical and experimental investigations on the origin of various defect families. Next, we delve into the fabrication of host materials and defect engineering of the quantum emitters using a range of strategies. We highlight some important works on integrating hBN quantum emitters into monolithic and hybrid photonic architectures. We subsequently overview the applications of quantum emitters in quantum technologies, such as quantum sensing, quantum cryptography, and quantum networks. We discuss the robustness of the quantum emitters and suggest areas that can be improved. Finally, we conclude the review with an outlook on this active and exciting research topic.

2.2. Principles of quantum emitters in hBN

Similar to other solid-state emitters, quantum emitters in hBN behave like a two-level atomic system that is locked inside a lattice. Not only such implantation immobilizes the defect centers, it also promotes significant coupling between the defect centers and the lattice vibrations—the phonons. A typical emission spectrum of a quantum emitter in hBN is shown in **Figure 2.1b**, right panel. The spectrum entails a sharper peak at

a shorter wavelength (higher energy), called a zero-phonon line (ZPL), and a broader peak at a longer wavelength (shorted energy), called a phonon-sideband (PSB). The term phonon-sideband here refers to optical phonons—phonons that can be excited by light. At low temperatures, while the ZPL arises from the pure electronic transition and does not involve any phonon coupling, the PSB involves the coupling with the optical phonons of the defect and bulk lattice. At higher temperatures, however, the ZPL does couple to acoustic phonons, which can be excited by sound waves, resulting in the linewidth broadening of the transition.

For this reason, the quantum emitters can be excited optically via three schemes. In the first scheme, the emitter can be pumped on resonance (**Figure 2.1b**, yellow dash box), where the excitation energy precisely matches that of the optical transition. Such an excitation protocol is the most efficient among the three methods and is similar to that for single atoms or single trapped ions in a vacuum. This is because of the huge absorption cross section at this excitation wavelength—the zero-phonon line. As efficient as it is, this excitation technique requires either advanced spectral filtering or orthogonal (cross) polarization. In the first method, only emitted photons falling into the PSB window are collected so that the majority of the back-reflected excitation laser can be rejected, rendering the high-purity single photons at the collection. The major drawback of

this technique is that it only collects photons in the PSB, which are not very coherent. These photons are not useful in implementations requiring highly coherent photons, such as quantum communication or quantum entanglement. In the second method, the excitation and collected light are cross-polarized, for example, vertical and horizontal polarization for excitation laser and emitted photons, respectively. In this way, the residual laser can be substantially attenuated. In some cases, the attenuation can reach seven orders of magnitude or more, resulting in highly pure and coherent photons being harvested at the ZPL. This technique, however, does not come without a weakness. To enable effective filtering based on the different polarization of light, the sample flatness is critical to prevent scattering of the excitation laser, which in turn alters the initial polarization state of the excitation. When the sample is in powder/particle form below a few microns, diffusive scattering becomes significant, transforming linearly polarized light into elliptically polarized photons. This unwanted modification, in turn, results in a substantially lower signal-to-noise ratio. Therefore, the technique can only be applied for bulk crystals and not for samples with sizes smaller than a few microns.

In the second scheme (**Figure 2.1b**, green dash box), the emitter is excited with laser energies higher than the optical transition—also known as Stokes excitation. Such a protocol is allowed due to the efficient coupling

with the local phonons. In this situation, the emitter emits a single or multiple phonons before generating a photon via the radiative decay channel—from the excited to the ground state. This scheme is the most popular choice for exciting defect centers in hBN since various laser wavelengths can be chosen, and the optical filtering procedure is straightforward due to the large spectral separation between the excitation laser and the emission signal. Unlike the resonant excitation procedure, Stokes excitation demands orders of magnitude higher in excitation power due to its low absorption cross-section. Such an increase in excitation power, in turn, induces local heating—causing the unwanted linewidth broadening. The broader the linewidth is, the less coherent the photons are, thanks to the inverse relationship between frequency and time. Furthermore, owing to the phonon relaxation process[3], the Stokes excitation is prone to excitation time jitter, worsening the photon coherence compared to that of the resonant excitation. For these reasons, Stokes excitation is considered a less popular choice when highly coherent photons are demanded. In the third scheme (**Figure 2.1b**, red dash box), the emitter is pumped with laser energies lower than that of the optical transition—called Anti-Stokes excitation. Seemingly counterintuitive at

[3] The phonon relaxation is usually very rapid compared to the optical relaxation into the ground state. This note is based on the recommendation of Examiner 2 during the Examination process of this thesis, and has been added only in this thesis (not in the published paper).

first, the excitation is permitted thanks to the efficient phonon absorption process, which, in conjunction with the Anti-Stokes excitation, pumps the emitter into its excited state. Similar to the Stokes transition, Anti-Stokes excitation gives rise to photons with less degree of coherence compared to that of resonant excitation. Interestingly, however, the optical transition follows the Arrhenius exponential scaling with temperature, making such an excitation valuable for thermal sensing applications.

Once in the excited state, the electron decays to the ground state, emitting a photon. The average amount of time spent in the excited state is called the lifetime of the emitter. The shorter the lifetime is, the faster the emitter replenishes and emits another photon, hence the higher repetition rate. Quantum emitters in hBN typically possess lifetime values of ~1–3 ns, significantly shorter than well-known color centers in bulk diamond such as the nitrogen-vacancy centers, which have lifetime values of ~12 ns.[41] Not only do hBN emitters feature short excited-state lifetimes, but they also own impressive intrinsic quantum efficiencies (QEs)—quantities corresponding to the percentage of radiative relaxation. A recent study suggests a QE value exceeding 80% has been observed in hBN quantum emitters,[42] which is superior to most group-IV centers in diamond, such as the silicon-vacancy (SiV) or the germanium-vacancy (GeV),[43-44] where values of ~10–30% are typically observed. Such short lifetime,

high quantum efficiency values, and the low refractive indexes of hBN (~1.8–1.9 for out-of-plane) and (~2.1–2.2 for in-plane)[45] make the quantum emitters one of the brightest solid-state sources to date, with a repetition rate exceeding several MHz.[14, 46]

The photon emitted from the hBN emitter can possess the wavelength of the ZPL or the PSB, depending on whether an optical phonon is simultaneously generated. For a typical hBN emitter, around 70% of the emission goes into the ZPL,[47-48] while the rest represents the PSB. This optical characteristic is another compelling feature of defect centers in hBN compared to competing platforms. To characterize the statistical nature of the emitted photons, the Hanbury Brown and Twiss interferometer is typically employed (**Figure 2.1c**, left panel). The setup features a 50:50 (transmission:reflection) free-space or fiber-based beamsplitter that divides the collected light into two beams. Each beam is counted by a single-photon avalanche photodiode (SPAPD)[4] capable of detecting extremely low light intensities. The two SPAPDs are time-tagged by an ultrafast time correlator with a typical resolution of a few picoseconds or better. The time-tagging scheme can be simplified as

[4] In general, acronym “SPAD” was used as conventional abbreviation of single photon avalanche photodiode, since it is a special case of the APD. This note is based on the recommendation of Examiner 2 during the Examination process of this thesis, and has been added only in this thesis (not in the published paper).

follows. The top SPAPD acts as a start switch upon the first photon arrival, which initiates the internal clock of the time correlator (**Figure 2.1c**, bottom panel). The bottom SPAPD then serves as a stop switch when the second photon is counted. The total delay time between the two consecutive photons is saved and binned into a histogram. After many cycles of collecting such time-correlated data, a histogram called the second-order correlation function is shown in **Figure 2.1c**, right panel. In the case of single photons, an antibunching dip value below 0.5, i.e. $g^{(2)}(0) < 0.5$ can be seen at the zero delay time—suggesting a sub-Poissonian statistic. Qualitatively, this indicates the low or zero probability of simultaneous detection of two photons at the two detectors. Theoretically, an antibunching value of zero is expected for a true single photon emitter. However, in real-world experiments, there are a few factors involved, such as background fluorescence, a second emitter located close to the excitation spot, or timing jitter due to the time-tagging errors. Realizing high-purity single photon emission is critical for various quantum applications that require the quantum interference effect. For quantum emitters in hBN, antibunching values below <0.1 were achievable in previous studies,[49-51] by using either thermal annealing treatment or laser writing to suppress contamination-induced background fluorescence. Higher purity single-photon emission $\left(g^{(2)}(0) = 6.4 \times\right.$

10^{-3}) has also been demonstrated using a combination of confocal microcavity and ultrashort pulsed excitation to efficiently couple the emission into the cavity mode and eliminate background fluorescence and multiple photon generation.[52]

One of the most important aspects of a quantum light source is its ability to generate indistinguishable photons—photons that are identical to each other. Such an attribute is critical since it determines the degree of quantum interference between two or multiple photons, the building block of various quantum applications such as quantum computing or quantum networks. Other than the high single-photon purity, the other vital criterion of a quantum emitter to achieve indistinguishability is to reach the natural emission linewidth, the narrowest possible. Such a linewidth is defined by a Fourier-transform of the emitter's radiative lifetime—i.e. the shorter the lifetime, the larger the linewidth and vice versa. This linewidth can only be reached, however, when the emitter is free of phonon-induced dephasing and spectral diffusion. The former can be eliminated by cooling the emitter to cryogenic temperatures (a few Kelvin or below). At these temperatures, the dephasing caused by phonons is minimized due to the reduction in both the phonon density of states and the electron-phonon coupling strengths. The latter is more challenging to overcome. Spectral diffusion—a jittering of the radiative transition

energy—causes the emission wavelength of the emitter to shift randomly. These random fluctuations usually range from nanoseconds to milliseconds and are induced by the surrounding environment of the emitter, such as surface states and trapped charges. These imperfections can be photo-ionized, causing electric noises.[53] These noises, in turn, interact with the emitter's dipole moment and cause randomly fluctuating Stark shifts. Spectral diffusion has been a major obstacle to achieving Fourier-transform-limited linewidths in hBN quantum emitters. Spectral diffusion can appear in various timescales and is usually classified into slow (milliseconds or slower) and fast (microseconds or faster). Early studies showed average spectral diffusion times ranging from ~hundreds of milliseconds to seconds.[54-56] However, recent works revealed spectral diffusion times of tens of microseconds with the linewidths approaching the transform-limited values for photons emitted in between the spectral jumps.[57] Although it is currently possible to achieve indistinguishable photons from hBN quantum emitters, it remains difficult to maintain such a photon stream for milliseconds or longer. To further circumvent this issue, improvements in chemical purity and crystallinity of hBN material need to take place alongside refinements in defect engineering. Such a holistic approach is expected to significantly enhance the

indistinguishability of hBN quantum emitters, making them a promising platform for various quantum applications.

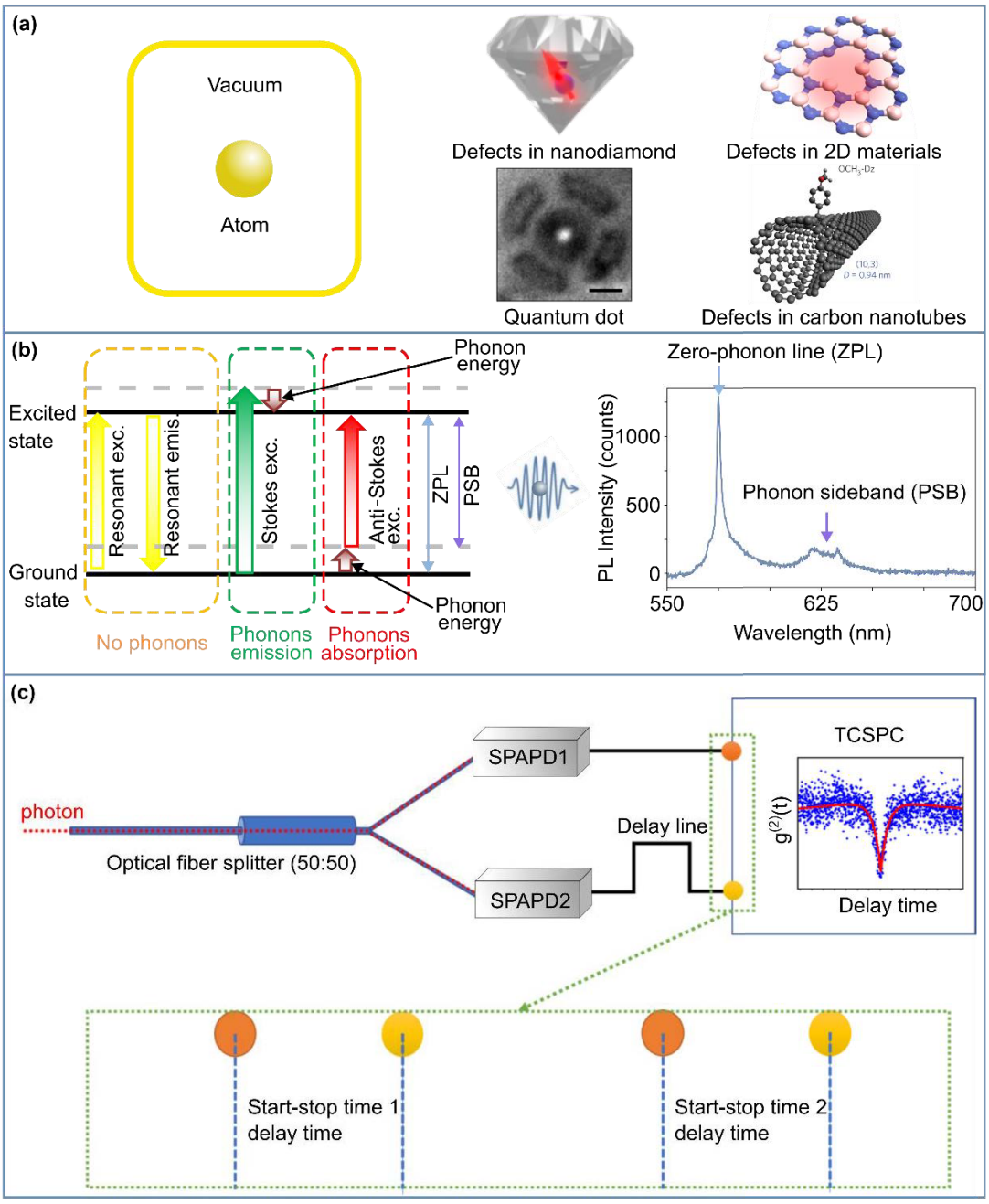

Figure 2.1: Basic principles of quantum emitters in hBN. (a) Classifications of quantum emitters: atom in vacuum (Left), and emitters

in solid-state materials (Right): defects in nanodiamond, 2D materials (hBN and TMDs), carbon nanotubes and quantum dot **(b)** Excitation of single defect center in hBN and a representative spectrum. **(c)** The Hanbury Brown and Twiss setup for single-photon source measurement. SPAPD - single-photon avalanche photon detector, TCSPC - Time correlated single photon counting. Figure proposed defect structure in hBN adapted with permission.[14] Copyright 2016, Springer Nature. Figure photoluminescence from a single quantum dot within the cavity (scale bar represents 5 μm) adapted under terms of the CC-BY 4.0 license.[58] Copyright 2015, The Authors, published by Springer Nature, Macmillan Publishers Limited. All rights reserved. Figure defect in carbon nanotubes adapted with permission.[59] Copyright 2017, Springer Nature.

2.3. Status of research on hBN quantum emitters

Research on hBN quantum emitters was pioneered by Tran and co-workers at the University of Technology Sydney, Australia, where they discovered the first quantum emitters operated at room temperature in 2016.[14] Since their first paper, the topic has gained significant traction in the research community, resulting in a sharp increase in publications and

citations, exceeding 150 publications and 7000 citations per year, as shown in **Figure 2.2a-b**. To date, research groups worldwide have been increasingly active on the topic, especially in the United States, Australia, China, Germany, Japan, the United Kingdom, and other European countries (**Figure 2.2c**). Initially spearheaded by Australian researchers, the field has recently witnessed the largest growth in the number of publications in the US and China. With the recent discovery of new spin-active defect centers in hBN,[60-62] the research topic is expected to grow significantly in the following decades. A significant increase in research interest will be in quantum sensing thanks to the unique two-dimensional nature of the hexagonal boron nitride lattice that facilitates more efficient near-surface defect engineering than diamond or silicon carbide. Quantum communication, particularly quantum key distribution, will be another area of strong growth thanks to recent advances in optical engineering, allowing for integrating the quantum light sources and supporting electronics into an ultra-compact CubeSat design.

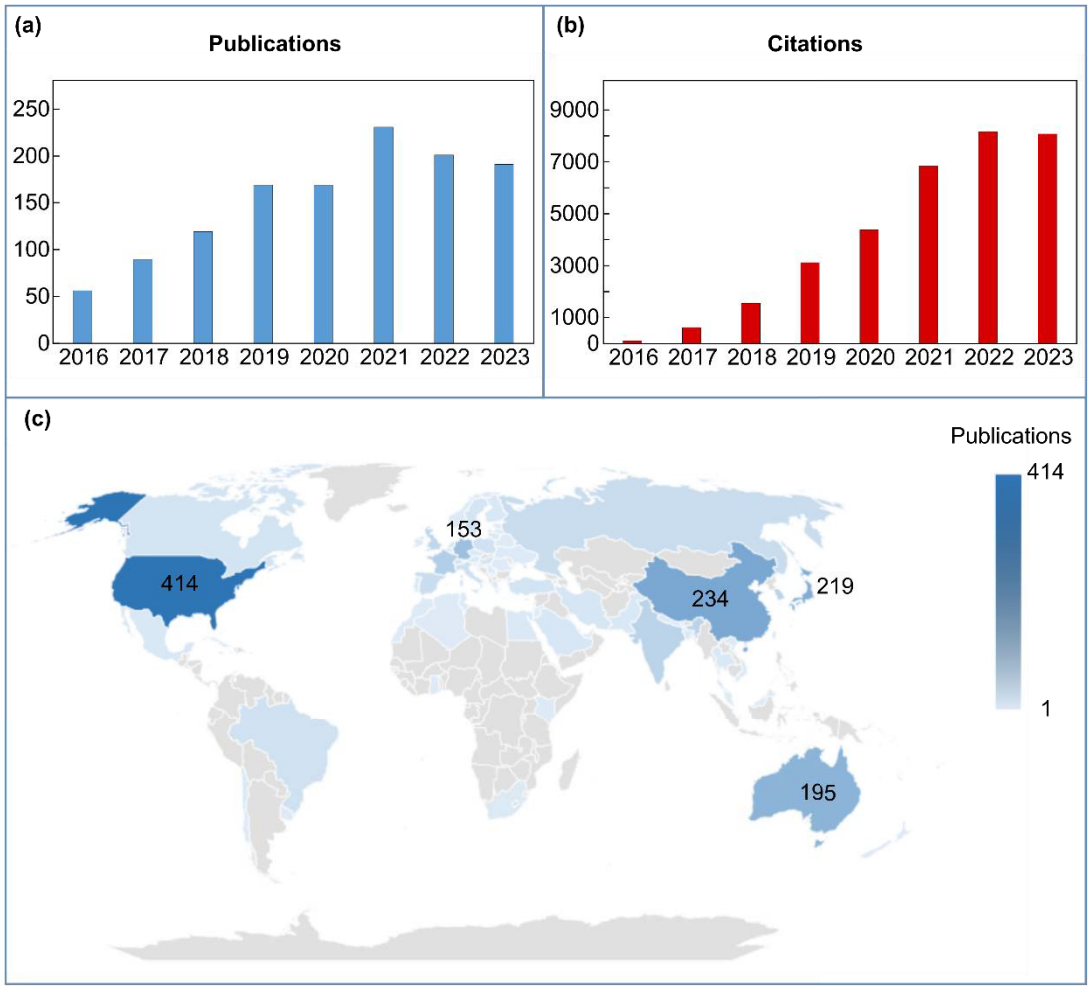

Figure 2.2: Statistics on global scientific research concerning hBN quantum emitters from 2016 to 2023. (a, b) Number of publications and citations using the Web of Science (Clarivate Analytics) with the keywords ["hexagonal boron nitride" OR "hexagonal boron-nitride" OR "hBN" OR "h-BN" (Topic) and "quantum emitter*" OR "color cent*" OR "color-cent*" OR "quantum light*" OR "single-photon*" OR "single photon*" OR "emitter*" OR "ensemble*" OR "dipole*" OR "quantum-emitter*" OR "quantum-light*" OR "defect*" (Topic) and "fluorescence*" OR "emission*" OR "photon*" OR "light*" OR

"optical"]. **(c)** Corresponding distribution of publications by countries, powered by Bing © Australian Bureau of Statistics, GeoNames, Microsoft, Navinfo, Open Places, OpenStreetMap, TomTom, Zenrin. The search was performed on August 09, 2024.

2.4. Theoretical and experimental investigations on the origin of various defect families

Unlike the case of most color centers in diamond, the exact chemical structures of most quantum emitters in hBN are largely unknown. This is in part due to the complexity involved within the hBN lattice. While diamond contains only a single element, carbon, hexagonal boron nitride comprises two elements, boron and nitrogen. Such poly atomic nature results in more possible defect configurations in hBN than in diamond. Additionally, hBN has more lattice imperfections and impurities than diamond, rendering the determination of the responsible defect centers a daunting task. Another factor is the built-in strain in hexagonal boron nitride. As hBN is a two-dimensional material, its single-layer sheet of atoms can sustain unusually high lattice strain of up to 5%, similar to graphite and other TMDs. Based on theoretical calculations, the built-in strain can shift the ZPL of an emitter up to tens or hundreds of

millielectronvolts.[63] Such a phenomenon significantly complicates the assignment of the defect structures since it can be mistakenly grouped into another defect family whose ZPL energy is close by.

Quantum emitters in hBN can be categorized into four families according to their emission wavelengths: UV (~4.1 eV), blue (~2.85 eV), visible (~2 eV), and spin-active (~1.5 eV) defects.[37] Variations in the emission wavelengths within each group are likely attributed to local built-in strains. In the UV-emitter group, carbon-related defects, such as the substitutional carbon at the nitrogen site (C_N) and the carbon dimers ($C_B C_N$) are proposed to be responsible for the emission.[64-65] Other candidates for the UV-family include the pentagon–heptagon Stone–Wales defect,[66] and carbon clusters (6C).[67] The so-called blue-emitters or B-center have recently been found and tentatively attributed to the carbon split interstitial defect (C_N^2)[68] or the carbon chain tetramer.[69] The visible emitters are the most studied among the four families thanks to their extraordinary optical properties, including ultrahigh brightness, linear polarization, and controllable emission wavelengths via external stimuli such as strain or electric fields. Emitters in this family cover a wide range of emission wavelengths ~550–850 nm (2.25–1.46 eV). Contrary to the other three families, the visible defect family appears to contain several sub-families of emitters due to their distinct spectral and optical

properties.[63, 70-72] Previous studies from various research groups suggest the existence of two to eleven different sub-families based on their optical signatures. Most notably, Islam et at. performed an extensive investigation of defect emission lines on over 10,000 defects and analyzed various parameters such as Franck−Condon-based factors, photoluminescence linewidths, phonon side bands, and spatial density.[73] The work identified 11 distinct groups of emitters based on their rigorous analysis over a large database of defect spectra. Initially, most of these visible emitters are attributed to non-carbon-related configurations such as the anti-site nitrogen-vacancy ($N_B V_N$).[14] Carbon is later thought to be involved in the chemical structure of these defects, such as the carbon antisite $C_B V_N$. Some defects in this group have recently been found to be spin-active and can be initialized, manipulated, and read out all optically—a technique called optical detected magnetic resonance (ODMR). Recent work suggests that the negatively charged $V_B C_N^-$ can be a candidate responsible for such optical characteristics.[60-61] Defect-based emission is, however, not the only hypothesis proposed. Alternative postulates include dangling bonds at grain boundaries and surfaces or donor-acceptor pair.[74-75] Overall, the most popular theoretical framework used thus far is the density functional theory (DFT), thanks to its efficiency, versatility, and accuracy for ground-state calculations.[76-78] Density functional theory

calculations are being used as a powerful tool in providing insightful understanding into the electronic structure of the materials and guiding the design of catalysts and functional materials with superior properties.[79-82] However, the use of conventional level of theory is not accurate in DFT studies on h-BN material, particularly when evaluating defect states and therefore higher level of theory is required.[39, 83-84] Reimers et al. comprehensively calibrated the performance of different DFT methods in describing spectroscopic and energetic properties of h-BN defect sites.[83] This study reported that DFT methods using the conventional generalized-gradient approximation functionals such as PBE performed poorly and could not be applied to defect states and higher levels such as hybrid functional HSE06 and long-range corrected functional CAM-B3LYP. Although those higher levels of theory implement more computational cost, they are making significant progress in shedding light on the origin of various defects sites in h-BN.

Huang et al.[85] used DFT calculations to gain mechanistic understanding on the formation of defects in hBN at microscopic scale and revealed the crucial role of interdefect electron pairing in stabilizing the donor- and acceptor-type defects combination. Dorn et al. used the integration between DFT calculations and high-resolution solid-state NMR spectroscopy to identify the detailed structure of the different defect sites

within h-BN.[86] Besides providing structural information, DFT calculations also delivered insightful information on electronic properties of the defect sites.[87] The stable spin states, charge transition levels, and optical excitations were computed at various defect center in h-BN, including boron antisite, boron vacancy, nitrogen vacancy, nitrogen antisite, etc, and the $C_B V_N$ defect was identified as the highly potential candidate for application in quantum bit and emitting.[82, 88-89] Other carbon-related defect configurations were also reported by several research groups, including the carbon trimers and tetramers.[76, 90-91] The unprecedented strong coupling of defect emission in hBN to stacking sequences was reported in Li et al.[92] shedding light on the design principles for precise controlling of defect emission. The optical properties of boron vacancy defect center were also evaluated in Ivady et al.[93] revealing the corresponding routes responsible for the spin dependent luminescence and optical spin polarization of this defect center. Recently, a notable effort in this area has resulted in a comprehensive online database of hBN optically active defect centers,[94] covering 257 triplet and 211 singlet electronic structures. In this work, the Vienna Ab initio Simulation Package (VASP) is used in conjunction with the HSE06 exchange-correlation functional to efficiently screen through many defect configurations. At first, 158 defect complexes from group III–V are

considered. Subsequent calculations determine the spin multiplicity: singlet, doublet, or triplet. Additional charges (positive or negative) are added for the doublet cases, followed by the geometrical optimizations. Some of the details are shown in **Figure 2.3a**. The defect complex is then added to the online library (https://h-bn.info). Interestingly, many useful parameters of these defects are collected, including their ZPL position, photoluminescence spectra, excitation and emission polarization, radiative lifetime, and quantum efficiency—making it among the most extensive theoretical investigations on hBN quantum emitters to date. Furthermore, with the recent development of machine learning techniques,[95-96] DFT calculations are expected to have more important role in advancing the knowledge of quantum bits in hBN-based materials.[97-98]

However, it has been shown that in some cases, a rigorous experimental framework alone could pinpoint a particular defect configuration with high confidence. Such an example is the discovery of the so-called spin-active defect family, which has an emission wavelength of ~850 nm. In this case, electron spin resonance angle-dependent (EPR) and ODMR, together, unveil the atomic origin of the defect, the negatively charged boron vacancy (V_B^-), as depicted in **Figure 2.3b**. Similar to the third defect family (the carbon-related spin-active group), the V_B^- defect

complex has a spin multiplicity of $S = 1$, meaning that it has a spin triplet with $m_S = \pm 1$ and $m_S = 0$ manifolds, with a zero-field splitting of ~3.5 GHz. Without the help of DFT, such a robust experimental framework has proven to be very effective in unveiling the chemical structure of these defect complexes in hBN. However, this situation is not always applicable, especially with defect complexes comprising multiple impurities and vacancies. It is, therefore, challenging to universally implement the scheme to all observed defect complexes.

Lately, transmission electron microscopy (TEM) and scanning transmission electron microscopy (STEM) have emerged as promising experimental techniques for investigating the defect structures in hexagonal boron nitride. For simplicity, we mention TEM as the umbrella term for both techniques. Owing to its atomic resolution, TEM was employed in studies of the formation of monovacancy or multi-vacancy defects in a monolayer hBN.[99-103] A recent study by Bui et al. demonstrated the creation of single vacancies in hBN under ultrahigh vacuum, where boron atom was twice as probable as nitrogen atom to be sputtered off below 80 keV of accelerating voltage.[104] Interestingly, other than creating vacancies, TEM were also utilized to insert mobile carbon atoms into these atom-sized voids. In their work, Park and co-workers showcased an elegant control of filling single carbon atom into

monovacancy and larger voids with the accuracy surpassing 2 nm.[105] Such abilities imply the potential of using TEM for on-demand defect engineering in hBN. Recent efforts have also been spent on correlative studies between optical and transmission electron microscopy to better understand the responsible defect configurations. For instance, a combination of photoluminescence, cathodoluminescence, and electron diffraction was attempted to gain insights into the atomic structures of the visible defect family.[71] In another attempt, high-resolution STEM-EELS (electron energy loss spectroscopy) was introduced in conjunction with photoluminescence, resulting in the tentative assigning of a carbon complex as the responsible defect structure for the 2.16-eV emitters—within the visible defect family.[106] While these joint approaches were not entirely successful in pinpointing the exact origin of these defects, it showed that a cross-platform correlative method is highly valuable in extracting hidden information about these defect complexes. It also highlights that TEM is among the most promising techniques for such defect structure studies.

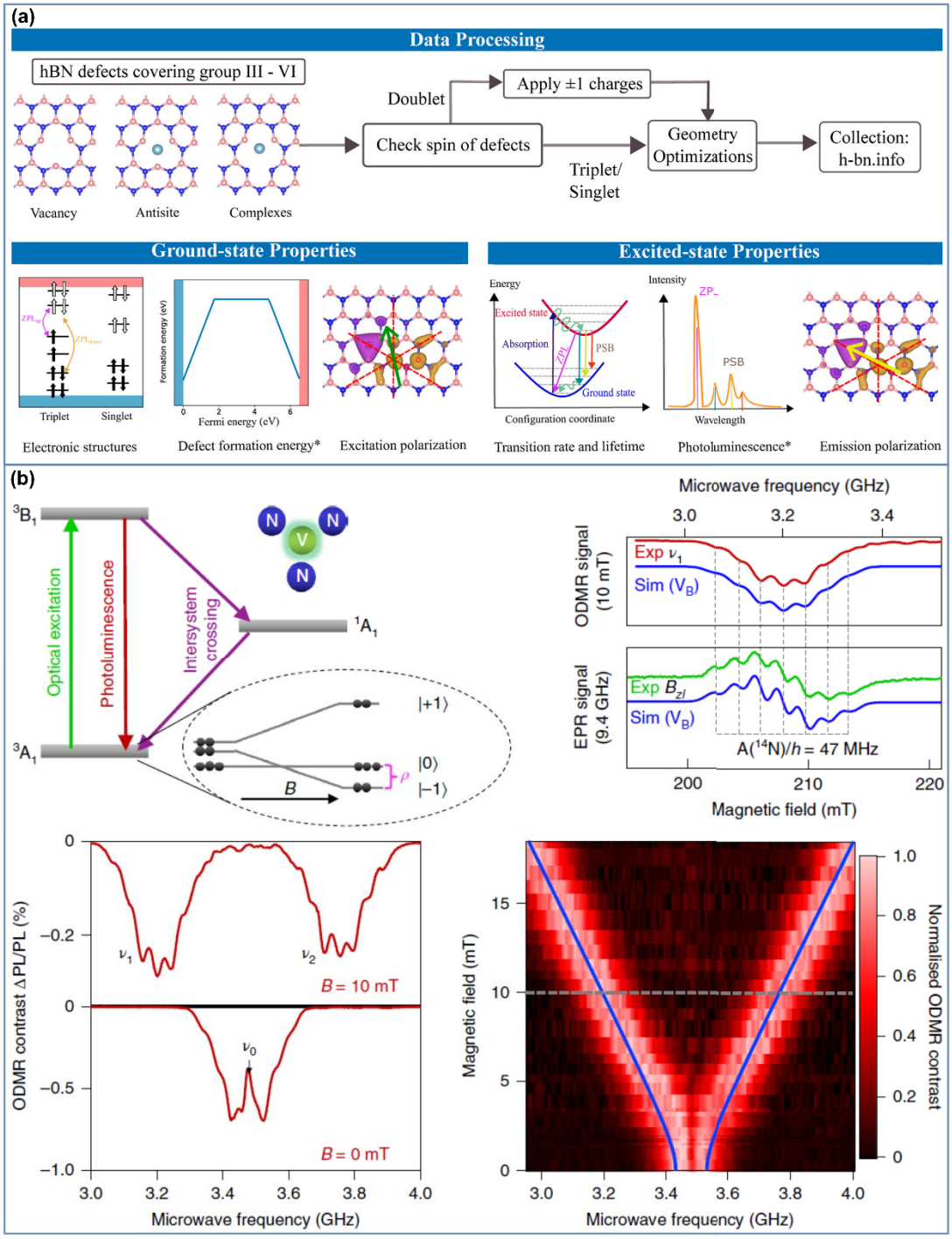

Figure 2.3: Theoretical calculations and experimental research on the origin of hBN quantum emitters. (a) The hBN defects database: A Theoretical compilation of color centers in hexagonal boron nitride **(b)** hBN spin defects read-out by electron paramagnetic resonance

spectroscopy and optically detected magnetic resonance measurements at room temperature. Figure a adapted under terms of the CC-BY 4.0 license.[94] Copyright 2024, The Authors, published by American Chemical Society. Figure b adapted with permission.[62] Copyright 2020, Springer Nature.

2.5. Host material fabrication and defect engineering

Compared to other host materials such as diamond or silicon carbide, hexagonal boron nitride bulk crystals and powder are significantly cheaper. Hexagonal boron nitride host can be categorized into three main morphological forms: thin film, micro/nanopowder, and bulk crystal as shown in **Figure 2.4a**. Each of these forms typically involves one or multiple growth techniques. For thin films, chemical vapor deposition (CVD), and metal–organic vapor-phase epitaxy (MOVPE) are the popular synthetic methods (**Figure 2.4a**, top panel). Chemical vapor deposition is a well-established method for growing hBN thin film with controllable thickness.[107-109] The technique involves the controlled flow of gaseous precursor(s) into a quartz tube heated at temperatures exceeding the decomposition threshold of the precursor(s). As such, the technique is straightforward and requires inexpensive apparatus. One of the most

significant advantages of this method is its scalability. Previous studies showed CVD growth at wafer-scale sizes,[110-111] enabling prospects of industrial integration. By adjusting the growth parameters such as temperature, duration, gas partial pressure, and precursor types, optically-active defect centers were embedded in situ.[112-113] The emission spectra from these CVD-grown hBN films feature a wider full-width-at-half-maximum (FWHM) and lower peak intensity than those from solvent-exfoliated nanoflakes. In addition, quantum emitters in these films tend to be susceptible to blinking and bleaching. The underlying reasons for this phenomenon remain largely unknown. Although there are still no techniques to effectively tune the defect density in these CVD hBN films, growth on pillar-patterned substrates exhibited a certain degree of control over the defect position within the films.[114] The following method is MOVPE, in which triethylboron and ammonia are the precursors. The technique is significantly more complex than CVD. Most notably, the technique demands highly pure metalorganic compounds and hydrides, and its operating parameters need to be controlled and synchronized precisely. The synthesis technique witnessed carbon incorporation during the hBN growth, resulting in thin hBN film with various densities of quantum emitters, depending on the input carbon concentrations within the precursors. While this method has only been introduced recently, it

has gained significant traction due to its ability to produce optically-addressable spin-active defect centers.[60-61] As such, MOVPE is expected to receive increasing attention in the research community even though the technique requires significant facility investment owing to its complex and stringent operations. The second morphological form of hBN is micro/nanopowder. Among the most popular techniques for synthesizing hBN powder is solvo/hydrothermal, where high pressure and high temperature are achieved by conducting the liquid-phase reaction in a pressurized vessel in an annealing oven. By controlling the parameters of the reaction, such as type of solvents, reaction time, filling factor, and temperature, the size of resultant hBN particles can be controlled. For instance, the middle panel of **Figure 2.4a** shows TEM images of hBN nanoparticles with sizes below 10 nm.[115] Such small particle sizes can be particularly useful for bioimaging, biosensing, or drug delivery applications.[116] Hexagonal boron nitride powder can also be synthesized via ammonolysis of boric oxide or borax at high temperatures, which is also known as the borax-urea method.[117] Chemical vapor deposition is another synthetic approach where gaseous precursors comprising nitrogen and boron are allowed to react in a chamber at high temperature, resulting in the powder form of hBN. The third form of hBN is bulk crystals—which provide the highest quality and purity of hexagonal boron nitride.

Bulk crystals can be synthesized in three main pathways: high-pressure high-temperature (HPHT), atmospheric pressure high temperature (APHT), or polymer-derived ceramics (PDC), as shown in the bottom panel of **Figure 2.4a**. In HPHT method, bulk hBN crystals are grown by high-pressure high-temperature process using Ba-BN solution , where temperature and pressure often exceed 1500°C and 4.5 GPa, respectively.[118] This approach yields the purest hBN crystals among the fabrication methods mentioned above. Most notably, bulk hBN fabricated by Taniguchi, Watanabe, and co-workers at the National Institute for Materials Science (NIMS) Japan, is widely regarded as the highest quality hBN to date and used for heterostructures in two-dimensional devices around the world.[119] As such, the material rarely contains optically active defects, and therefore, defect engineering techniques are required to implant suitable defects into the hBN lattice. Unlike HPHT, atmospheric-pressure high-temperature also gives rise to similar crystal quality, albeit at ambient pressure. Bulk hBN crystals synthesized by such a pathway, however, contain ten-fold more defects than the HPHT method.[120] The APHT approach involves the mixing of boron and nitrogen into a molten solvent that is created by melting metals at high temperatures. Common metal pairs used as the solvents include Ni-Cr, Fe-Cr, or Cu-Cr.[121-124] Upon being cooled, hBN crystals are precipitated out

of the metallic solvent and are collected. Interestingly, using this method, the growth of isotopically pure hBN—hBN with enriched ^{10}B- or ^{11}B were realized.[122, 125] The growth of single-crystal hBN can also be achieved by the polymer-derived ceramics approach which produces bulk crystals close to the quality achieved by APHT.[120, 126] The PDC approach comprises three steps. The first involves the polycondensation of borazine into polyborazilene. The second step entails the pre-ceramization of the mixture of polyborazilene and lithium nitride at moderately high temperature (~650°C). In the final step, the preceramic powder is sintered at high temperature (~1800°C) and high pressure (~180 MPa) to produce hBN single crystals as large as millimeters. Although bulk hBN crystals offer superior purity and crystallinity compared to other two forms, the optical properties of the emitters hosted within are less impressive. Many native quantum emitters in bulk hBN exhibited significant optical blinking and possessed multiple dark manifolds,[14, 127] making them unsuitable for most quantum applications.

Besides the thin film form, hBN powder or bulk crystals are routinely exfoliated into thin flakes for further use. The exfoliation of hBN can be divided into solvent- and mechanical exfoliation. The former technique is almost exclusively used for hBN micro/nanopowder. In this method, the obtained powder is dispersed in suitable solvents such as ethanol,

isopropanol (IPA) or N-methylpyrrolidone (NMP), whose surface energies match the cross-plane interactions between hBN sheets. The hBN flakes are gradually exfoliated in the solution by the sheering motions induced by the ultrasonication bath. The cavitation effect creates randomly distributed, localized spots with extremely high temperature and pressure, causing the flakes to separate in the out-of-plane direction.[128] Prolonged sonication promotes thinner hBN flakes in the solution at the expense of smaller flake diameters due to the breakdown of the flakes in the sonication process. The resultant solvent-exfoliated flakes possess a typical dimension of 200–500 nm in diameter and 20–100 nm in thickness.[128] The defects are embedded within the exfoliated flakes and can be activated by simple annealing at a temperature >850°C.[63] Although inferior in terms of crystallinity compared to CVD and MOVPE, solvent exfoliation provides a low-cost alternative for applications where high-quality crystalline material is not required, such as heterogeneous integration of the quantum emitters with on-chip photonic architectures or quantum key distribution. Another technique is mechanical exfoliation, which are originated from the Scotch tape method.[129] This method, on the other hand, is only employed for exfoliating bulk hBN crystals. Though simple, the method can produce high-quality flakes with large sizes. The typical flakes feature a thickness

ranging from a few layers to a few hundred nanometers and a lateral dimension of a few to tens of microns. On the one hand, the technique is often used in the laboratory setting owing to its lack of scalability. On the other, the most important advantage of this method is its simplicity and versatility, which allows for rapid building of complex 2D heterostructures from various 2D materials whose lattice parameters are mismatched. For these reasons, mechanically exfoliated hBN is a preferred choice for device fabrication, such as electrically driven single-photon emitting devices or widely tunable single-photon light sources.[130-133]

We now turn to defect engineering strategies for the hBN hosts (**Figure 2.4b**). The first method involves thermal annealing at high temperatures, typically >850°C. At these temperatures, quantum emitters were observed to be activated, and the quantity seemed to be weakly correlated with the annealing temperature.[63] However, the exact mechanism for such activation remains elusive. The thermal treatments effectively activate optically active defects in various hosts, including bulk, solvent- and mechanical-exfoliated flakes.[128, 134-135] In addition, the method is also used as a post-treatment for a main structural modification process, as discussed later in the text. Though simple and effective, thermal treatments lack spatial determinism and are challenging to implement on

substrates/structures that are temperature-sensitive. The second approach, laser writing, for example, tackles this issue. In this approach, a femtosecond laser (pulse width <1000 fs) is tightly focused onto an hBN flake, releasing pulse energies in the order of tens of nanojoules.[51] Beyond a certain pulse energy threshold, laser-induced damage was observed, with defective structures ranging from bubble-like to crater-like formations. Bright and stable quantum emitters were observed after the subsequent thermal annealing treatment. The yield of such a technique reached ~43%, which is relatively high among other competing methods. Nevertheless, the mechanism of defect formation is still poorly understood, making it difficult for further improvements to occur. Plasma-induced etching is another promising technique for creating emitters in hexagonal boron nitride. This method relies on the mild etching created by the accelerated ions in the plasma.[50, 136] The ion species can be selected by introducing different types of gas, such as oxygen, argon, and hydrogen.[50, 135-136] These highly energetic ions bombard the hBN lattice, causing bond breakage and vacancies, and the defect density is shown to have a strong correlation to the plasma power. The subsequent thermal treatment then induces lattice reconstruction, which promotes the formation of optically active defect centers. When executed with a lithography-defined mask, the plasma etching process can create an array

of site-specific quantum emitters. The following method is electron-beam-induced defect creation. In this technique, highly accelerated electrons in a scanning electron microscope (SEM) are directed toward hBN flakes, inducing atomic-sized defects in the lattice. Due to the negatively charged nature of the electrons, their interactions with the lattice are complicated and require simulation platforms such as Monte Carlo simulation of electron trajectories (CASINO) in solids to extract crucial interaction parameters.[137] These parameters include electron trajectories, energy loss, backscattered, and secondary electron generation. Early attempts using electron beams to create emitters in hBN resulted in randomly distributed optically active defects that tend to localize near edges and grain boundaries.[63, 138] Recent studies, however, showed that electron irradiation effectively created quantum emitters in a deterministic manner. The method produced emitters from both the visible and blue families.[139-142] . Unlike the visible family, the blue emitters possess a narrow linewidth distribution of ~3 meV,[140] allowing for the first two-photon quantum interference from emitters in hBN.[143] A closely related technique is ion implantation which arises from an ion implanter or a focused ion beam (FIB). Previous studies reported increases in emitter density with various ion species.[138] The spatial distribution of optically active defects was, however, arbitrary. Spatial localization of the quantum

emitters was recently achieved by gallium FIB,[144] with a yield as high as 31%. The milling process created an array of holes with edges at their circumferences, where hBN emitters were located. Further optimization of the ion implantation conditions can be obtained by detailed simulations on platforms such as the stopping range of ions in matter (SRIM) since it can provide insightful information about ion range and distribution, energy loss, sputtering yield, and vacancy concentration.[145] Another method involves using indentation by an atomic force microscope (AFM) to induce “crater-like” pits on the hBN flakes.[146] The damage created at the rim of the pits was found to host quantum emitters, with a yield of ~36%. The ZPL distribution of the emitters fabricated by this technique is relatively wide, however, ranging from ~582–633 nm, and the PL lineshapes vary significantly from emitter to emitter. Another drawback of the method is its destructive nature—making it difficult to seamlessly integrate into on-chip photonic structures.

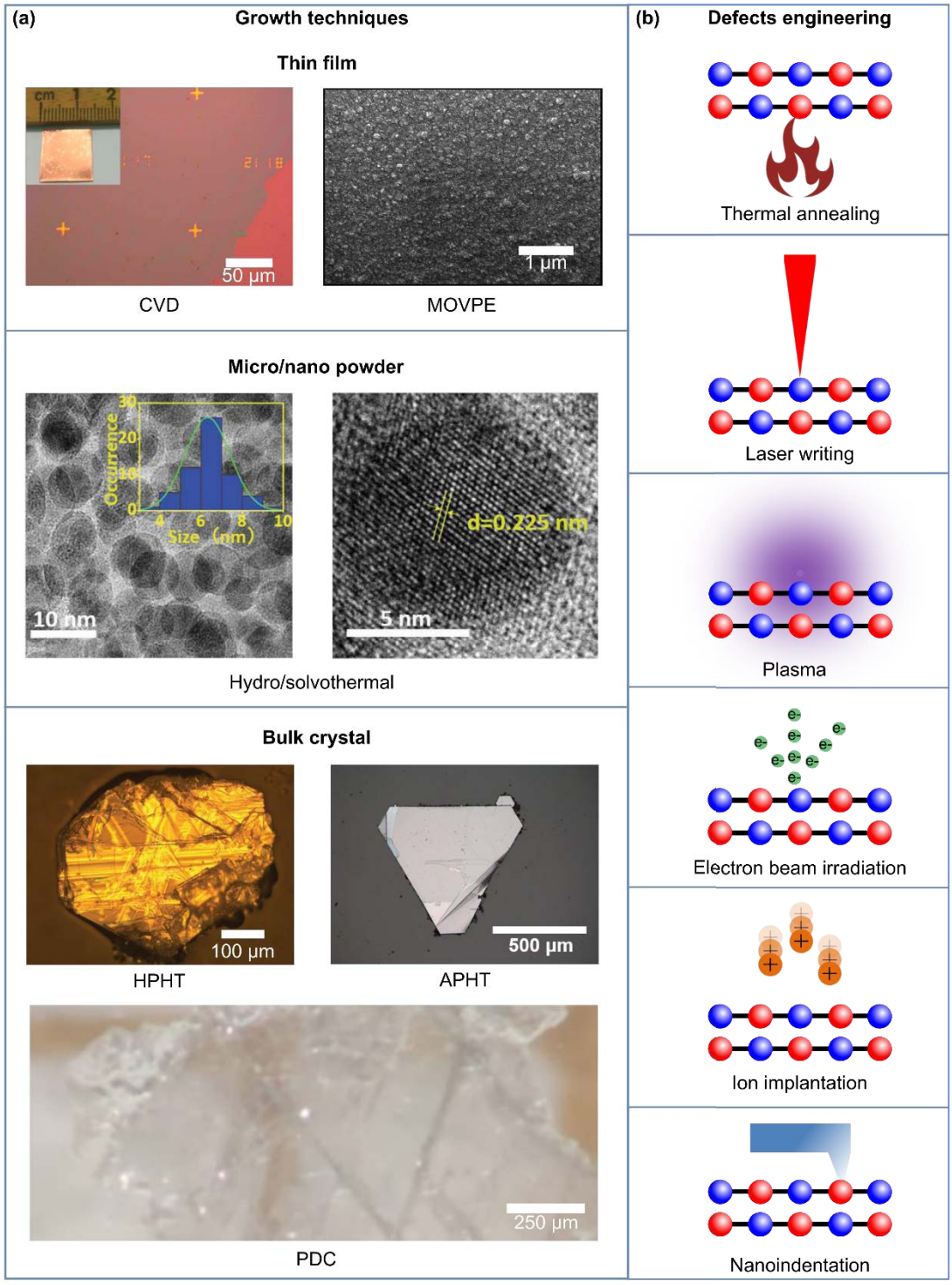

Figure 2.4: Fabrication of hBN quantum emitters. (a) Techniques to growth hBN in three different forms: thin film hBN by chemical vapor deposition (CVD) and metal-organic vapor-phase epitaxy (MOVPE),

micro/nano hBN powder by hydro/solvothermal method, bulk crystals hBN by high pressure high temperature (HPHT), atmospheric pressure high temperature (APHT) and polymer-derived ceramics (PDC). **(b)** Schematic representations of six methods to create optically active defects in hBN: thermal annealing, laser writing, plasma, electron beam irradiation, ion implantation, and nanoindentation. Figure optical image CVD hBN adapted with permission.[112] Copyright 2019, American Chemical Society. Figure SEM image MOVPE hBN adapted under terms of the CC-BY 4.0 license.[147] Copyright 2021, The Authors, published by Springer Nature. Figure TEM and HRTEM images taken from hBN nanoparticles growth by hydrothermal method adapted with permission.[115] Copyright 2021, Wiley-VCH GmbH. Figure optical image HPHT hBN adapted with permission.[134] Copyright 2016, American Physical Society. Figure optical micrograph APHT hBN adapted with permission.[124] Copyright 2017, American Chemical Society. Figure optical image PDC hBN adapted with permission.[126] Copyright 2024, American Chemical Society.

2.6. Monolithic integration into photonic cavities and waveguides

Most quantum applications demand the quantum light source to be emitted into a particular well-defined optical mode that is directional. Therefore, integrating individual hBN quantum emitters into photonic cavities and waveguides is a vital step toward any practical implementations. Such incorporation schemes can be classified into two main categories: monolithic and non-monolithic integrations. In the monolithic scheme, the emitter and the photonic structures share the same host material—hexagonal boron nitride. It must be noted that hexagonal boron nitride is a dielectric that has a birefringence value $\Delta n = n_{\perp} - n_{\parallel} = \sim -0.35$,[45] which needs to be taken into account in the design. The main advantage of this approach is that the photon coupling from the emitter to the cavity or waveguide is usually superior to that of the non-monolithic counterpart. This is because the emitter can be accurately positioned at the optimal location within the photonic structures, rendering maximum coupling efficiency. The fabrication process typically involves several steps. First, a type of photonic structure, say a cavity, is designed using finite-difference time-domain (FDTD) software where the resonant wavelength and the quality (Q) factor can be calculated. Second, the

fabrication of the cavity structure follows the standard electron beam lithography (EBL) process on hBN flakes deposited on silicon substrates. The procedure entails e-beam resist patterning, developing, dry-etching (sulfur hexafluoride, SF_6), undercut (KOH solution), and thermal annealing. Third, the emitters are created by a site-specific method, such as electron beam irradiation, to produce individual emitters at locations with maximal field intensities. Early attempts, however, rely primarily on the random distribution of the emitter with respect to the optimal sites. Such an approach is known as probabilistic integration. For instance, one-dimensional (1D) photonic crystal cavity (PCC) was created, and emitter-cavity weak-coupling was demonstrated,[148-149] as shown in **Figure 2.5a**. The estimated Purcell factor—a photoluminescence enhancement ratio of the coupled emitter to the bare emitter—was estimated to be ~15. Such a value is considerable, considering that dielectric cavities often feature significantly larger mode volumes compared to their plasmonic counterparts.

By further fine-tuning the fabrication procedure by employing a combination of low SF_6 concentration, low gas partial pressure, and low etching power, Nonahal and co-workers showcased a slow etching process, resulting in very smooth sidewalls in the photonic structures. The smoothness of the structures gives rise to Q factors of the two-dimensional

PCC as high as 2000 (**Figure 2.5b**). Microdisk resonators were fabricated using the same approach, exhibiting Q factors exceeding 3000 (**Figure 2.5c**). Complicated photonic structures such as the bound state in the continuum (BIC) metasurfaces have also been fabricated monolithically.[150] Coupling of spin-active defects to the structures were reported, yielding 25-fold increase in photoluminescence and spectral linewidth reduction to under 4 nm. Couplings of quantum emission into a waveguide mode were demonstrated by Li et al. using a similar technique, which resulted in a relatively modest coupling efficiency of ~3% (**Figure 2.5d**).[151] The monolithic fabrication of hBN photonic architectures has advanced significantly during the last several years, with suspended, fully integrated quantum photonics (IQP) recently realized.[152] Continuous improvements in the fabrication steps, especially dry-etching and mask removal, are needed to reach the Q factors closer to what was achievable in bulk dielectrics such as silicon and III-V semiconductors. Ultimately, the hard limit in the performance might be set by the two-dimensional nature of the material per se. The weak out-of-plane interactions between atomically thin sheets of hBN make it challenging to sustain a high degree of smoothness during the etching process, unlike other bulk materials, such as silicon, whose lattice integrity is isotropic. Contrary to the probabilistic nature of these integrations, recent studies leverage the site-

specific creation of emitters within the photonic structures, significantly increasing the device's performance. For example, Gérard et al. demonstrated site-controlled coupling of the blue emitters into monolithic photonic waveguides, thanks to the use of site-specific focused electron beam irradiation.[153] In a similar fashion, Spencer and co-workers showcased deterministic coupling of blue emitters into bullseye cavities, also known as circular Bragg gratings (CBG), resulting in a 6-fold emission collection enhancement.[154]

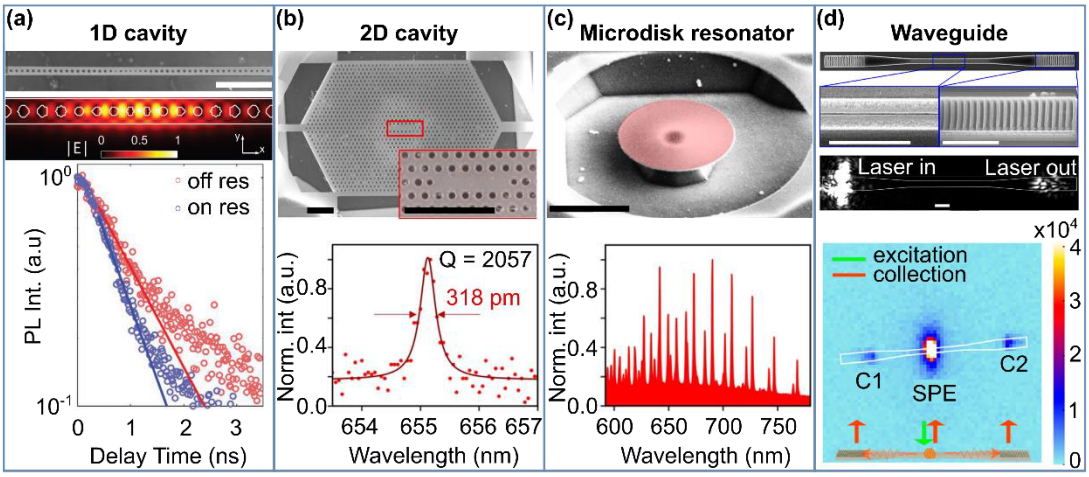

Figure 2.5: Monolithic integration of hBN quantum emitter in photonic structures. (a-d) SEM images and representative optical signatures of 1D, 2D photonic crystal cavities, microdisk resonator, and waveguide, respectively. Scale bars in all figures are 2 µm. Figure a adapted with permission.[148] Copyright 2021, Wiley-VCH GmbH. Figure

b, c adapted with permission.[152] Copyright 2023, Wiley-VCH GmbH. Figure d adapted with permission.[151] Copyright 2021, American Chemical Society.

2.7. Hybrid integration into dielectric and plasmonic architectures

In the non-monolithic category, two platforms are considered: hybrid dielectric and plasmonic integration. The form scheme encompasses the positioning of individual quantum emitters embedded in hBN micro flakes or nanoflakes atop pre-fabricated dielectric structures. Compared to the monolithic counterpart, the hybrid approach is significantly more versatile since various dielectrics, such as silicon, silicon carbide, or III–V semiconductors, can be used as the material for fabricating cavities or waveguides. As such, the approach makes integrating hBN quantum emitters into well-established integrated photonic chips a straightforward task. Hybrid dielectric architectures, however, suffer from a significant weakness—that is, the suboptimal coupling efficiency of the emitter to the photonic structures. The quantum emitters are usually placed on the dielectric cavities or waveguides. At the same time, the maximal field intensities are located inside the photonic formations, resulting in a spatial

mismatch between the two. An example of this strategy was conducted by Froch et al. Here, an hBN film grown by CVD was transferred onto a silicon nitride (SiN) substrate, and the composite was patterned with EBL and dry-etched into hybrid CVD hBN/1D PCC structures, as depicted in **Figure 2.6a**. A quality factor of 2400 and a PL enhancement of 9 folds were reported.

Vogl and co-workers integrated quantum emitters in mechanically exfoliated microflakes into microcavities (**Figure 2.6b**). The cavities are a modified Fabry-Perot type consisting of a hemispherical and a flat mirror that confines the cavity mode to the emitter location. The cavity mode is tunable thanks to the adjustable thickness of the sandwiched PDMS layer between the two mirrors. When on resonance, the cavity-emitter composite features a Purcell factor of 2.3 and a 25-fold reduction in linewidth values. Owing to the compact design of the microcavities and other miniaturized optical components, the single-photon source setup is entirely self-contained within an $10 \times 10 \times 10$ cm^3 enclosure. Unlike the previous two designs, the third example demonstrates a coupling of hBN quantum emitters, the V_B^- defect center in particular, to the plasmonic nanopatch antennas (NPAs),[155] as shown in **Figure 2.6c**. The hybrid system comprises a bottom thin silver film, a thin hBN flakes, and a top silver nanocube. Such a design not only offers extremely tight

confinement of electromagnetic fields of a plasmonic cavity but also produces directional emission of a plasmonic antenna. As a result, an overall PL enhancement of ~250 folds was achieved, significantly better than any other coupling schemes.[156-157] A drawback of this design, however, lies in the probabilistic nature of the coupling since the extreme mode confinement induced by the silver film and nanocube requires the perfect spatial matching of the emitter to the mode. Besides cavities, hybrid waveguides were also demonstrated using a similar strategy. For instance, Kim and co-workers fabricated the hybrid hBN-AlN composite waveguide structures by placing the hBN nanoflakes on top of the pre-existing aluminum nitride formations (**Figure 2.6d**).[158] The significant spatial mismatch between the emitter and the waveguide mode and the mode leakage induced by the underlying sapphire substrate resulted in a modest coupling efficiency of < 2%. Other more sophisticated integrations between hBN emitters and photonic structures such as metalenses or BICs were also realized experimentally.[159-160] The former showcased the ability to spatially separate quantum emission with different polarization states. The latter featured the first room-temperature strong-coupling between an hBN quantum emitters and a cavity, resulting in a noticeable Rabi splitting of ~4 meV. Though challenging, the spatial mode mismatch issue mentioned above can be tackled. An innovative

strategy has recently been demonstrated using a composite SiN-hBN microring resonator structure in which the hBN flake was sandwiched between the top and bottom halves of the SiN resonators.[161] Such a composite structure addressed the spatial matching issue mentioned above, though with a significantly higher degree of complexity in the fabrication process. Such a clever integration is a step in the right direction to improve the performance of the hybrid photonic architectures, rivaling those of monolithic counterparts.

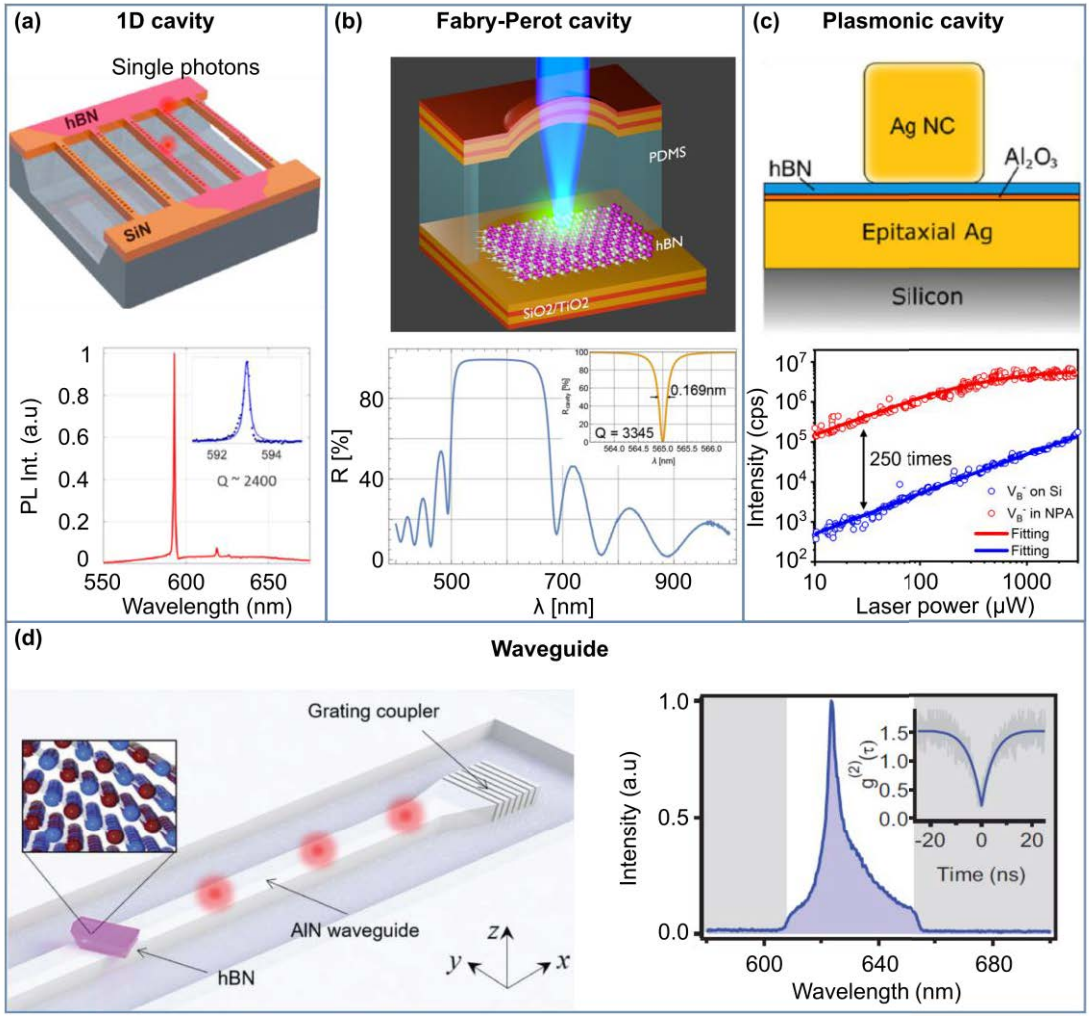

Figure 2.6: Non-monolithic integration of hBN quantum emitter in photonic structures. (a-d) Schematic and corresponding results of various hybrid integration of hBN quantum emitters: one-dimensional photonic crystal cavity, Fabry-Perot cavity, plasmonic cavity, and waveguide structure, respectively. Figure a adapted with permission.[162] Copyright 2020, American Chemical Society. Figure b adapted with permission.[163] Copyright 2019, American Chemical Society. Figure c adapted with permission.[155] Copyright 2022, American Chemical

Society. Figure d adapted with permission.[158] Copyright 2019, Wiley-VCH Verlag GmbH & Co. KGaA, Weinheim.

2.8. Applications in quantum sensing

Quantum emitters in hBN have recently emerged as a promising alternative to established platforms such as color centers in diamonds or silicon carbide. Hosted in atomically thin sheets of hexagonal boron nitride, quantum emitters can be positioned closer to the material surface without being severely disturbed by the surface states and trapped charges, thanks to the dangling-bond-free nature of the material. One of the simplest examples of quantum sensing is quantum thermometry—the measurement of local temperature using quantum systems. Chen et al. reported using individual quantum emitters in hBN nanoflakes to monitor temperature down to the sub-micron scale (**Figure 2.7a**).[164] The spectral characteristics of hBN quantum emitters, such as the broadening of the linewidths or the shifting of the ZPLs, are well-correlated with the temperature changes. As a result, local temperature readouts at different spots of a microheating circuit were demonstrated by an individual quantum emitter. Since the emitter is around a nanometer in size, the work implies that a few-nanometer-sized thermal probe can be realized with

further improvements in the material engineering aspect. Another exciting example is nanofluidic sensing, reported by Radenovic and co-workers (**Figure 2.7b**). In their work, surface defects in hBN were submerged inside solvents with various polarities, such as ethanol, acetonitrile, dimethylsulfoxide, pentane, etc. Owing to the dipole-dipole interaction between the defects and the solvent molecules, the defects became optically activated and emitted photons. Solvents with stronger dielectric induced stronger red-shift of the emission from the quantum emitters due to the enhanced dipolar interactions. Levering such a mechanism, hBN quantum emitters were used to image confined solvents down to the nanoscale and probe the changes in the liquid dielectric constants in nanoscale-confine circumstances. The work demonstrated the potential use of hBN quantum emitters for studying the liquid-solid interface at the nanoscale. Quantum emitters in hexagonal boron nitride were also utilized for magnetic and temperature sensing (**Figure 2.7c**). In particular, Healey et al. fabricated thin hBN flakes hosting the negatively charged boron vacancy defects by ion implantation. The defects are optically active and can be initiated, manipulated, and read out using the ODMR technique. By leveraging the even distribution of these near-surface quantum sensors, the team showcased the multimodalities of the technique by simultaneously mapping thermal and magnetic field distributions in a 2D

magnet $CrTe_2$.[165] They also demonstrated visualizing the electron currents and Joule heating in a working graphene-based device. Measuring other physical parameters, such as pressure and strain, was also realized using the V_B^- defects, from other research groups.[166-167]

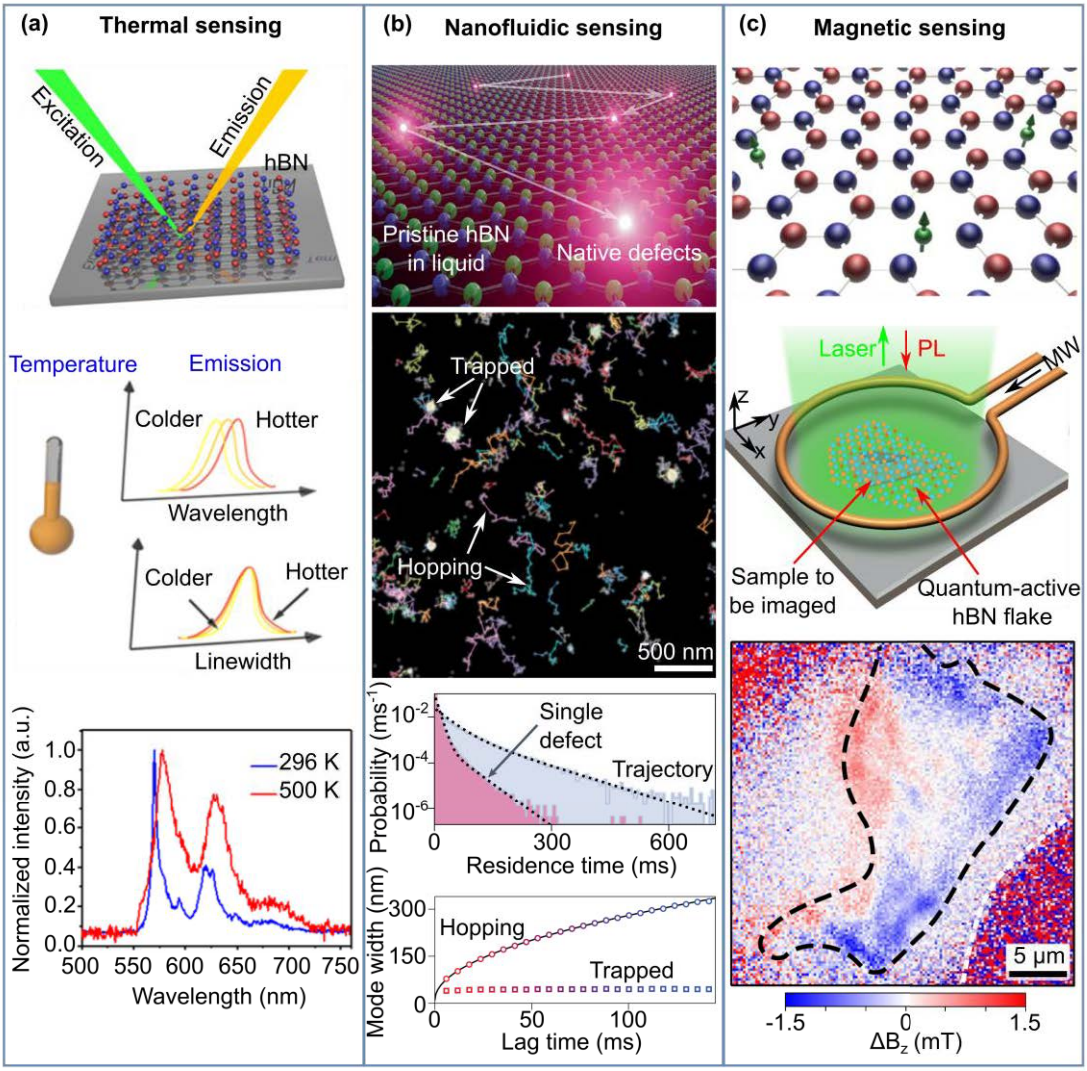

Figure 2.7: Applications of hBN quantum emitters in quantum sensing. (a) Optical thermometry with quantum emitters in hBN

nanoflakes **(b)** Nanofluidic sensing with quantum emission from pristine hBN **(c)** Quantum microscopy with spin defects in hBN. Figure a adapted with permission.[164] Copyright 2020, American Chemical Society. Figure b adapted under terms of the CC-BY 4.0 license.[168] Copyright 2023, The Authors, published by Springer Nature. Figure c adapted with permission.[62] Copyright 2020, Springer Nature.[165] Copyright 2023, Springer Nature.

2.9. Applications in quantum cryptography

Besides quantum sensing, quantum cryptography—quantum key distribution—is another area where hBN quantum emitters are expected to shine. Quantum key distribution has gained tremendous traction recently, owing to its ultrasecure encryption procedure governed by the no-cloning theorem in quantum mechanics. The quantum emitters are ultrabright, room-temperature operational, feature high single-photon purity, and possess linearly polarized emission, the criteria demanded in QKD. Based on the BB84 protocol, Al-Juboori et al. demonstrated quantum key distribution in free-space using quantum emission (ZPL at 645 nm) from an hBN emitter.[169] In their experiment protocol (**Figure 2.8a**), single photons with randomly selected polarizations from the four

possible states, horizontal (H), vertical (V), right-handed (R) and left-handed (L) circular, were synchronized with the exciting pulsed laser and prepared by the first electro-optic modulator (EOM) at Alice, the sender. These polarized photons were sent to Bob, the receiver, and measured by a pair of SPAPDs using one of the two bases, H/V or R/L, thanks to the second EOM and the time-gated detection based on the pulsed laser. Once finished, Alice and Bob exchanged the bases used for each photon via a public channel, but they did not share the measurement results. Together, they discarded photons measured by the wrong bases and kept the correct ones. With additional error correction algorithms and privacy amplification, the string of the correct photons formed the secret key. A secret key of ~70000 bits and a security level of 10^{-10} were reported. Another quantum key distribution protocol—the B92 with hBN quantum emitters in visible range also were reported by Samaner and colleagues.[170] Quantum key distribution was also demonstrated in a water environment by the same team using a blue emitter whose ZPL is at ~ 436 nm (**Figure 2.8b**).[171] It must be noted that the team only simulated the underwater transmission conditions by using water tubes between the optical components. Such fluorescent emission is desirable since it closely matches the dip in the water absorption spectrum (~ 417 nm).[172] Although the underwater performance was inferior to that in the

air, the study laid a foundation for further developments in water-based quantum key distribution. Unlike the underwater setting, QKD during daylight conditions requires a different transmission wavelength. Vogl and co-workers identified the Hα Fraunhofer line at 656 nm as the optimal wavelength for QKD protocols in such conditions.[173]

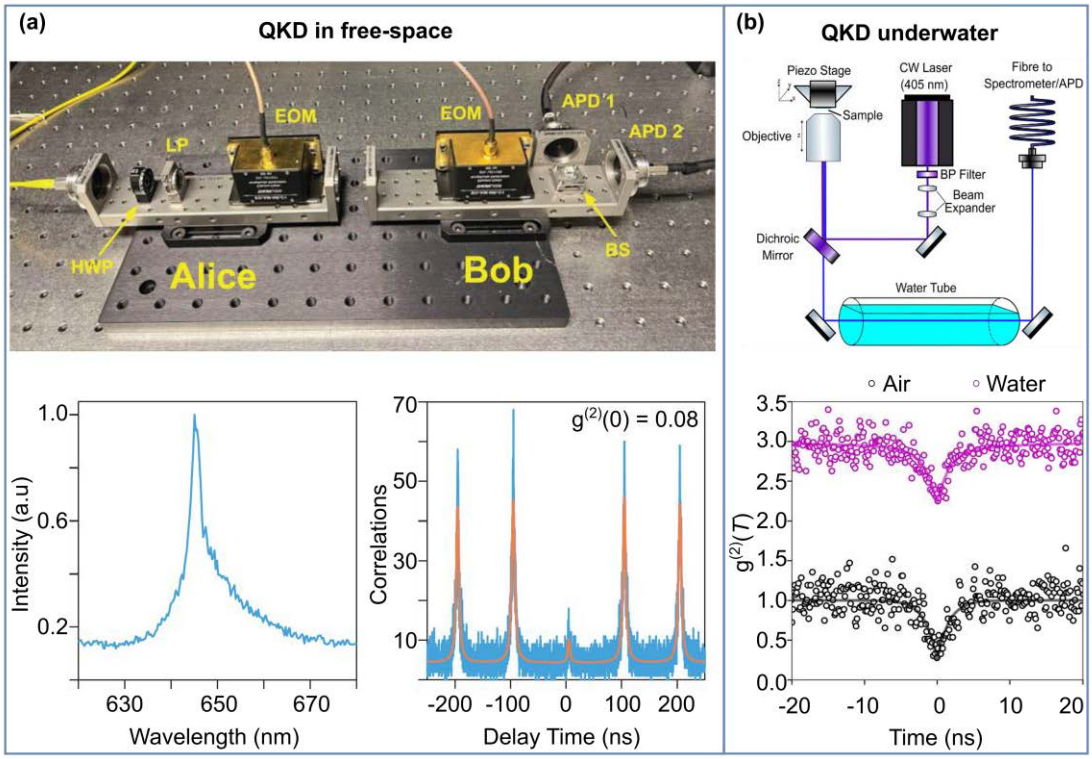

Figure 2.8: Application of hBN quantum emitters in quantum key distribution. (a) The first proof of finite-key BB84 QKD system realized with hBN quantum emitters in free-space (optical components of the transmitter (Alice) and the receiver (Bob) setup including EOM: electro-optic modulator, LP: linear polariser, APD: avalanche photodiode, PBS:

polarizing beam splitter, HWP: half-wave plate **(b)** Optical communications with hBN quantum light sources underwater. Figure a adapted with permission.[169] Copyright 2023, Wiley-VCH GmbH. Figure b adapted under terms of the CC-BY 4.0 license.[171] Copyright 2024, The Authors, published by IOP Publishing Ltd.

2.10. Applications in quantum networks and quantum memories

Another critical area where hBN quantum emitters can be deployed is quantum communication. A prerequisite for such applications is the ability to produce indistinguishable photons—photons that can interfere with each other. For a light source to generate indistinguishable photons, it needs to (i) have high single-photon purity, (ii) produce photons with the same wavelength, polarization, and spatial mode, and (iii) create photons whose spectra are Fourier-transformed-limited—their linewidths defined only by the excited state lifetime.[13] Fournier and co-workers established the first experimental demonstration of the two-photon quantum interference experiment, the Hong-Ou-Mandel, using a blue emitter in hBN.[143] In their experiment (**Figure 2.9a**), the emitter was excited non-resonantly with an 80 MHz pulsed laser, and the emission

from the ZPL was exclusively collected using a combination of high-resolution grating and single-mode-fiber coupling. By introducing a 12.5-ns delay time, the two photons interfered with one another on a fiber-based beam-splitter, resulting in a HOM dip of 0.32 for the parallel polarization case, corresponding to an indistinguishability of 0.56. The deviation from a perfect HOM dip (zero) was due to the dephasing caused by the non-resonant excitation. It was calculated that the indistinguishability could approach 90% if the emitter were coupled to a cavity (Purcell factor of ~15) and excited resonantly. The work shed light on using blue emitter in hBN for quantum applications that require HOM protocol. In another attempt, Vogl and co-workers proposed a quantum photonic circuit to test an extended theory in space using hBN quantum emitters as a single-photon source as shown in **Figure 2.9b**, top panel.[174] Specifically, the team conceptualized a circuit that comprised a 1-to-3 beam divider, three optical switches that were active Mach-Zehnder interferometers, and a 3-to-1 beam combiner, resulting in a 3-path interference. The three-arm interferometer could be used to test Born's rule—the correlation between the probability density and the wavefunction—in low Earth orbit (LEO). Another potential application for hBN quantum emitters is quantum memory. To be useful for quantum memory, the emitter-cavity system has to possess the following: a Λ electronic structure, a compatible ZPL, a

practical Q factor of a cavity, and a wide bandwidth. Cholsuk et al. identified 257 defect configurations with triplet-states, which possess Λ energy levels, using DFT (**Figure 2.9b**, bottom panel).[175] Of these, 25 complexes closely matched the ZPLs of other quantum systems. In addition, most defect centers required a cavity Q-factor from 10^5 to 10^7 and received wide bandwidths to achieve 95% writing efficiency. The work showcased the potential of hBN quantum emitters for efficient quantum memory systems.

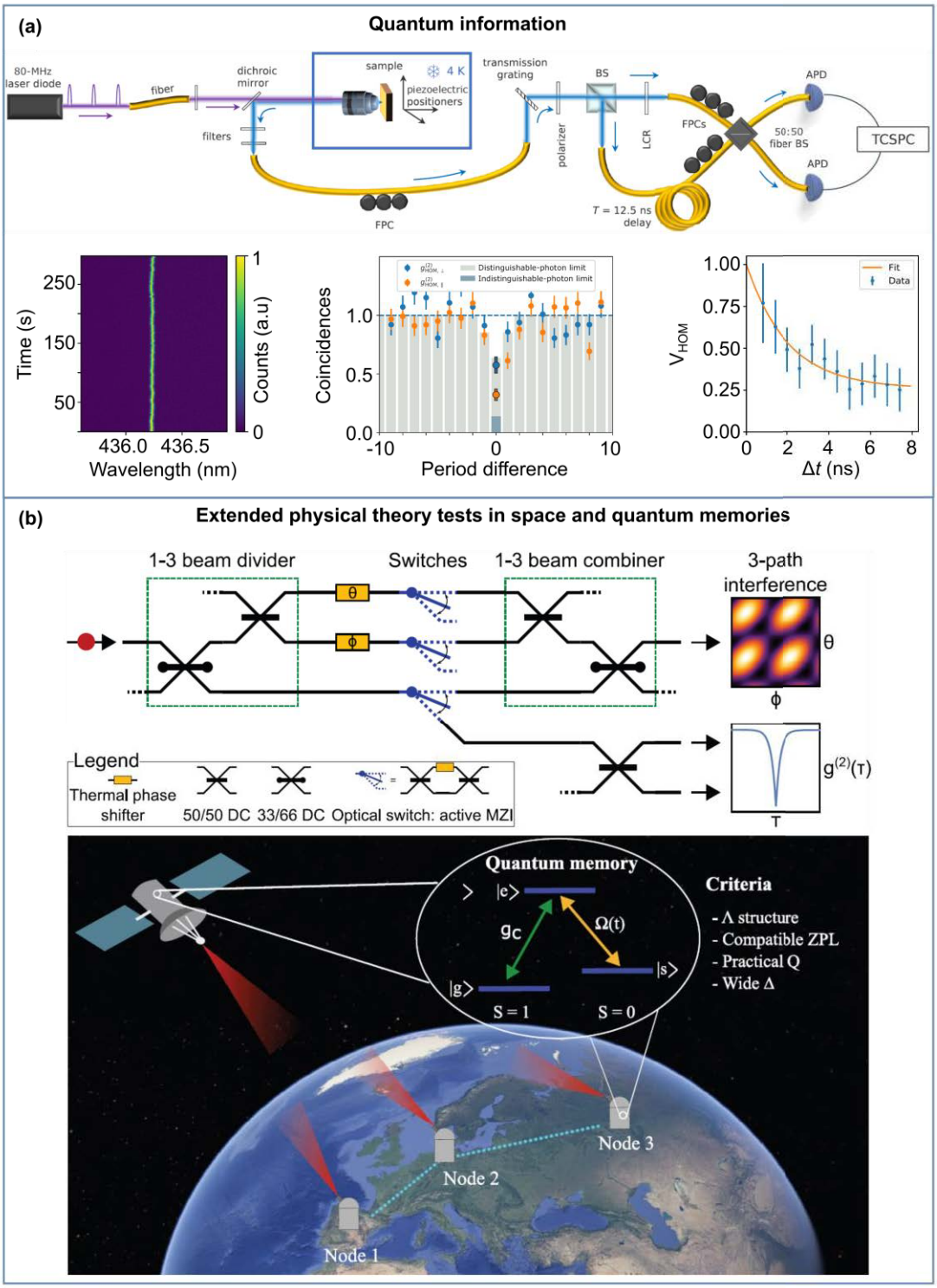

Figure 2.9: Prospective approach for hBN quantum emitters. (a) Quantum information with indistinguishability two-photon interference from quantum emitter generated from hBN via Hong-Ou-Mandel

interferometer **(b)** Extended physical theory tests in space and quantum memories with hBN quantum emitters. Figure a adapted with permission.[143] Copyright 2023, American Physical Society. Figure b adapted with permission.[174] Copyright 2024, Wiley-VCH GmbH.[175] Copyright 2024, Wiley-VCH GmbH.

2.11. Robustness of the quantum emitters

To enable the aforementioned applications, hBN quantum emitters must be robust towards environmental factors such as chemicals, ionized radiation, temperature, and mechanical stress. Quantum emitters were tested against gaseous substances such as argon, hydrogen, oxygen, and ammonia at 500°C for 1 hour (**Figure 2.10a**).[63] While some emitters bleached out, most survived the test with preserved photoluminescence spectra and quantum emission characteristics. Such a feat implied the excellent chemical resistance of the quantum emitters thanks to the high inertness of the hBN lattice structure. Next, the quantum emitters were subject to γ-ray irradiation to examine if they were space-qualified. Vogl and co-workers employed the isotope $^{22}_{11}Na$, which emitted 1.28 MeV photons and decayed to $^{22}_{11}Ne$, to study the robustness of the quantum emitters.[176] Interestingly, even with such highly energetic photons, hBN

quantum emitters remained mostly intact, exhibiting the same PL lineshape and single-photon purity as shown in **Figure 2.10b**. To validate the high-temperature operation of quantum emitters in hBN, Kianinia et al. characterized the photophysics of the emitters in a home-built high-temperature PL chamber. They observed the emission characteristics of the quantum emitters from room temperature to 800 K, and negligible changes were observed for the photoluminescence, antibunching dip, and lifetimes (**Figure 2.10c**). The quantum emitters were also examined against tensile stress in an experimental attempt by Mendelson and co-workers.[177] The team observed that the emission was red-shifted significantly when the tensile strain was applied to the hBN film, which was attributed to perturbation onto the transition dipole moment. As shown in **Figure 2.10d**, reversible strain values as large as 5% were recorded during the experiment, indicating the high resistance of hBN towards strain-induced damage. Overall, quantum emitters have been shown to exhibit a high degree of robustness toward a variety of environmental elements and external fields, making them a promising candidate for ground-based and extraterrestrial quantum applications.

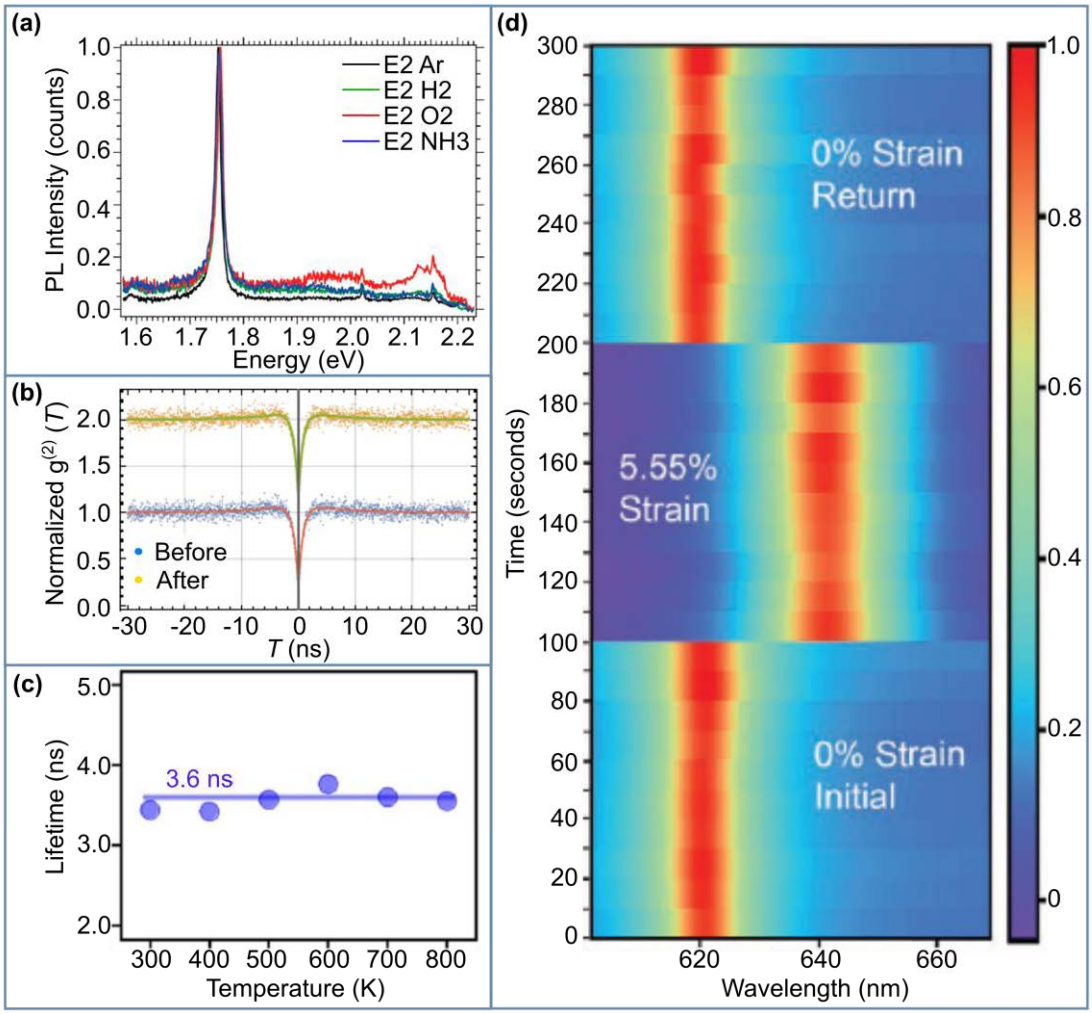

Figure 2.10: Robustness of hBN quantum emitters in harsh conditions. (a) Robust single photon emission at room temperature from hBN quantum emitters after the 30-minute sequential annealing in argon, hydrogen, oxygen and ammonia environments **(b)** Negligible differences in second-order correlation function dipping at zero time delay of hBN quantum emitter before (0.185) and after (0.188) gamma ray irradiation tolerance testing for space applications **(c)** Optically stable single photon source in hBN operating at high-temperature (800K) **(d)** Reversible tuning of the emission and related photophysical properties of hBN

quantum emitters upon applying tensile strain. Figure a adapted with permission.[63] Copyright 2016, American Chemical Society. Figure b adapted under terms of the CC-BY 4.0 license.[176] Copyright 2019, The Authors, published by Springer Nature. Figure c adapted with permission.[178] Copyright 2017, American Chemical Society. Figure d adapted with permission.[177] Copyright 2020, Wiley-VCH Verlag GmbH & Co. KgaA, Weinheim.

2.12. Conclusion and Outlook

Eight years after its inception, quantum emitters in hBN have witnessed tremendous growth in interest from the research community worldwide. Such growing interest stems from the accessibility of the quantum material, which is inexpensive and readily available. Unlike other existing quantum sources, hBN quantum emitters feature a balanced suite of room-temperature operation, high brightness, good single-photon purity, high chemical robustness, spin-accessible (some families), and low fabrication costs. Being atomically thin and flat, hBN can be easily integrated into various photonic structures, monolithically or non-monolithically, from photonic crystal cavities and plasmonic antennas to hybrid architectures and integrated quantum photonic chips. Moreover, owing to their vicinity

to the surface, hBN quantum emitters have garnered significant attention as frontrunners for the quantum sensing of various physical quantities and chemical species. Quantum key distribution, quantum communication, and physical theory testing in extraterrestrial contexts are other exciting applications for quantum emitters in hBN. Space qualification and other relevant testing and planning for the self-contained integrated quantum source have been established and are ready for the initial experiments in space. With the help of high-throughput DFT approaches, over two hundred defect complexes were proposed, many possessing the triplet-singlet intercrossing system critical for quantum sensing and quantum memory.

On the one hand, research into expanding the possible quantum applications for hBN emitters will be proliferating. Implementations such as quantum repeaters or teleportation are expected to be realized soon, considering the readiness of hBN emitters for such settings. On the other hand, the hunt for new defect families with superior quantum optical properties will continue with the help of efficient computational simulations. More unification between simulations and experiments, especially those with extreme resolution, such as TEM or STM, will help identify the chemical structures of these defect complexes. Furthermore, an electrically driven quantum source in hBN is another exciting research

area—that is reachable thanks to the recent developments in two-dimensional heterostructure fabrication. Electrical excitation is essential for scalability since it can be implemented in complementary metal-oxide semiconductor technology. Recent advancements in the fabrication of high-quality two-dimensional heterostructures have enabled the first realization of electrically-driven hBN single-photon sources—opening the door to integrating hBN quantum sources into existing silicon-chip technologies.[179-180] There are, however, several critical challenges remaining. First, although the ZPL distribution among emitters has been significantly improved with the discovery of the blue emitter family, such a parameter is still larger than competing platforms such as the NV or group IV centers in diamonds. Strain-engineering during or after growth may alleviate this heterogeneous linewidth broadening issue as it did in other platforms.[181] Second, spectral diffusion has been a long-standing problem for hBN emitters.[56] Such a phenomenon gives rise to low quantum interference visibility,[143] affecting many applications underpinned by the performance of this metric. Current directions include the preparation of ultrapure hBN surfaces/interfaces to minimize surface states, feedback-driven active tuning, or resonant excitation.[131] Third, due to its intrinsically large bandgap, making good electrical contact with hBN and introducing charges into the defect levels is incredibly

challenging. Such a roadblock might be tackled by growing p-type and n-type hBN materials. While the former has been achieved, the latter has remained out of reach. Recent computational studies, however, shed light on the potential use of sacrificial impurity coupling to realize n-type hBN.[182] While it is a long journey ahead for the quantum source, it holds great promise to be a prime candidate for many quantum technologies of tomorrow.

Acknowledgments

T. T. T acknowledges the financial support from the Australian Research Council (DE220100487, DP240103127). T. T. T. and T. D. thank the Queensland Department of Environment, Science and Innovation for their financial support (Q2032010).

Conflict of Interest

The author declares no conflict of interest.

ToC

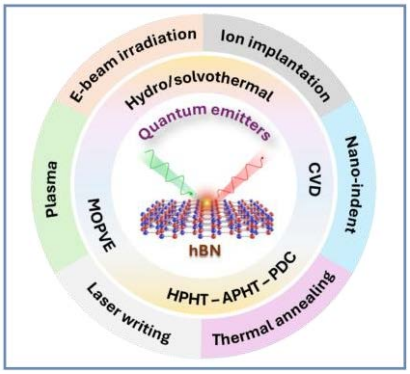

Quantum emitters in hexagonal boron nitride have emerged as a promising candidate for quantum information science. This review examines the fundamentals of these quantum emitters, including their level structures, defect engineering, and their possible chemical structures. It also explores the integration of these emitters into various photonic architectures and examines their current applications in quantum technologies.

First and corresponding author biographies and photographs

Thi Ngoc Anh Mai received her Bachelor degree in Physics and Education from the Hanoi National University of Education, Vietnam (2017) and Master of Science degree in Physics and Applications from the ENS Paris–Saclay, University of Paris–Saclay, France (2018). She worked as an university lecturer at the Faculty of Engineering Physics and Nanotechnology, VNU University of Engineering and Technology (VNU-UET), Hanoi, Vietnam (2019-2022). She is currently a Ph.D. student at the University of Technology Sydney, Australia (2022–Current). Her research interests focus on novel quantum emitters in wide-bandgap materials and their applications for quantum technologies.

Toan Trong Tran is a Senior Lecturer at the University of Technology Sydney, Australia. He received his Bachelor of Science in Materials Science from Vietnam National University, Vietnam (2008) and Master of Engineering in Chemical Engineering from the National University of Singapore, Singapore (2011). He previously received his PhD (2018) from UTS and worked there as a Chancellor Research Fellow and a DECRA Fellow. Along with his colleagues at UTS, he pioneered research in hBN quantum emitters and has remained active since. His research interests include quantum optics, nanophotonics, solid–state physics, thermometry, and nanofabrication.

Preamble for chapter 3 and chapter 4

Quantum emitters in hexagonal boron nitride have emerged as the most promising candidate for quantum communication and quantum physic tests in extraterrestrial contexts. In this thesis I delve into one fundamental space qualification test of hexagonal boron nitride quantum emitters in the cryogenic thermal shock and under several thermal shock cycles by using very low temperatures of liquid nitrogen. This pioneering study of solid-state quantum emitters under space-like conditions provides insights into their robustness, stability, and potential for integration into space-based quantum technologies. The results pave the way for applications in space in the future and advance our understanding of quantum materials in extreme environments.

Chapter 3

Research Methodology

Preamble

In this chapter, I detail all the experiment and simulation methods I used in this thesis. It includes four main parts: the first section is the sample fabrication method of hexagonal boron nitride quantum emitters, the second section is the cryogenic cooling experiments, the third section is the optical and structural characterization of hBN quantum emitters before and after the experiments, and finally the last section is dedicated to the numerical calculations of the electronic structure of quantum emitters upon the exposure to the cryogenic experiment.

A significant portion of this chapter is copied and compiled by adding more figures and detailed information from the **Methods** section of the peer-reviewed article "*Cryogenic Thermal Shock Effects on Optical Properties of Quantum Emitters in Hexagonal Boron Nitride"* **Thi Ngoc Anh Mai**, Sajid Ali, Md Shakhawath Hossain, Chaohao Chen, Lei Ding, Yongliang Chen, Alexander S. Solntsev, Hongwei Mou, Xiaoxue Xu, Nikhil Medhakar, and Toan Trong Tran, ACS Applied Materials & Interfaces 2024, 16, 19340.[7]

3.1. Sample fabrication

The hexagonal boron nitride flakes used in this work were prepared by solvent exfoliation method as illustrated in **Figure 3.1**. The average thickness of the flakes is ~320 ± 227 nm based on our atomic force microscopy measurements. 10 mg hBN powder of PlasmaChem was added into 20 mL isopropanol–**Figure 3.1a**, followed by a probe ultrasonication for 10 minutes for exfoliation–**Figure 3.1b**, and diluted 100 times in IPA. The hBN diluted solution was dropped onto a 1 cm x 1 cm silicon substrate. Then, it was heated at 80°C on a hotplate for 10 minutes to dry as depicted in **Figure 3.1c**. Finally, the substrate was annealed at 850°C in a tube furnace (Lindberg Blue Mini-mite)–**Figure 3.1d** with a 50 sccm argon flow rate for 30 minutes to activate and stabilize the hBN flakes. The sample was stored in a vacuum bag to avoid other contamination for further experiments.

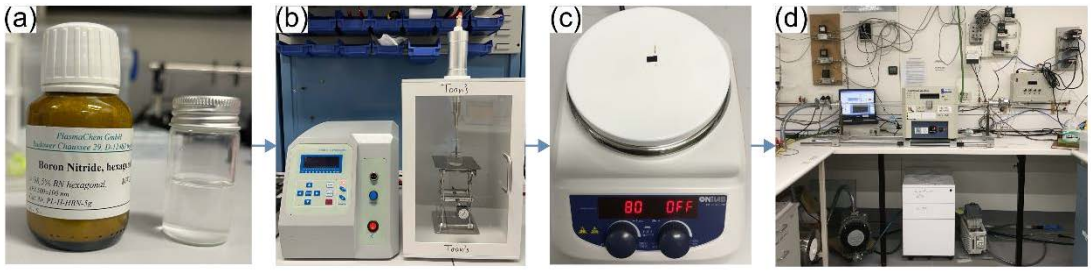

Figure 3.1: Fabrication of solvent-exfoliated hexagonal boron nitride nanoflakes. (a) Hexagonal Boron Nitride powder PlasmaChem and 20 mL isopropanol to dissolve 10 mg hBN powder (b) probe ultrasonication machine for exfoliate hBN solution (c) hotplate at 80°C to dry silicon substrate after dropcast hBN exfoliated solution (d) tube furnace setup to anneal hBN sample.

3.2. Thermal shock experiments

3.2.1. Cryogenic thermal shock experiment

The 1 cm^2 silicon substrate with hBN flakes (was kept in tweezer in **Figure 3.2a**), as in the above fabrication technique, was dipped directly in a 30L liquid nitrogen dewar using a bucket/canister, as in **Figure 3.2b-c**. It causes the temperature to drop down suddenly to - 190°C. After waiting for 3 minutes–**Figure 3.2d**, the sample was taken out

immediately–**Figure 3.2e** to room temperature (25°C) and let dry naturally for 10 minutes.

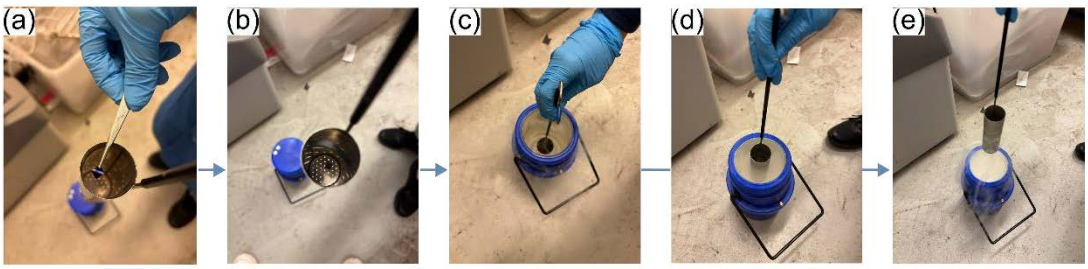

Figure 3.2: Cryogenic thermal shock experiment process. Bucket with hBN sample before (a-b), during (c-d) and after (e) dipping into liquid nitrogen dewar.

3.2.2. Slow cooling experiment

Another duplicated 1 cm^2 silicon substrate with hBN flakes–**Figure 3.3a** was placed in a thermal vacuum heating/cooling stage (Microoptik-MHCS-622)–**Figure 3.3b**. The thermal vacuum cooling stage was assembled to a high-performance temperature controller (Microoptik-MDTC600) with a temperature accuracy of 0.1°C, a liquid nitrogen pump, and a liquid nitrogen dewar as in **Figure 3.3c**. The sample was glued on the stage with a silver conductive grease to improve the heat transfer process. The sample in the stage was cooled down from room temperature

to -190°C gradually for 30 minutes with a cooling rate of 6°C/minute, stayed at -190°C for 10 minutes, and then heated up to room temperature slowly for 6 hours as in **Figure 3.4**.

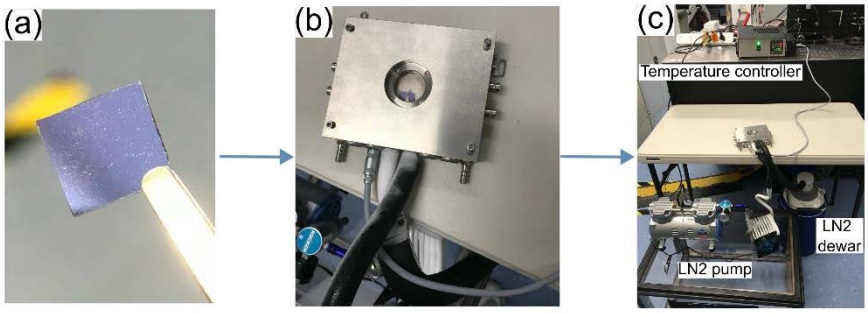

Figure 3.3: Slow cooling experiment setup. (a) Hexagonal Boron Nitride sample (b) Thermal vacuum cooling stage with hBN sample inside (c) Thermal vacuum cooling stage connects with temperature controller, liquid nitrogen pump and dewar setup. LN2–Liquid nitrogen.

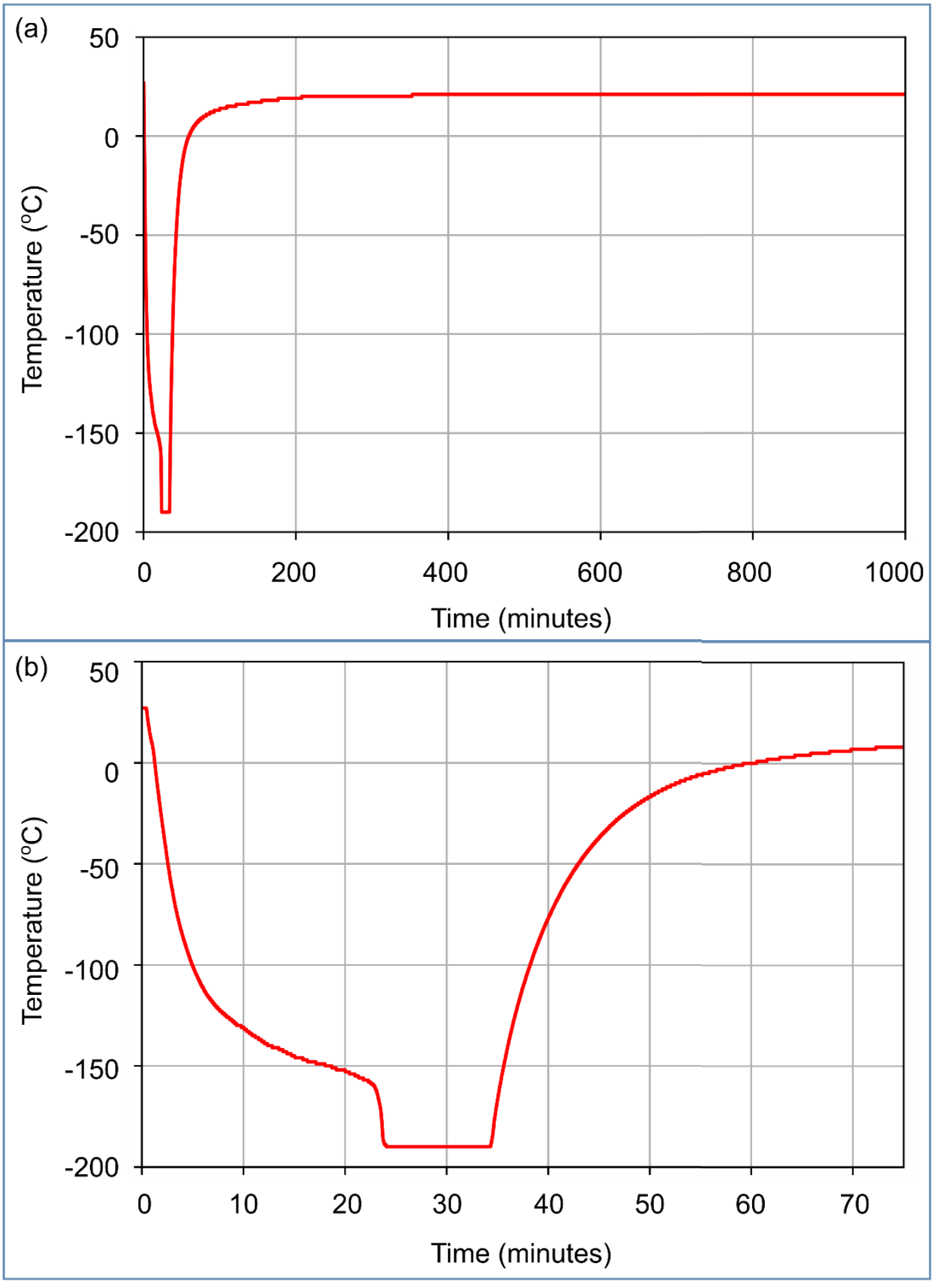

Figure 3.4: Time-temperature profile of slow cooling experiment. (a) The plot of time vs temperature of prepared hBN flakes on silicon substrate from starting at room temperature, slowly cool down to liquid

nitrogen temperature (-196ºC) in 25 minutes, stay there for 10 minutes and then slowly come back to room temperature. (b) Zoom-in temperature profile.

Note that: There is no time-temperature profile of shock cooling experiment, since described in **Section 3.2.1** the silicon substrate (1 cm^2) was dropped directly into the liquid nitrogen dewar (30L, -196ºC), the silicon substrate is very small compared to the volume of the liquid nitrogen in the dewar, resulting in the immediate drop in temperature down to the liquid-nitrogen temperature, so the plot of time vs temperature should be very close to a step function as illustrated in **Figure 4.1a**.

3.3. Characterization methods

3.3.1. Optical characterization

Photoluminescence and Raman spectra of all single-photon emitters in hexagonal boron nitride samples before and after cryogenic thermal shock and slow cooling process were collected by an Andor spectrometer (SR-500i-A) equipped with a CCD camera in a lab-made confocal microscope set up as illustrated in **Figure 3.5**. The sample was excited with a 532 nm

continuous wave (CW) laser (Cobolt Samba 532 nm) with an excitation power of 300 μW, and the power meter was placed right above the objective lens. For safety reasons, the laser was connected with an interlock at the lab door to protect people entering when the laser is working. The laser was coupled into a single-mode fiber to easily manipulate and propagate the light with less loss. A bandpass filter (Thorlab, BP 532 nm) was placed at the fiber port to allow only that wavelength to go through. Variable neutral density (ND) filters were placed on the excitation path to adjust the excitation power of the laser.

A scanning mirror (Newport, SFM-CD300B) was used to navigate the laser spot position in the sample plane to generate the confocal map. A 4F system and an objective that has a numerical aperture (NA) of 0.7 (Thorlabs, MY100X-806, 100×) were used to focus the laser spot on the surface of the sample, which was put on a three-dimensional micro-positioner stage. The collection and excitation arms were separated by a cube beam splitter (30R/70T; Thorlabs). A long pass filter (Semrock, LP 561) was placed in the collection path to completely suppress the 532 nm excitation. Mirrors were used to shape the direction of the light. The emission signal from the collection arm was divided into two pathways by a plate beam splitter (50R/50T; Thorlabs), coupled into two graded-index multimode fibers (Thorlabs, GIF625). One path was connected to a

single-photon avalanche photodiode (Excelitas Technologies, SPCM-AQRH 14-FC) to count all the incoming photons, and the other was connected to the spectrometer to visualize the spectra from each single photon emitter.

LabVIEW software was used to control all the hardware, analyze the photon rates, and generate the confocal map based on the signal collected in APD. Andor Solis software was used to analyze the spectra collected in the spectrometer. For each single-photon emitter, zero phonon line and phonon sideband were fitted with the Lorentzian function to extract both the peak position and the full-width half maximum of the peak. An example of a fitted spectrum is shown in **Figure 3.5** (top right conner) and in **Supporting Information Figure S2**. The second-order autocorrelation measurements were conducted with the Hanbury Brown-Twiss setup equipped with two APDs and a time-correlated single photon counting module (Time Tagger 20). A typical $g^{(2)}(\tau)$ measurement was placed in **Figure 3.5** (bottom right conner). All data was processed by using Python programming.

All photoluminescence spectra, Raman spectra, second-order autocorrelation, and photostability (such as **Figure 4.1c, d**; **Figure 4.4a, b, c**) of hBN quantum emitters in this thesis were recorded by this setup

on an optical table (TMC LaserTable-Base) in Photonics Labs, UTS Tech Lab.

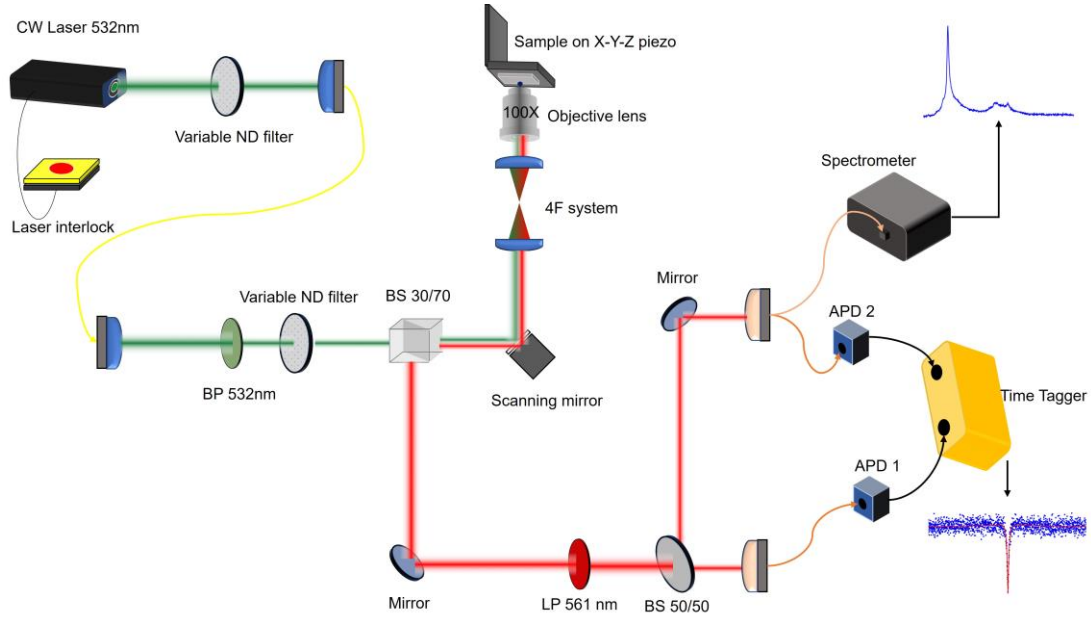

Figure 3.5: Schematic of confocal microscope and Hanbury Brown and Twiss setup for characterizing optical properties of hBN quantum emitters. In the top left conner, the laser source connects with interlock goes through variable neutral density filter and couples into a single-mode fiber optics. At the center, the scanning mirror navigates the excitation laser into sample and a beam splitter splits the excitation and collection signal from each other. In the right, the collection part equipped with two photodetectors and spectrometer to measure the photoluminescence spectra and qualify the quantum emission of the quantum emitter. CW-continuous wave, ND-neutral density, BP-

bandpass filter, BS-beam splitter, LP-long pass filter, APD-avalanche photodiode. Single-mode optical fiber was illustrated by yellow curve while the multi-mode optical fiber was used orange curve.

3.3.2. Structural characterizations

i) Atomic force microscopy

The topography and morphology of hBN samples before and after cryogenic thermal shock were obtained by an atomic force microscope (Park System XE70) that is capable of 12 μm in z-direction and 100 μm x 100 μm in xy-direction. All AFM images were taken under ambient conditions. A standard silicon probe (Nanoworld, NCH, spring constant of 42 N/m, and a natural frequency of 320 kHz) was used. The line profiles of hBN flakes were extracted from AFM images which were flattened and corrected using XEI software (Park Systems) as in **Figure 4.3** and **Supporting Information Figure S4**.

ii) Transmission electron microscopy

The inside crystal structures of hBN flakes before and after the cryogenic thermal shock experiment were done by using a transmission electron

microscope (JEOL 2200FS). The TEM images, thickness mapping images, and selected area electron diffraction (SAED) patterns of selected hBN flakes on a copper grid with an accelerating voltage of 200 kV. The JEOL 2200FS has a lattice resolution of 0.1 nm. The images were taken right before and after the cryogenic thermal shock experiment, as shown in **Figure 4.5 a-d** and **Figure 4.3 j-l**.

iii) X-ray diffraction

To examine the crystal phase and lattice structures of the hBN flakes before and after cryogenic thermal shock exposure, we used the X-ray diffraction (XRD) technique. The XRD patterns were obtained using a Bruker D8 Discover A25 X-ray diffractometer with Cu K1 radiation (40 kV, 40 mA, λ=0.15406 nm). The XRD spectra were taken in three cases: pristine (before shock), after slow cooling, and after shock cooling processes. The scan step was 0.02 deg/min, and the scanning time was 0.4 s/step. The XRD results are presented in **Figure 4.5e**.

3.4. Theoretical calculations – density functional theory

In this thesis, to investigate the effect of cryogenic shock on the optical properties of hBN quantum emitters, we used the most successful/ powerful computational methods named the density functional theory calculations. The ground states, excited states, and normal modes were conducted using the VASP electronic structure code with a plane-wave wave cut-off of 800 and a gamma point[5] sampling of the Brillouin zone. For accurate calculation of electron spin density close to the nuclei, the projector augmented wave method (PAW) was applied together with a plane wave basis set. The defects were represented in a 9 x 9 x 1 supercell (monolayer) and allowed to fully relax until the maximum force was below 0.01eV/Å. A vacuum of 15 Å was used along the vertical direction. The HSE06 exchange-correlation functional was used for all calculations.

[5] A complete band structure calculated to justify a gamma point calculation. The complete band structure shows flat defect levels, then it is sufficient to only perform a gamma point calculation. This note is based on the recommendation of Examiner 2 during the Examination process of this thesis, and has been added only in this thesis (not in the published paper).

Chapter 4

Results and Discussion

Preamble

In this chapter I present the investigation of the impact of cryogenic temperature shock on spectral, photostability, quantum emission and structure of hexagonal boron nitride flakes.

A significant portion of this chapter is copied verbatim from the peer-reviewed article "*Cryogenic Thermal Shock Effects on Optical Properties of Quantum Emitters in Hexagonal Boron Nitride*" **Thi Ngoc Anh Mai,** Sajid Ali, Md Shakhawath Hossain, Chaohao Chen, Lei Ding, Yongliang Chen, Alexander S. Solntsev, Hongwei Mou, Xiaoxue Xu, Nikhil Medhakar, and Toan Trong Tran, *ACS Appl. Mater. Interfaces* **2024**, 16, 19340.[7]

All graphics have been reproduced to match the style of this thesis.

Cryogenic Thermal Shock Effects on Optical Properties of Quantum Emitters in Hexagonal Boron Nitride

Thi Ngoc Anh Mai,[†] Sajid Ali,[‡] Md Shakhawath Hossain,[†] Chaohao Chen,[§,∥] Lei Ding, [#] Yongliang Chen,[††] Alexander S. Solntsev,[‡‡] Hongwei Mou,[#] Xiaoxue Xu,[#] Nikhil Medhekar[‡] and Toan Trong Tran[†,*]

[†]School of Electrical and Data Engineering, University of Technology Sydney, Ultimo, NSW, 2007, Australia.

[‡]School of Physics and Astronomy, Monash University, Victoria 3800, Australia.

[§]Department of Electronic Materials Engineering, Research School of Physics, The Australian National University, Canberra, Australian Capital Territory 2601, Australia.

[∥]ARC Centre of Excellence for Transformative Meta-Optical Systems (TMOS), Research School of Physics, The Australian National University, Canberra, Australian Capital Territory 2601, Australia.

[#]School of Biomedical Engineering, University of Technology Sydney, Ultimo, NSW, 2007, Australia.

[††]Department of Physics, The University of Hong Kong, Pokfulam, Hong Kong 999077, China.

[‡‡]School of Mathematical and Physical Sciences, University of Technology Sydney, Ultimo, NSW, 2007, Australia.

*Corresponding author: trongtoan.tran@uts.edu.au

Abstract

Solid-state quantum emitters are vital building blocks for quantum information science and quantum technology. Among various types of solid-state emitters discovered to date, color centers in hexagonal boron nitride have garnered tremendous traction in recent years thanks to their environmental robustness, high brightness, and room-temperature operation. Most recently, these quantum emitters have been employed for satellite-based quantum key distribution. One of the most important requirements to qualify these emitters for space-based applications is their optical stability against cryogenic thermal shock. Such understanding has, however, remained elusive to date. Here, we report on the effects caused by such thermal shock which induces random, irreversible changes in the

spectral characteristics of the quantum emitters. By employing a combination of structural characterizations and density functional calculations, we attribute the observed changes to lattice strains caused by the cryogenic temperature shock. Our study shed light on the stability of the quantum emitters under extreme conditions—similar to those countered in outer space.

Keywords: shock-cooling, cryogenic thermal shock, quantum emitters, hexagonal boron nitride, spectral shift.

4.1. Introduction

Quantum information science has held the promise to revolutionize the way we communicate, resembling the way the Internet did to our society in the 20th century.[15, 20, 183] At the heart of quantum information science lies one of the most important pieces of quantum hardware—the quantum emitters. Such emitters can send information in the form of individual photons, also known as "the flying qubits".[184] To date, many solid-state quantum emitters have been discovered, including epitaxial quantum dots, colloidal quantum dots, single molecules, and point defects in wide bandgap materials.[8, 16, 20, 185] Among these candidates, color centers in

hexagonal boron nitride have received intense research focus thanks to their high repetition rate, robust photostability, ease of fabrication and ability to be incorporated into other van der Waals heterostructures.[14, 37, 46, 63, 127, 186-187] The impressive traits of these quantum emitters can be attributed to the strong in-plane B-N bond that gives hBN its optical transparency, physical robustness, and chemical inertness. Most notably, however, is the robustness of the quantum emitters against extreme temperatures, up to 500ºC in a vacuum as well as in harsh chemical conditions. Along with their high single photon purity and short lifetime, quantum emitters in hBN have recently been considered for satellite-based quantum communications.[174, 176] In a recent study, the quantum emitters have been subject to various types of radiation conditions including, γ-ray, photons and electrons, to test their suitability for space-based communication applications.[176] Surprisingly, the emitters did not show any degradation in their optical properties, making them very compelling for such applications. Nevertheless, to qualify for space-based applications, the emitters' optical attributes must remain the same under cryogenic thermal shocks, i.e. instantaneous drop from room temperature to cryogenic temperature. This is because such cryogenic thermal shocks closely resemble conditions encountered by the emitters operating in the

Earth's orbits[6]. The impact of the cryogenic thermal shocks on hBN quantum emitters has, however, remained poorly understood to date. In this work, we perform experimental investigation on such a thermal shock effect to better understand its repercussions on the optical properties of these emitters.

4.2. Results and discussion

We started with the sample preparation, following previous procedures published elsewhere.[128] Briefly, commercially available hexagonal boron nitride micropowder was dispersed in isopropanol and sonicated in an ultrasound bath to exfoliate them into thinner flakes (cf. Methods). The flakes were dropcast onto a marked silicon substrate, and the substrate was annealed at 850ºC under 5 mTorr of argon (50 sccm) for half an hour in a tube furnace. Such an annealing procedure has been shown to help improve the stability of the quantum emitters in hBN.[50, 188]

To examine the effect of cryogenic thermal shock on the optical properties of the hBN emitters, we designed two experiments. In the first experiment,

[6] The thermal shock is faster than the typical temperature gradient that expects for a quantum communication satellite which would orbit typically in low Earth orbit. Also, LEO satellites will not experience temperatures down to 77 K. This test in harsher conditions confirmed that hBN quantum emitters are really good and will sure work in space environment. This note is based on the recommendation of Examiner 2 during the Examination process of this thesis, and has been added only in this thesis (not in the published paper).

the hBN sample was directly dropped into liquid nitrogen, causing a sudden shock in temperature experienced by the hBN flakes. As a result, the temperature dropped to liquid nitrogen temperature (77K) instantaneously, as depicted in **Figure 4.1a**. The sample was removed from the liquid nitrogen tank and allowed to heat up to room-temperature for further optical characterization. In the second experiment, the hBN sample was slowly cooled to liquid nitrogen temperature by using a temperature-controlled heating/cooling stage (cf. Methods) over 30 minutes, as shown in **Figure 4.1b**. The sample was allowed to heat up to room-temperature in a similar fashion performed as the first experiment. The second experiment is our controlled experiment as the slow cooling process closely mimics the typical cryogenic photoluminescence procedure typically conducted in optics laboratories. To prepare for both experiments, we first characterized two different groups of emitters, each on a separate marked silicon substrate. Our optical system is a home-built laser scanning confocal microscope that features a 0.7 NA air objective where excitation and emission light was focused through and collected from, respectively. A non-polarizing beam splitter (70T:30R) was used to split the excitation path from the collection path. For the excitation source, we used a 532 nm continuous-wave laser with a power of 300 μW to excite the emitters since the laser energy is well below the electronic band

gap of hexagonal boron nitride, thus eliminating any unwanted excitonic emission from the hBN lattice. Specifically, we collected the emission spectra from 46 quantum emitters for the first experiment as shown in **Supporting Information Figure S1a**. During the experiments, we observed that 6 emitters bleached out after being exposed to the cryogenic thermal shock whereas the rest of the emitters were optically stable under 532 nm excitation at 300 μW power (**Supporting Information Figure S1b**). **Figure 4.1c** shows emission spectra taken from an exemplary emitter before (red) and after (blue) being subject to the cryogenic thermal shock. To determine the changes in the emission spectra, we fit the data with a single Lorentzian peak—an example of which can be found in the **Supporting Information Figure S2**. Surprisingly, a strong red shift of the zero-phonon line of ~5.5 nm occurs, from 622.46 nm to 627.95 nm, after the emitter experiences the thermal shock. Not only does the thermal shock induce the spectral shift, but it also causes an increase of 4.1 nm in the linewidth, also known as the full width at half maximum, from 6.67 nm to 10.81 nm. Such modifications in the spectral characteristics resemble the effect caused by applied strains to the hBN lattice.[46, 177] Detailed discussion will be given later in the text. On the contrary, for the second experiment, we observed no bleaching phenomenon across the 40 quantum emitters whose emission spectra were recorded in **Supporting**

Information Figure S3. **Figure 4.1d** features two representative spectra taken from an emitter before (red) and after (blue) being exposed to the slow cooling process. Unlike the observation in the first experiment, there was no visible shift in ZPL nor change in FWHM recorded, indicating that such a slow cooling process does not affect the optical properties of the emitters per se.

To further understand the effect of cryogenic thermal shock on the emitters' optical properties, we collected statistical data of the ZPL shifts and changes in FWHM for 40 emitters in both the first and second experiment. **Figure 4.1e and 4.1f** show the ZPL shift plotted as a function of emission wavelength for the thermal shock and slow cooling experiment, respectively. For both cases, the ZPL shifts are relatively independent of the emission wavelengths. Such an observation might imply that these emitters share very similar defect configurations with some differences in their neighboring dielectric environments. In the case of cryogenic thermal shock, the ZPL shifts are very significant, with the maximum redshift and blueshift of up to 5.5 nm and 2 nm, respectively. Conversely, for the slow cooling process, the largest redshift and blueshift are only 0.83 nm and 0.79 nm, respectively, several times smaller than that of the former case. A similar trend was observed for plots of FWHM changes versus FWHM as shown in **Figure 4.1g and 4.1h** for thermal

shock and slow cooling, respectively. The magnitude of change in linewidths for the case of thermal shock is 2–3 fold larger than that of the slow cooling case. Notably, in the cryogenic thermal shock, the FWHM increases for emitters whose linewidths are around 7.5 nm or less, while the FWHM decreases for those with linewidths larger than 7.5 nm. A different tendency was observed for the case of slow cooling, however. Emitters whose linewidths are smaller than 5 nm exhibit small changes in the FWHM values (< 1 nm) while those with linewidths larger than 5 nm feature significant changes in FWHM, with values clearly exceeding 1 nm. Such divided trends can be attributed to the different optical characteristics of different groups of hBN emitters.[39, 61, 189] Emitters from different groups possess dissimilar optical properties due to their unique chemical compositions and structural arrangements.[71, 190]

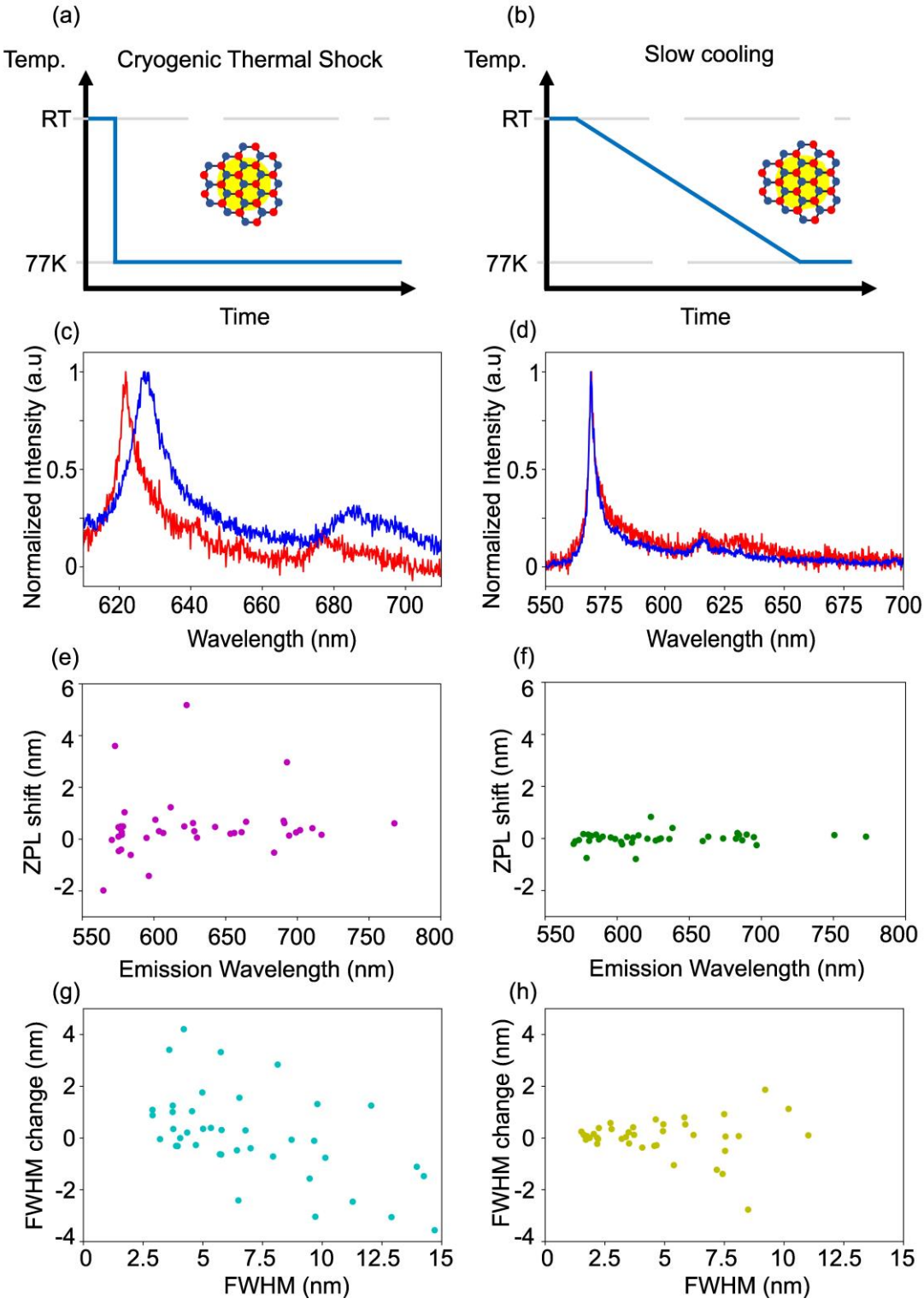

Figure 4.1. Spectral changes of hBN quantum emitters before and after exposure to cryogenic thermal shock or slow cooling process. (a-b) Schematics showing the qualitative differences in the cooling rates of

cryogenic thermal shock versus slow cooling. In both experiments, silicon substrates with hBN flakes were cooled to liquid nitrogen temperature. **(c-d)** Representative spectra of two emitters before (red) and after (blue) the thermal shock and slow cooling processes, respectively. **(e-f)** Zero-phonon line shifts plotted against emission wavelength and **(g-h)** changes in full-width at half maximum versus FWHM after the emitters are subject to thermal shock and slow cooling, respectively. Data from forty quantum emitters were chosen for (e-h). All optical characterizations in (c-h) were conducted using a 532 nm continuous-wave excitation at 300 μW at room temperature.

When the data in **Figure 4.1 e-h** are plotted in the form of histograms, the effect of the cryogenic thermal shock compared to that of slow cooling is clearly recognized. The thermal shock induces a ZPL shift distribution with a mean value, μ, of 0.47 nm—a clear redshift—and a standard deviation, σ, of 1.18 nm **(Figure 4.2a**). By contrast, the slow cooling process gives rise to a distribution with the mean value of almost zero (-0.006 nm) and a standard deviation of 0.25 nm—less than a fourth of that caused by the thermal shock **(Figure 4.2b**). Such a sub-nanometer redshift in ZPLs in conjunction with a relatively large distribution width created by the cryogenic thermal shock can be a major concern for quantum

applications that are wavelength-sensitive such as quantum communication or quantum teleportation—where quantum emitters need to be resonantly excited to generate the highly coherent photons.[20] In such situations, the resonant laser has to be periodically swept across the ZPL of the emitter to lock into its resonance, making the procedure arduous and time-consuming.[55] A similar trend is also observed for the FWHM of the emission spectra. **Figure 4.2c and 4.2d** entail the distribution of changes in FWHM for the case of thermal shock and slow cooling, respectively. While both the distributions are mostly symmetrical around zero, the distribution in the case of slow cooling is more than two-fold narrower (0.74 nm vs 1.72 nm) compared to that from the thermal shock case.

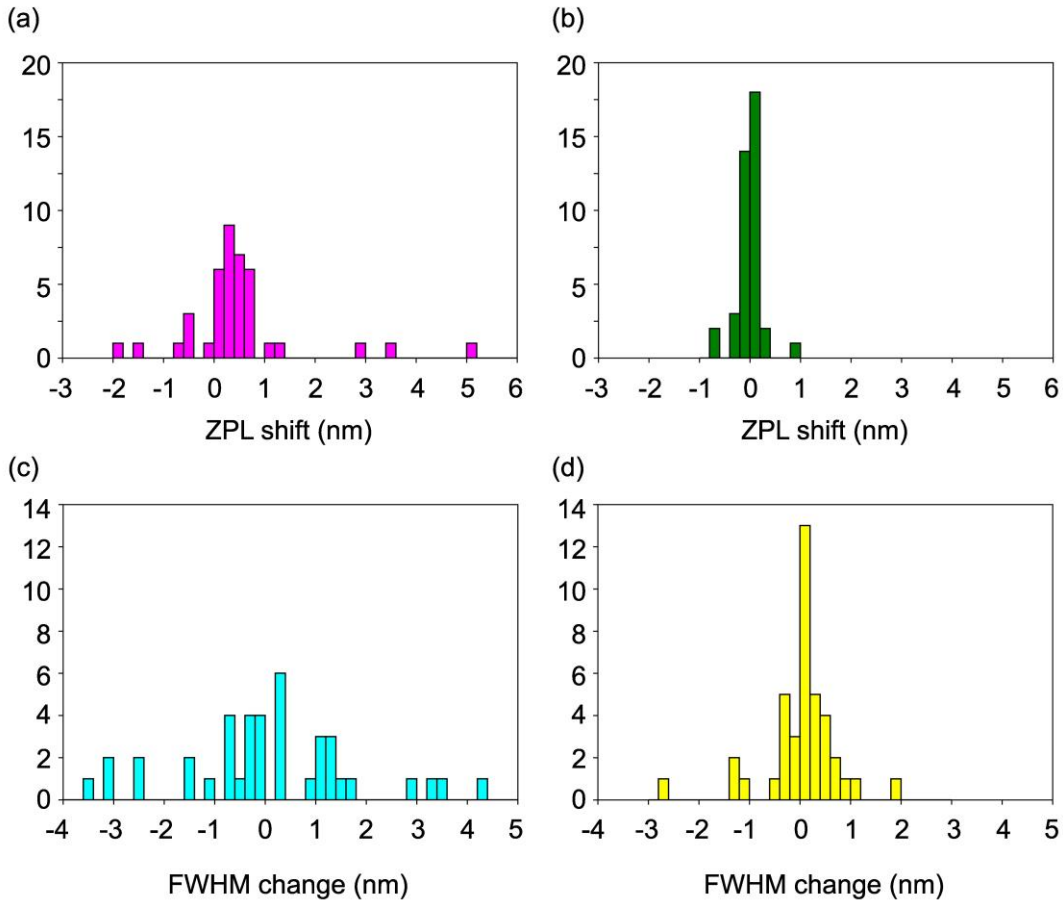

Figure 4.2. Statistical analysis of modifications in spectral characteristics of the quantum emitters after the cryogenic thermal shock and slow cooling. (a-b) Histograms of ZPL shifts after the thermal shock and slow cooling, respectively. **(c-d)** Histograms of FWHM changes after being exposed to thermal shock and slow cooling, respectively. The bin width is 0.2 nm for all the figures. Each histogram is plotted with data taken from the 40 emitters mentioned in Figure 4.1.

To gain more insights on the effects of thermal shock to the quantum emitters, we first looked at the morphological information from the hBN flakes before and after the thermal shock exposure. Specifically, we identified and measured three representative flakes using a standard commercial atomic force microscope since AFM measurements are extremely sensitive in the vertical direction (z-direction). **Figure 4.3a, d, g** shows the topographical image featuring the three hBN flakes with various thickness, from 668 nm (Flake 1) to 701 nm (Flake 2) and 217 nm (Flake 3). **Figure 4.3b, e, h** entails the image of the same flakes after being exposed to thermal shock. Some reduction in lateral dimensions were observed across the three flakes. By analyzing the line profiles of the flakes (**Figure 4.3 c, f, i**), we noticed that there were consistent decreases in the flake thickness across all the flakes: 7 nm for Flake 1, 45 nm for Flake 2, and 135 nm for Flake 3. Another AFM measurement with three different flakes in another position with the same reduction evidence can be found in **Supporting Information Figure S4**. Such reduction in the flake thickness might be attributed to the sudden in-plane contraction of the hBN lattice, causing the exfoliating/peeling effect to the flakes. A reduced thickness can, in turn, give rise to variations in the dielectric environments—most notably, allowing the emitters to come closer to the

trapped charges and surface states. Such proximities can induce ZPL shifts and FWHM changes via a Stark effect.

In addition, from the TEM measurement, we can extract thickness mapping of hexagonal boron nitride flakes before and after the cryogenic thermal shock cooling process as shown in **Figure 4.3j and 4.3k.** The mean free path (MFP) line profiles (**Figure 4.3l**) of the flake before and after the thermal shock shows a decrease in the flake thickness, which is in good agreement with the AFM measurements.

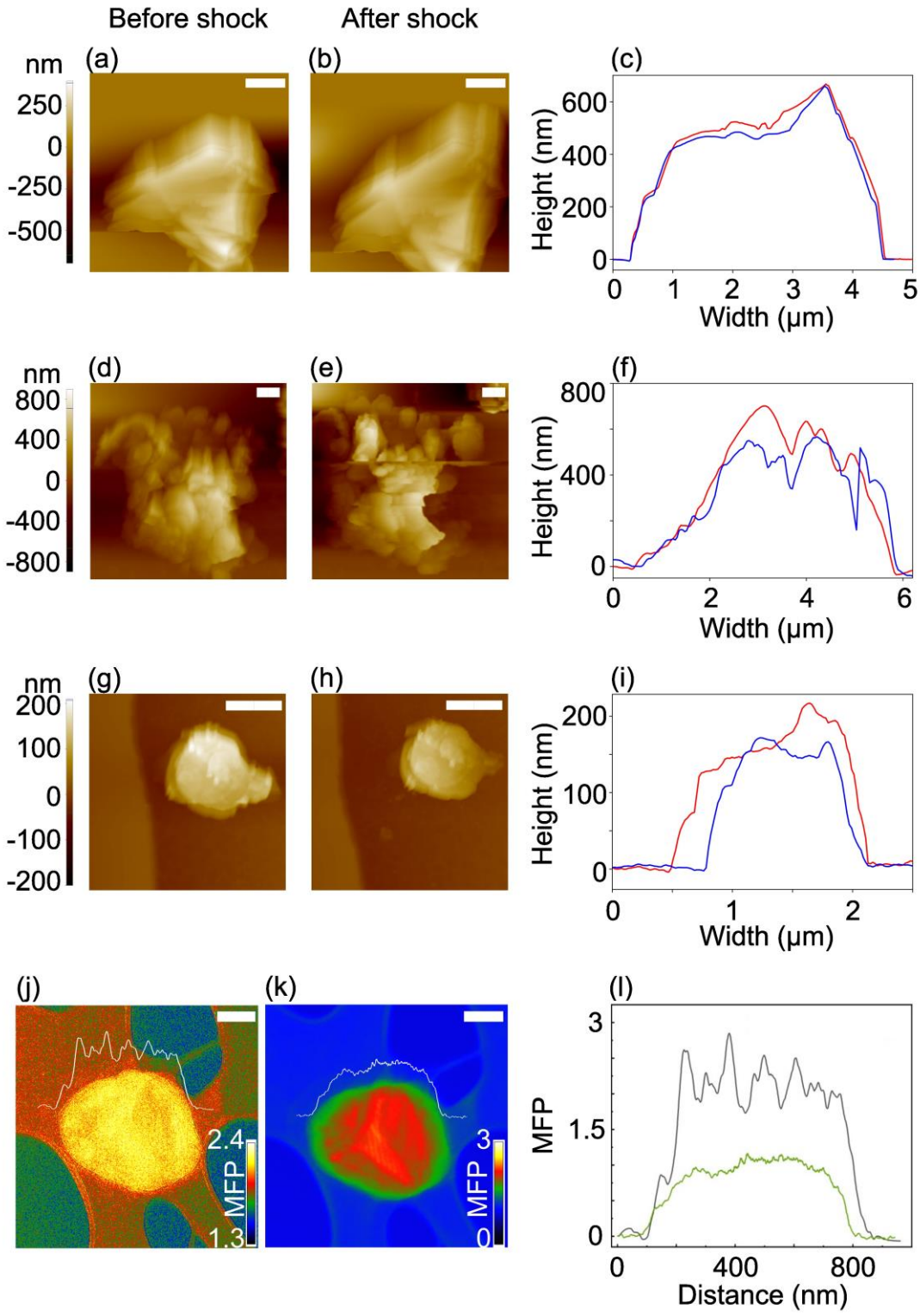

Figure 4.3. AFM characterizations and TEM thickness mapping of hexagonal boron nitride flakes before and after the cryogenic thermal shock. (a-b, d-e, g-h) High-resolution topographical AFM images for

three hBN flakes before and after thermal shock exposure, respectively. The pixel color corresponds to the thickness of the flakes, brighter color means thicker and vice versa. The scale bars in a-b, d-e, g-h are 1 μm. **(c, f, i)** Line profiles of the three hBN flakes before (red line) and after (blue line) the thermal shock exposure. (**j-k**) Transmission electron microscopy thickness mapping of one representative hexagonal boron nitride flake before and after the cryogenic thermal shock cooling process, respectively. The scale bar is 200 nm. (**l**) The mean free path (MFP) line profiles of the hBN flake before and after the shock cooling exposure.

While AFM offers insights on the topographical modifications of the hBN flakes after thermal shock exposure, it is not capable of providing structural information about the flakes per se. Raman spectroscopy is, on the other hand, the right tool for such characterization. By collecting the Raman spectra on a representative flake before and after the thermal shock process (cf. Methods), we can unveil any changes in the hBN crystal lattice. **Figure 4.4a** showcases two peaks at ~1369.2 cm^{-1} obtained before (red) and after (blue) the thermal shock. The peaks can be attributed to the E_{2g} in-plane phonon mode in hexagonal boron nitride. The Lorentzian-fitted spectra for both cases are, however, identical to one another, suggesting that the in-plane crystal lattice remains unchanged

after the flakes are exposed to the thermal shock. To examine the quantum emission nature of the emitters after the thermal shock, we employed the second-order autocorrelation function, also known as the $g_2^{(t)}$ measurement on an exemplary emitter,[191] as shown in **Figure 4.4b**. Unlike the visible changes in the spectral characteristics mentioned above, we observed no significant changes in the antibunching dips (clearly below 0.5) and the antibunching times. The results indicate that there were no visible changes in the photon statistics of the emitter—a strong implication that the emitter did not undergo any compositional changes. In terms of photostability of the emitter, we notice a significant increase in fluorescence fluctuations after the emitter was subject to the thermal shock (**Figure 4.4c**), however. The surge in fluorescence instabilities can be attributed to the proximity to trapped charges or surface states as mentioned earlier.

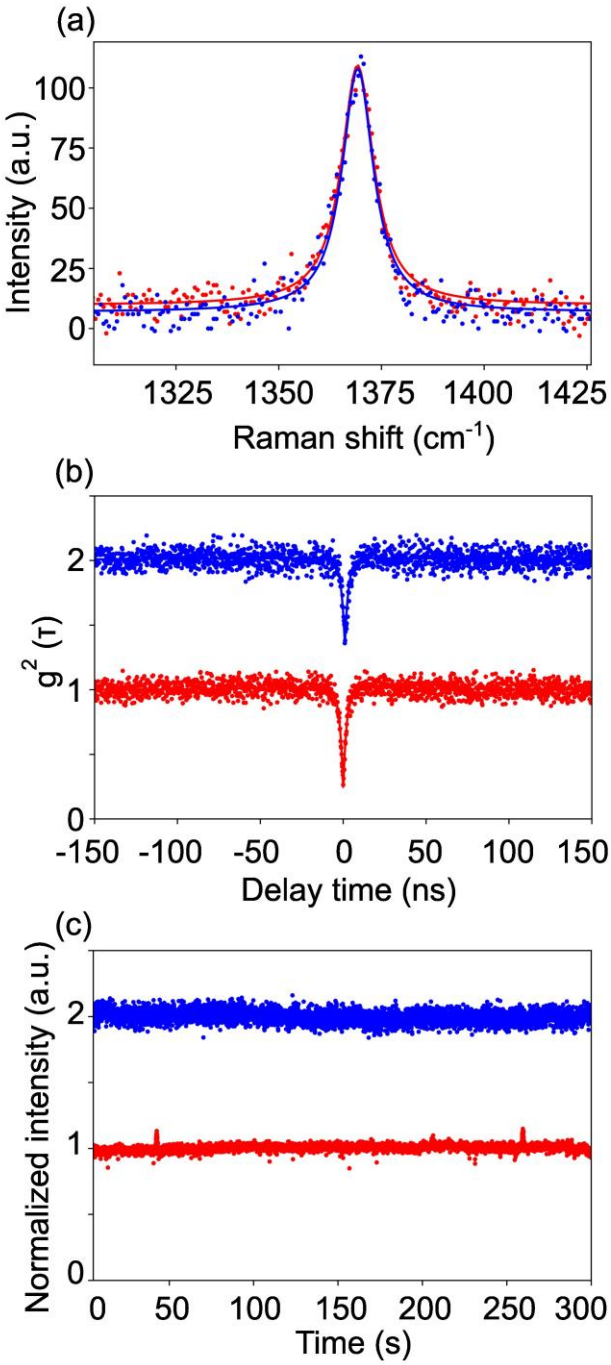

Figure 4.4. Spectroscopic characterizations on hBN flakes before and after thermal shock exposure. (a) Raman spectra, **(b)** second-order autocorrelation measurements and **(c)** photostability of a representative quantum emitter in an hBN flake before (red) and after (blue) the shock-

cooling process. In (a-c), the raw and fitted data were illustrated by circle markers and solid straight lines, respectively and offset by one unit for clarity.

To obtain more in-depth information about the crystal structures of the hBN flakes subjected to the thermal shock, we resorted to the combination of transmission electron microscopy, selected area electron diffraction and X-ray diffraction. First, we conducted the TEM imaging on a representative flake before and after the thermal shock. **Figure 4.5 a-b** features the images of an hBN flake in the two cases in which no visible differences can be discerned. The selected-area diffraction patterns taken from the same flake before and after the thermal shock were shown in **Figure 4.5 c-d**, respectively. Both reciprocal images consist of three individual diffraction patterns (red, yellow, and green)—which individually belong to different sets of d-spacing of hBN in real space. It must be noted that the smaller spots within the groups of diffraction spots can be attributed to the Moire pattern in real space. The Moire pattern is formed due to the misalignment of the three hBN films stacking on top of one another, as shown in the **Supporting Information Figure S5**. Regardless, from our detailed analysis of these patterns, there were no

significant variations in all the indexed hBN d-spacing, in good agreement with the above Raman analysis.

X-ray diffraction measurements were used to give further information about the out-of-plane d-spacings. **Figure 4.5e** depicts the XRD spectra taken for the three cases: pristine (black), after slow cooling (red) and after thermal shock (green), respectively. The peaks at the 2θ angles of 26.71°, 41.10°, 43.23°, 49.11° and 53.67° can be assigned to the (002), (100), (101), (102) and (004) planes on the pristine sample, respectively. Surprisingly, except for the (002) and (004) peaks, the in-plane d-spacing, which does not show any changes in the d-spacing after the thermal shock or slow cooling, the rest of the peaks that contain the out-of-plane component (the c-axis in hexagonal lattice) do show noticeable increases in the 2θ angle, which translate into shrinkages in the d-spacings. Most notably, the (002) and (004) planes feature the most significant reduction in the interplanar spacing, which is in good agreement with the overall observation of the interplanar shrinkage in the hBN lattice. The shrinkage occurring mainly in the out-of-plane direction of the flakes can be attributed to the anisotropic nature of hexagonal boron nitride. As a van der Waals material, the hexagonal boron nitride lattice features strong covalent bonding in the in-plane direction and weak van der Waals interaction in the out-of-plane direction. Such compression in the

interplanar direction could be the reason for the shift in ZPLs and changes in FWHM seen previously.

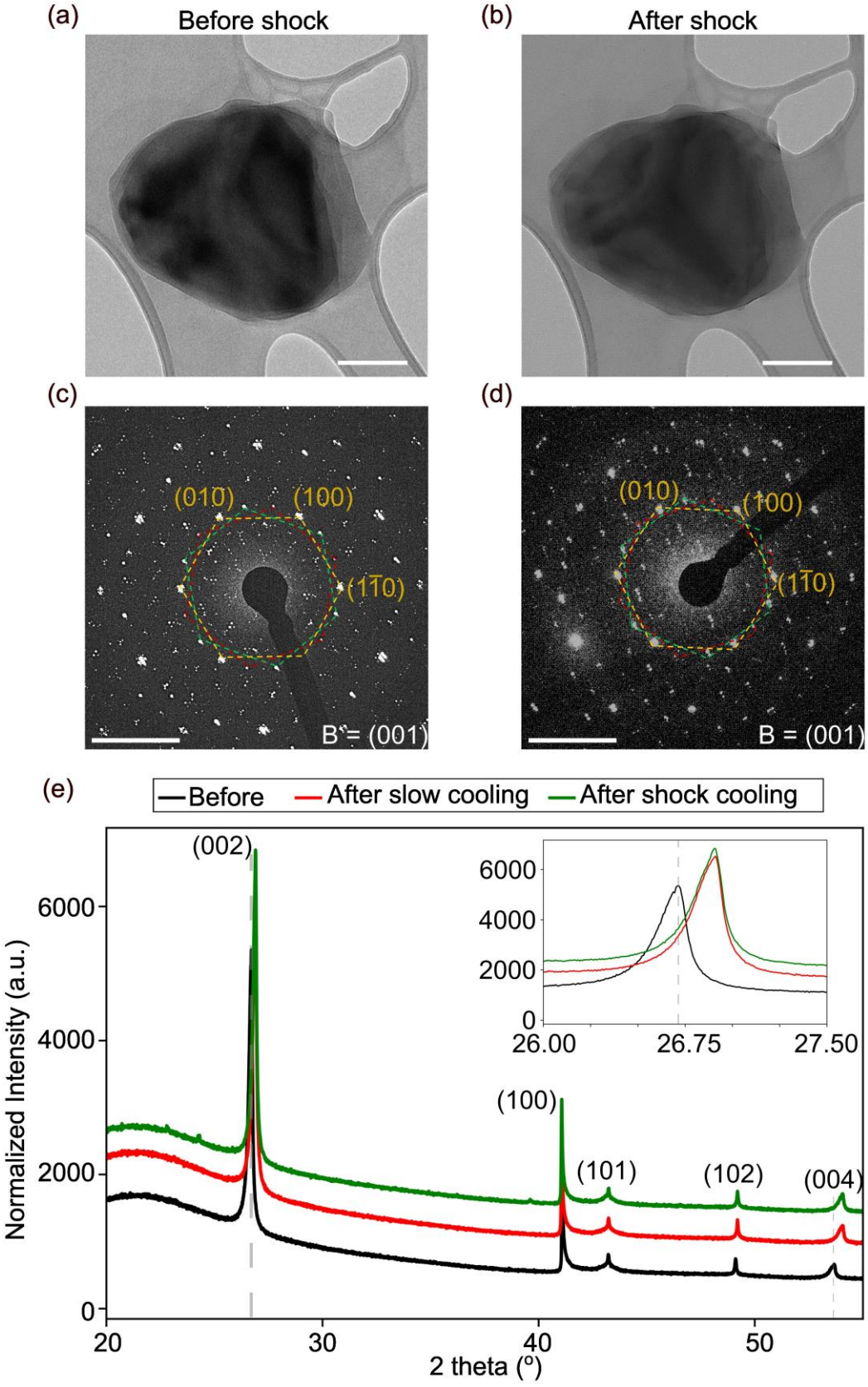
(a)
Before shock
(b)
After shock
(c)
(010)
(100)
(1$\bar{1}$0)
B = (001)
(d)
(010)
(100)
(1$\bar{1}$0)
B = (001)
(e)
Before
After slow cooling
After shock cooling
(002)
(100)
(101)
(102)
(004)
Normalized Intensity (a.u.)
2 theta (°)
0
2000
4000
6000
20
30
40
50
26.00
26.75
27.50

Figure 4.5. Crystal structure characterization of the hBN flakes before and after cooling processes. (a-b) Representative transmission electron microscopy images taken before and after the cryogenic thermal shock, respectively. The scale bars in a, b are 200 nm. **(c-d)** Representative selected area electron diffraction images taken before and after the cryogenic thermal shock, respectively. The scale bars in c, d are 5 (1/nm). **(e)** X-ray diffraction patterns obtained from three cases: pristine, after slow cooling and after thermal shock cooling. The broad peak between 20–25° in the XRD spectra of hBN is attributed to the glass capillary used as the sample holder in the XRD characterization.

DFT Calculations

To understand the relationship between induced strain and ZPL shifts, we employed the density function theory calculations of strain induced shift in ZPL energies and PL lineshapes. All the DFT calculations for the ground states, excited states and normal modes were performed within the VASP electronic structure code using a plane-wave wave cut-off of 800 eV and a gamma point sampling of the Brillouin zone. For accurate calculation of electron spin density close to the nuclei, the projector augmented wave method was applied together with a plane wave basis set. The defects were represented in a 9 x 9 x 1 supercell (monolayer) and

atoms allowed to fully relax until the maximum force was below 0.01 eV/Å. A vacuum of 15 Å was used along the vertical direction. The HSE06 exchange correlation functional was used for all calculations.

Since $(2)^2A_2 \rightarrow (1)^2A_2$ transition of the C_2C_N defect (**Figure 4.6a**) is thought to be the source of single photon emission (SPE) from hBN.[192] We have calculated the PL lineshape for this transition and compared with the experimental luminescence spectra to confirm the origin of emission in our experiments (**Figure 4.6b**). Our calculated luminescence line shape plotted against the experimental spectra shows a very good agreement, given the fact that the only fitting parameter in the calculation is gaussian smearing of 0.02 eV and a rigid shift of 0.51 eV to align the zero phonon lines. After confirming the origin of emission in our samples, we study the strain induced shift in the ZPL energies as shown in **Figure 4.6c**. We applied uniform strain within the plane of hBN and calculated the change in the ZPL energies. We find that ±1% strain causes meV shift in the ZPL energies, consistent with experimental observations. From the combination of experimental characterization and theoretical predictions, we believe that the cryogenic thermal shock induces an irreversible shrinkage in the out-of-plane direction due to the instantaneous change in temperature of the flake. Such a phenomenon results in the locally induced strain in the lattice. Depending on the local dielectric environment, i.e. the

lattice imperfections in the vicinity, and intrinsic strain, each defect complex may respond differently to such strain, leading to various changes in the optical properties such as the shift in ZPL or the changes in FWHM. On the contrary, in the slow cooling process, the hBN lattice has enough time to respond to the stress induced by the decrease in temperature—allowing for significantly smaller modifications in the optical properties of the emitters. In addition, we believe that the effect of substrate on the thermal shock is negligible. All the flakes we chose to study are at least several tens of nanometers in thickness. Such thickness translates to several tens to hundreds of monolayers. Since the out-of-plane interactions are primarily dictated by van der Waal forces, the strain induced by the thermal expansion coefficient mismatch at the interface between hBN and silicon is largely suppressed after the first few layers from the bottom due to the interlayer sliding.[193]

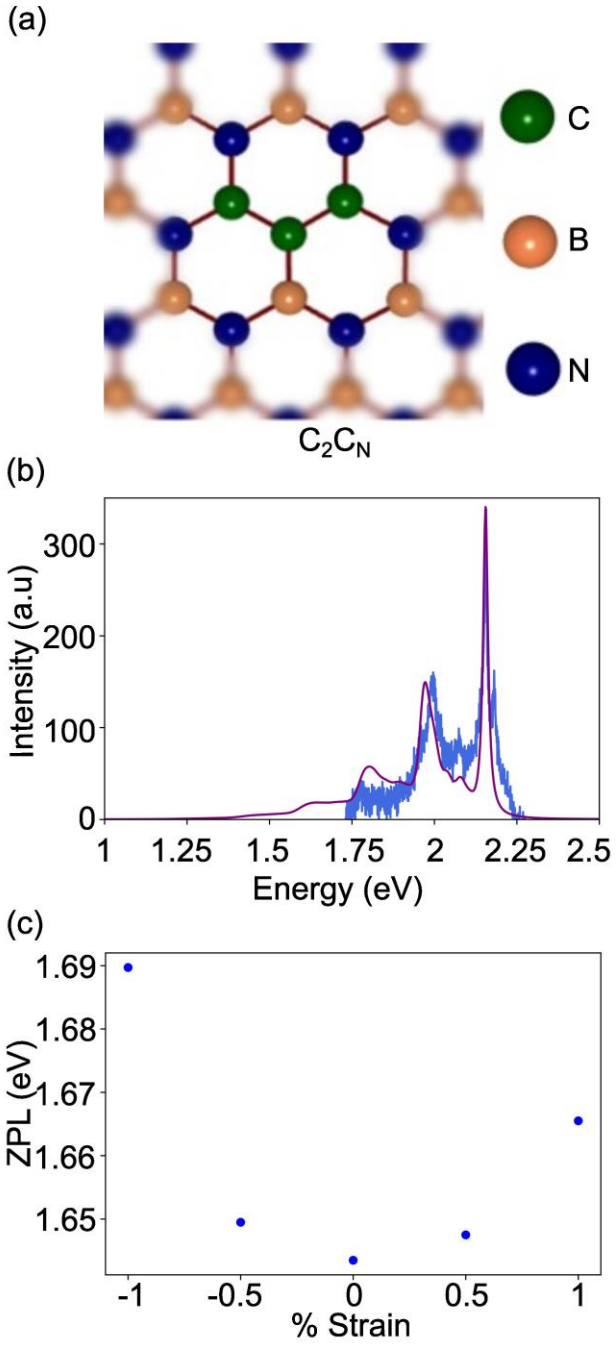

Figure 4.6. Density functional theory calculations on strain-induced emission shift. (a) C_2C_N defect with the C_{2v} symmetry in hBN **(b)** Calculated photoluminescence spectrum compared to the experimental spectrum, the calculated spectrum with adiabatic ZPL energy has been shifted rigidly by 0.51 eV to match the high intensity peak of the

experimental spectrum at 575.4 nm (2.15 eV). The blue and purple lines are the experimental data and the fit, respectively. **(c)** Strain induced shift in the ZPL energies of $(2)^2A_2 \rightarrow (1)^2A_2$ transition of the C_2C_N defect.

Since the slow cooling process has only minor effects on the optical properties of the emitters, we mainly focus to the effect caused by the thermal shock process. For practical implementations, especially in the case of space-based applications, quantum emitters need to be spectrally stable against multiple cryogenic thermal shock cycles. As such, we designed an experiment in which the quantum emitters were exposed to three thermal shock cycles to gain more insights on the effect of repeated exposure to the thermal shock on the quantum emitters. After each cycle, we optically characterized the same emitters and recorded their spectral data, similar to that in the earlier experiments. To be as consistent with the previous experiments as we can, we conducted the second and third thermal shock cycles on the same sample that was exposed to the first thermal shock cycle (in **Figure 4.1 c, e,** and **g**). As mentioned earlier, we started the experiment with 46 emitters. After each cycle, a small portion of emitters bleached out. Specifically, after the first, second and third thermal cycle, the numbers of emitters that bleached out were 6, 7 and 3, respectively. After the third cycle, only 30 emitters remained optically

stable while the other 16 emitters were optically inactive. This means that ~35% of emitters bleached out after the three thermal cycles—implying the detrimental effect of the consecutive cryogenic thermal shocks on the optical properties of the emitters. The remaining thirty emitters were identified and characterized, and their spectra were fitted using a single Lorentzian peak. To compare the ZPL shifts and FWHM changes after each thermal shock cycle, we subtracted the fitted values obtained from each thermal shock cycle to that from the original emission before the thermal shock, $\gamma_{r,i} = \gamma_i - \gamma_0$, where $\gamma_{r,i}$ is the subtracted value, γ_i is the fitted value after thermal shock cycle i, and γ_0 is the fitted value before the first thermal shock. **Figure 4.7a and 4.7b** show the ZPL shifts plotted in category and box plots, respectively, for three consecutive thermal shock cycles. It is clear that the second and third thermal cycles cause significantly more ZPL shifts, on average, than that from the first cycle, with the median values of 1.09 and 0.90 nm, respectively, compared to 0.31 nm from the first cycle. Moreover, compared to the first and second cycles, the third cycle induces more than two-fold increase in the distribution of ZPL shifts—1.12 nm versus 0.39 and 0.43, respectively. Such an increase in the distribution width is also observed for the FWHM changes as shown in **Figure 4.7c and 4.7d**.

While we only showed the susceptibility of quantum emitters in hBN towards cryogenic thermal shock in this work, the same protocol can be extended to test and validate quantum emitters hosted in other semiconductors such as the color centers in carbon nanotubes, diamond, silicon carbide, or gallium nitride as part of the space-qualification testing suite. In a similar fashion, the quantum emitters will be subject to the thermal shock cycles, and optical characteristics will be monitored and analyzed. These include the ZPL shifts, FWHM changes, photostability, and second-order autocorrelation function measurements. The changes in optical properties of the emitters will then be compared against requirements for the intended applications so that further optimization can be done to improve the stability of the quantum emitters to make them ready for space-related applications.

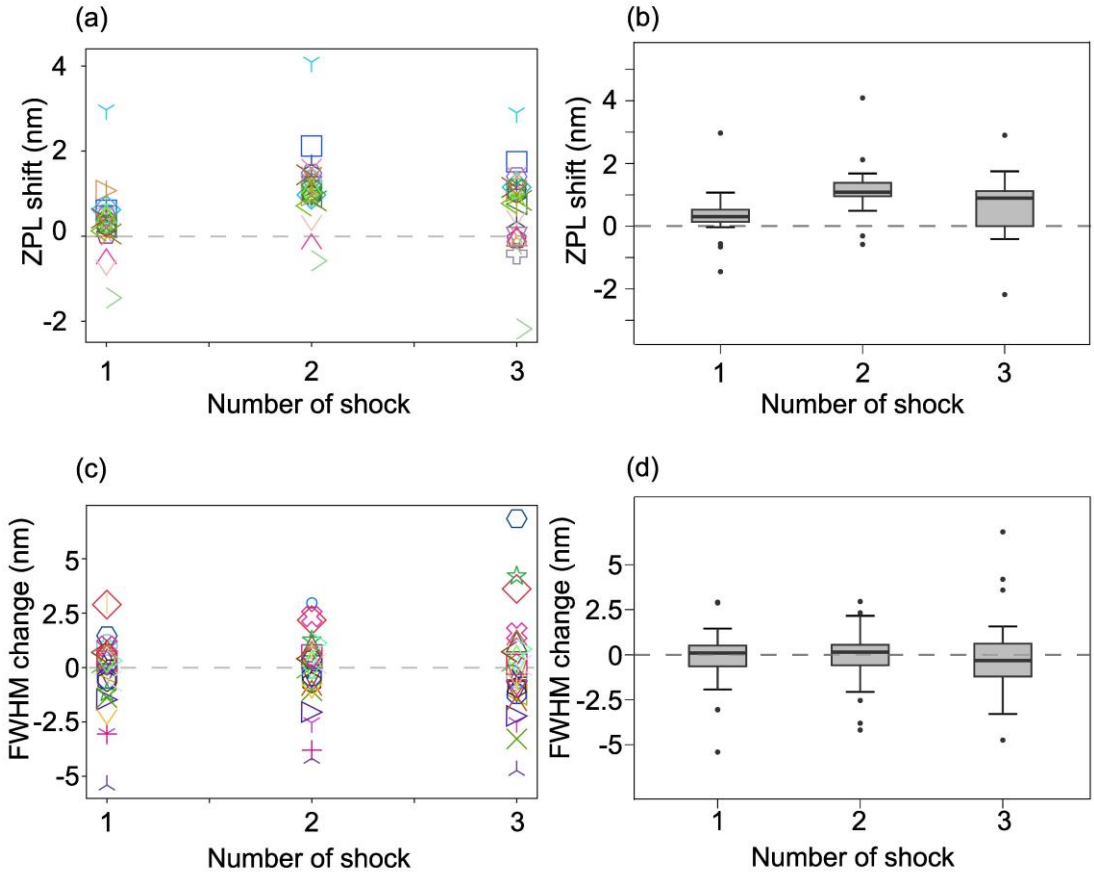

Figure 4.7. Modifications in optical characteristics of hBN quantum emitters upon three consecutive cryogenic thermal shock cycles. The ZPL shifts after three consecutive thermal shock cycles plotted as category (**a)** and box plot **(b)**, respectively. The FWHM changes after three consecutive thermal shock cycles plotted as category (**c)** and box plot **(d)**, respectively. A total number of thirty emitters were considered for this experiment. All data were calculated by subtracting the fitted values after each thermal shock to the fitted values before the thermal shock. The grey dash line at zero was added as the reference to improve visualization.

4.3. Conclusions

In this study, we have presented a comprehensive analysis of the cryogenic thermal shock effects on the optical properties of quantum emitters embedded in hBN. Our experimental data, supported by structural characterizations and density functional theory calculations, demonstrate that cryogenic thermal shocks induce spectral shifts in these emitters. This is a result of lattice strains, which lead to random and irreversible alterations in their emission characteristics. Notably, these findings underscore the sensitivity of hBN quantum emitters to extreme temperature fluctuations, despite their otherwise robust performance under high-temperature and chemically harsh environments. The resilience of these quantum emitters to radiation further accentuates their potential for space-based applications, particularly in quantum communication technologies.

Looking ahead, the implications of our research are twofold. Firstly, there is a clear imperative to further explore materials engineering strategies that could enhance the thermal shock resistance of hBN quantum emitters. This could involve the development of novel fabrication techniques or the investigation of composite materials that could mitigate lattice strain effects. Secondly, our findings pave the way for new experimental

protocols that specifically simulate the harsh conditions of outer space, providing a more rigorous testing ground for quantum emitters in future quantum communication networks. As the quest for quantum-enabled technologies progresses, the insights provided by our research will be invaluable in navigating the challenges posed by the extreme conditions of space, ensuring that the promise of quantum communication can be realized fully and reliably.

ASSOCIATED CONTENT

Data Availability Statement

The datasets generated during and/or analyzed during the current study are available from the corresponding author upon reasonable request.

Supporting Information

Spectra taken from quantum emitters in hexagonal boron nitride before shock-cooling; fitting of an exemplary spectrum taken from a quantum emitter in hBN; spectra taken from quantum emitters in hexagonal boron nitride before slow-cooling; topographical AFM images for three hBN flakes before and after thermal shock exposure; high-resolution TEM

image of the three misaligned hBN thin films, resulting in the Moire pattern.

AUTHOR INFORMATION

Author contribution

T. N. A. M. and T. T. T conceived the idea of the project. T. N. A. M. and T. T. T built the optical system and its software. T. N. A. M. fabricated the quantum emitters in hBN and performed all the optical characterization. X. X. and H. M. conducted the TEM, SAED and XRD experiments and analyzed the data. S. A. and N. M. carried out the DFT calculations for strain effect on hBN quantum emitters. T. T. T supervised the project. All authors discussed the results and commented on the manuscript.

Acknowledgement

T. N. A. M. is grateful to UTS and VNU for the financial support to this research through the Joint Technology and Innovation Research Centre (JTIRC) scheme. The authors thank the UTS node of Optofab ANFF for the assistance with nanofabrication. The authors acknowledge the

technical and scientific assistance of Sydney Microscopy & Microanalysis, the University of Sydney node of Microscopy Australia.

Funding Sources

T. T. T. acknowledges the Australian Research Council (DE220100487) for the financial support.

Notes

The authors declare no competing financial interest.

TOC graphic

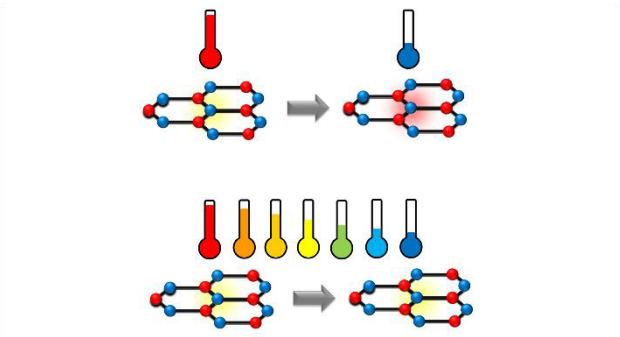

Chapter 5

Conclusions

In this thesis, I reported a comprehensive and up-to-date review of hexagonal boron nitride quantum emitters with fundamental principles, atomic structure calculations, experimental investigations, fabrication and integration into devices, and potential application directions. Then, I investigated the optical properties of hBN quantum emitters after exposed to a specific and extreme condition—cryogenic temperature shock as part of space qualification testing to prepare it for satellite-ground quantum key distribution and space-related communication applications. Most recently, hexagonal boron nitride quantum emitters have been used to test the extended quantum theory[52] and were proposed to be the first qualified quantum emitters for testing extended physical theory in space. The hBN quantum emitters have been shown to be optically stable under different conditions, such as high temperatures at 800K, different aggressive gas annealing, and under gamma ray and proton irradiation tests. However, there is still a lack of results on the optical properties of quantum emitters against some harsh and inconceivable conditions, such as cryogenic shock temperature and multiple repeat shock temperature cycles. These

conditions are also challenging to realize and test in laboratories on earth. In this thesis, I presented the first investigation and experiment to mimic the outer space shock conditions on hexagonal boron nitride quantum emitters by using liquid nitrogen. The results showed that cryogenic thermal shock can induce random, irreversible spectral shifts and photo-bleaching in hBN quantum emitters. These spectral shifts are attributed to lattice strain caused by the extreme temperature changes. We also did consider the thermal shock on hBN quantum emitters in the other way—the hot regime for instance between high temperature (e.g. 500-1000ºC) to liquid nitrogen temperature. Such experiments, however, pose a couple of issues. First, performing a thermal shock at these temperatures involves high-risk activities since the samples need to be removed from a tube furnace and placed into the liquid-nitrogen-containing dewar instantaneously. Second, the realistic temperature changes in orbits are at least a few folds smaller than the said range. Based on the results of the cryogenic shock experiments, we believe that the cryogenic thermal shock from room- to liquid nitrogen- temperature is highly indicative of the experimental result of thermal shock in hot regimes and space environments. The cryogenic thermal shock experiment protocol, designed to simulate the harsh conditions of outer space, could be used for ground-testing other potential quantum emitters. This protocol

highlights the necessity of enhancing the thermal shock resistance of hBN quantum emitters before they can be reliably integrated into space instrumentation.

To sum up, my thesis has laid a foundation for further investigation of behaviors of solid-state quantum emitters in extraterrestrial conditions. This mainly applies to future quantum optics tests such as long-range entanglement and quantum gravity. It will open up quantum technologies in space with various applications, some of which still have to be identified and realized.

Appendix

Supplementary information: ACS Appl. Mater. Interfaces 2024, 16, 19340-19349

Supporting information for

Cryogenic Thermal Shock Effects on Optical Properties of Quantum Emitters in Hexagonal Boron Nitride

Thi Ngoc Anh Mai,[†] Sajid Ali,[‡] Md Shakhawath Hossain,[†] Chaohao Chen,[§,∥] Lei Ding, [#] Yongliang Chen,[††] Alexander S. Solntsev,[‡‡] Hongwei Mou,[#] Xiaoxue Xu,[#] Nikhil Medhekar[‡] and Toan Trong Tran[†,*]

[†]School of Electrical and Data Engineering, University of Technology Sydney, Ultimo, NSW, 2007, Australia

[‡]School of Physics and Astronomy, Monash University, Victoria 3800, Australia

[§]Department of Electronic Materials Engineering, Research School of Physics, The Australian National University, Canberra, Australian Capital Territory 2601, Australia.

[‖]ARC Centre of Excellence for Transformative Meta-Optical Systems (TMOS), Research School of Physics, The Australian National University, Canberra, Australian Capital Territory 2601, Australia.

[#]School of Biomedical Engineering, University of Technology Sydney, Ultimo, NSW, 2007, Australia.

[††]Department of Physics, The University of Hong Kong, Pokfulam, Hong Kong, China.

[‡‡]School of Mathematical and Physical Sciences, University of Technology Sydney, Ultimo, NSW, 2007, Australia.

*Corresponding author: trongtoan.tran@uts.edu.au

The Supporting Information includes:

Figure S1 Spectra taken from quantum emitters in hexagonal boron nitride before shock-cooling.

Figure S2 A Lorentzian fit (blue line) to an exemplary spectrum (red circle) taken from a quantum emitter in hBN.

Figure S3 Spectra taken from quantum emitters in hexagonal boron nitride before slow-cooling.

Figure S4 Topographical AFM images for three hBN flakes before and after thermal shock exposure.

Figure S5 High-resolution TEM image of the three misaligned hBN thin films, resulting in the Moire pattern.

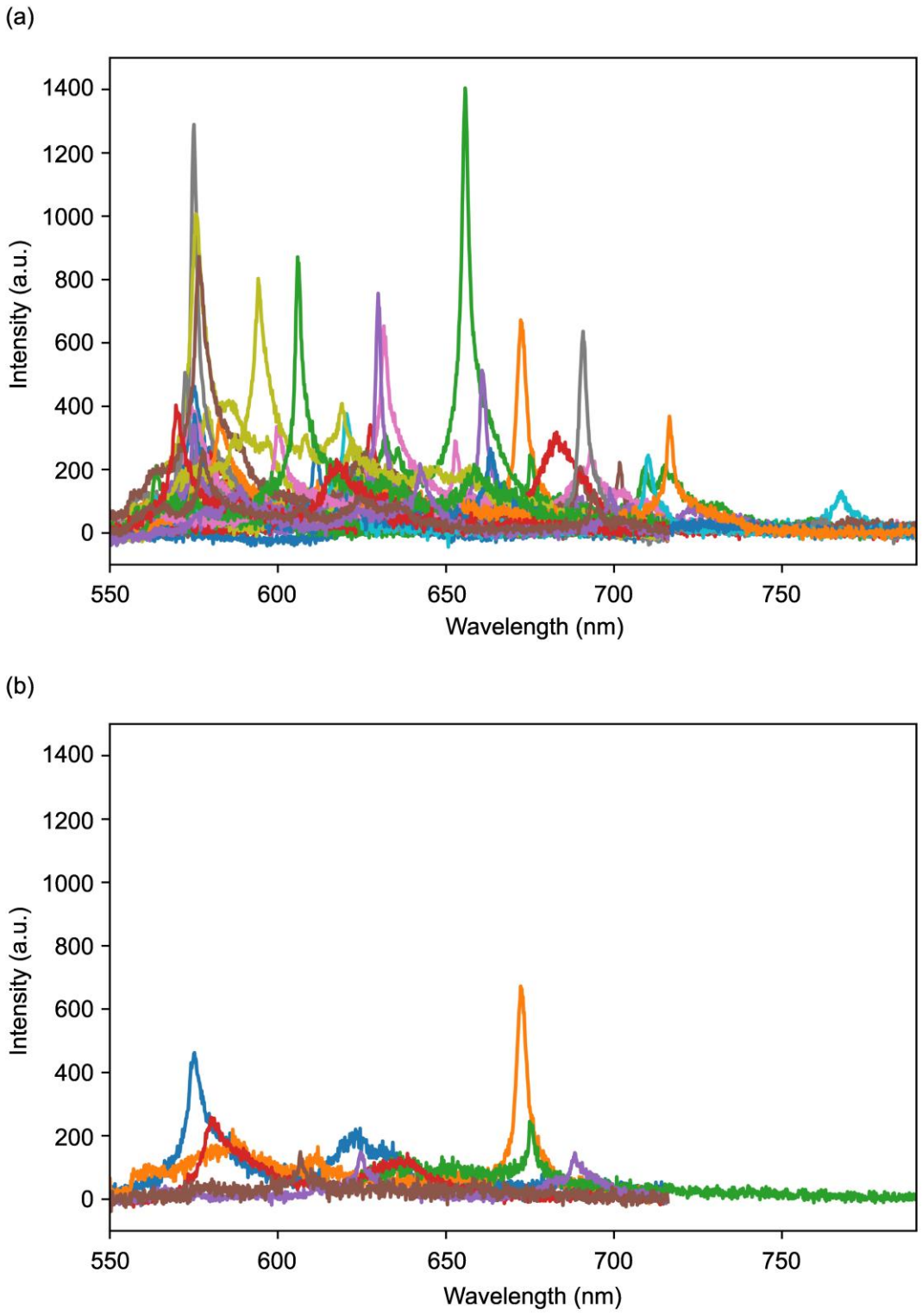

Figure S1 a) Spectra taken from 46 quantum emitters in hBN before cryogenic thermal shock exposure. b) Spectra taken from the 6 emitters that bleached out after the thermal shock process.

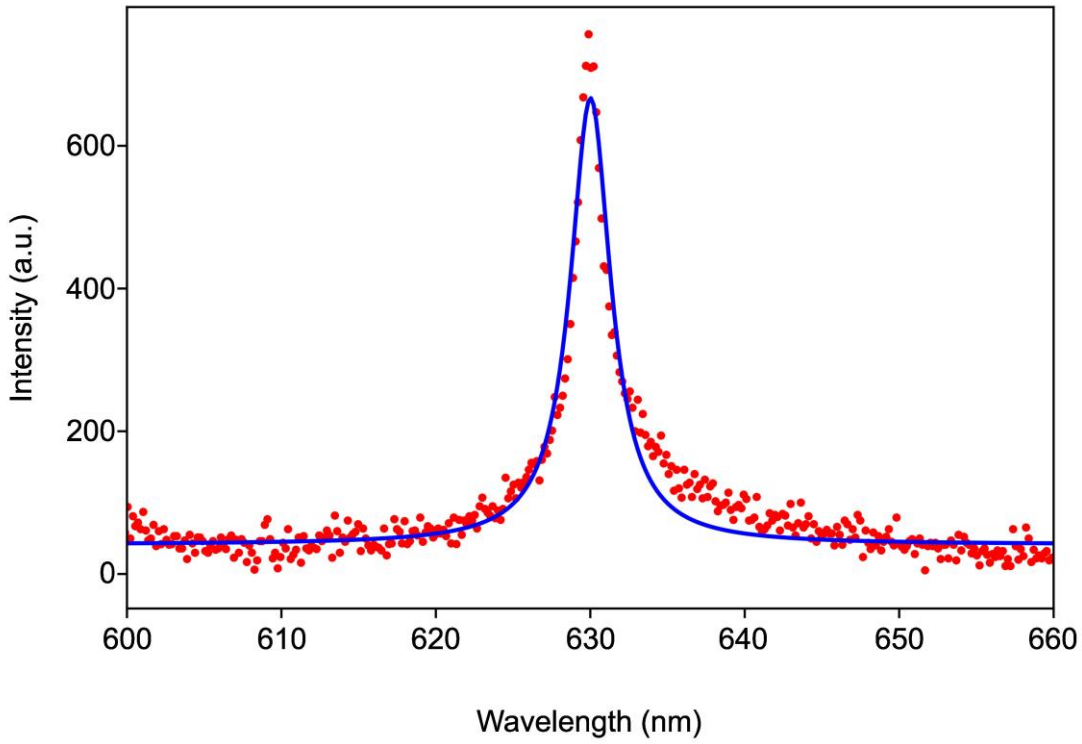

Figure S2 A Lorentzian fit (blue line) to an exemplary spectrum (red circle) taken from a quantum emitter in hBN.

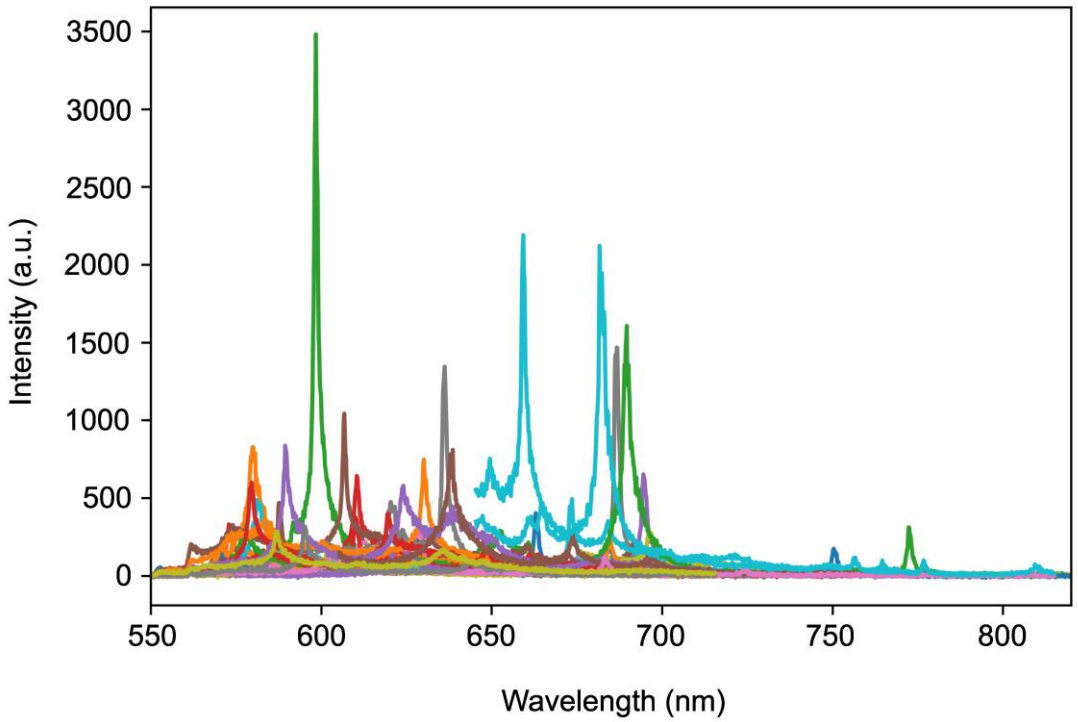

Figure S3 Spectra taken from 40 quantum emitters in hBN before slow-cooling.

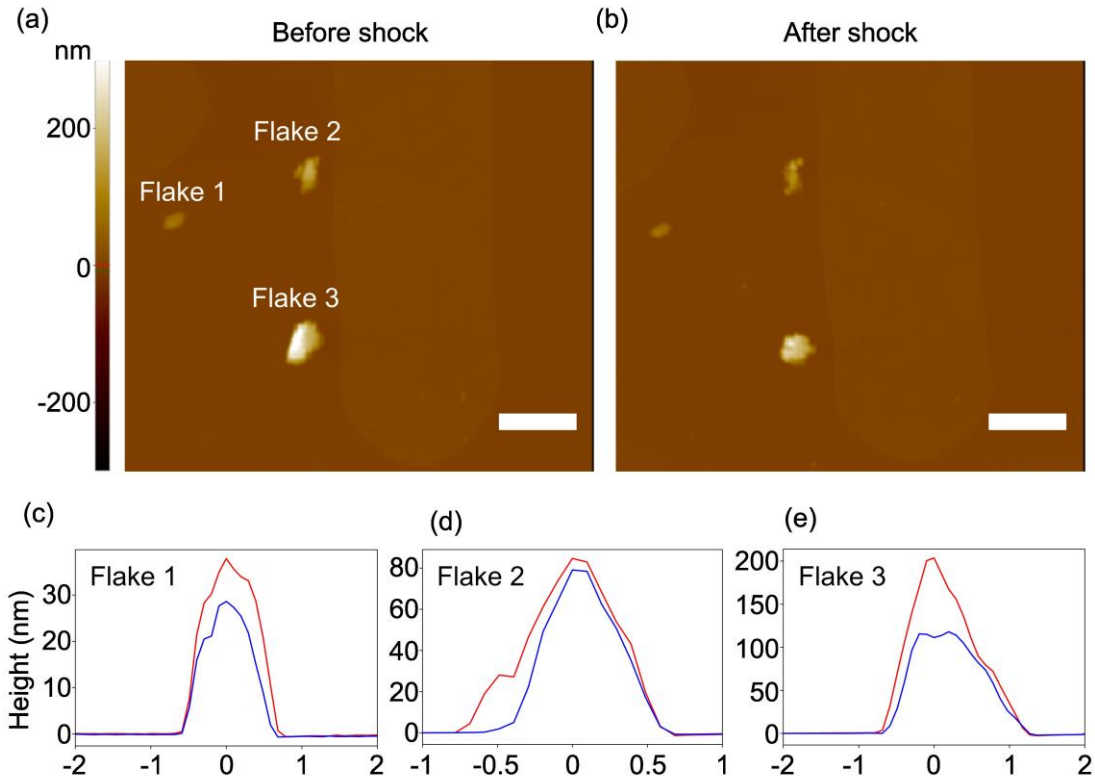

Figure S4 Topographical AFM images for three hBN flakes before and after thermal shock exposure. The pixel color corresponds to the thickness of the flakes, brighter color means thicker and vice versa. The scale bars in a, b are 4 μm. **(c-e)** Line profiles of the three hBN flakes before (red line) and after (blue line) the thermal shock exposure. The faint, oval shapes in the background come from the etch-in markers used to locate the flakes in question.

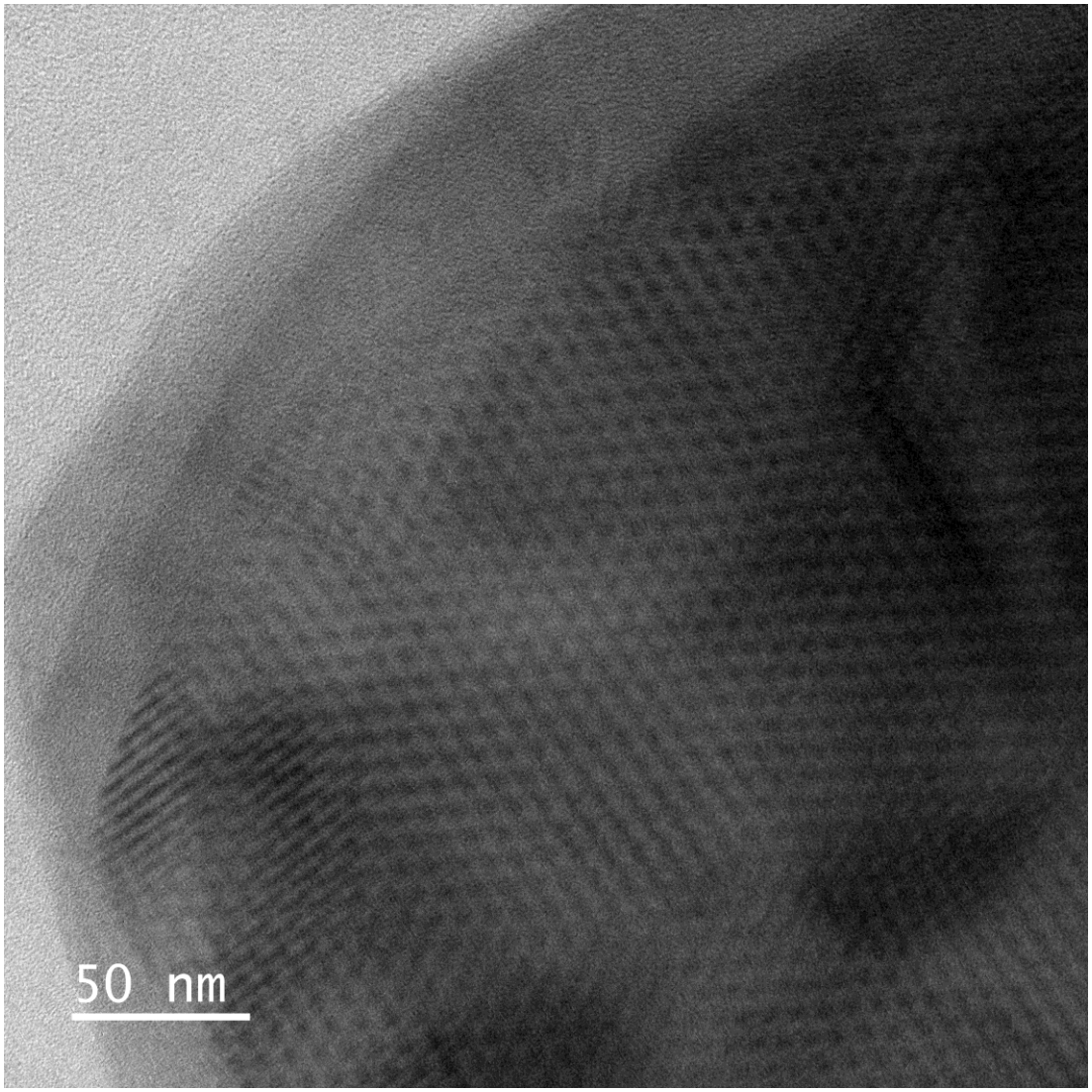

Figure S5 High-resolution TEM image of the three misaligned hBN thin films, resulting in the Moire pattern.

Bibliography

[1] C. H. Bennett, G. Brassard, *Proceedings of the IEEE International Conference on Computers, Systems and Signal Processing* **1984**, 175.
[2] C. H. Bennett, G. Brassard, Quantum cryptography: Public key distribution and coin tossing, *Theoretical Computer Science* **2014**, *560*, 7.
[3] W. K. Wootters, W. H. Zurek, A single quantum cannot be cloned, *Nature* **1982**, *299*, 802.
[4] P. Migdał, K. Jankiewicz, P. Grabarz, C. Decaroli, P. Cochin, Visualizing quantum mechanics in an interactive simulation – Virtual Lab by Quantum Flytrap, *Optical Engineering* **2022**, *61*, 081808.
[5] S.-K. Liao, W.-Q. Cai, W.-Y. Liu, L. Zhang, Y. Li, J.-G. Ren, J. Yin, Q. Shen, Y. Cao, Z.-P. Li, F.-Z. Li, X.-W. Chen, L.-H. Sun, J.-J. Jia, J.-C. Wu, X.-J. Jiang, J.-F. Wang, Y.-M. Huang, Q. Wang, Y.-L. Zhou, L. Deng, T. Xi, L. Ma, T. Hu, Q. Zhang, Y.-A. Chen, N.-L. Liu, X.-B. Wang, Z.-C. Zhu, C.-Y. Lu, R. Shu, C.-Z. Peng, J.-Y. Wang, J.-W. Pan, Satellite-to-ground quantum key distribution, *Nature* **2017**, *549*, 43.
[6] T. N. A. Mai, M. S. Hossain, N. M. Nguyen, Y. Chen, C. Chen, X. Xu, Q. T. Trinh, T. Dinh, T. T. Tran, Quantum Emitters in Hexagonal Boron Nitride: Principles, Engineering and Applications, *Advanced Functional Materials* **2025**, *n/a*, 2500714.
[7] T. N. A. Mai, S. Ali, M. S. Hossain, C. Chen, L. Ding, Y. Chen, A. S. Solntsev, H. Mou, X. Xu, N. Medhekar, Cryogenic Thermal Shock Effects on Optical Properties of Quantum Emitters in Hexagonal Boron Nitride, *ACS Applied Materials & Interfaces* **2024**, *16*, 19340.
[8] I. Aharonovich, D. Englund, M. Toth, Solid-state single-photon emitters, *Nature Photonics* **2016**, *10*, 631.
[9] A. M. Fox, Solid-State Quantum Emitters, *Advanced Quantum Technologies* **2025**, *8*, 2300390.
[10] A. M. Fox, *Quantum optics: an introduction*, Vol. 15, Oxford university press, **2006**.
[11] S. Haroche, J.-M. Raimond, *Exploring the quantum: atoms, cavities, and photons*, Oxford university press, **2006**.
[12] M. O. Scully, M. S. Zubairy, *Quantum optics*, Cambridge university press, **1997**.
[13] S. Buckley, K. Rivoire, J. Vučković, Engineered quantum dot single-photon sources, *Reports on Progress in Physics* **2012**, *75*, 126503.
[14] T. T. Tran, K. Bray, M. J. Ford, M. Toth, I. Aharonovich, Quantum emission from hexagonal boron nitride monolayers, *Nature Nanotechnology* **2016**, *11*, 37.

[15] D. D. Awschalom, R. Hanson, J. Wrachtrup, B. B. Zhou, Quantum technologies with optically interfaced solid-state spins, *Nature Photonics* **2018**, *12*, 516.
[16] A. R. P. Montblanch, M. Barbone, I. Aharonovich, M. Atatüre, A. C. Ferrari, Layered materials as a platform for quantum technologies, *Nature Nanotechnology* **2023**, *18*, 555.
[17] K. Azuma, S. E. Economou, D. Elkouss, P. Hilaire, L. Jiang, H.-K. Lo, I. Tzitrin, Quantum repeaters: From quantum networks to the quantum internet, *Reviews of Modern Physics* **2023**, *95*, 045006.
[18] C. H. Bennett, D. P. DiVincenzo, Quantum information and computation, *Nature* **2000**, *404*, 247.
[19] B. Lounis, M. Orrit, Single-photon sources, *Reports on Progress in Physics* **2005**, *68*, 1129.
[20] G. Wolfowicz, F. J. Heremans, C. P. Anderson, S. Kanai, H. Seo, A. Gali, G. Galli, D. D. Awschalom, Quantum guidelines for solid-state spin defects, *Nature Reviews Materials* **2021**, *6*, 906.
[21] H. J. Kimble, M. Dagenais, L. Mandel, Photon Antibunching in Resonance Fluorescence, *Physical Review Letters* **1977**, *39*, 691.
[22] A. J. Shields, Semiconductor quantum light sources, *Nature Photonics* **2007**, *1*, 215.
[23] M. Esmann, S. C. Wein, C. Antón-Solanas, Solid-State Single-Photon Sources: Recent Advances for Novel Quantum Materials, *Advanced Functional Materials* **2024**, *34*, 2315936.
[24] F. Kulzer, M. Orrit, Single-molecule optics, *Annu. Rev. Phys. Chem.* **2004**, *55*, 585.
[25] C. Bradac, W. Gao, J. Forneris, M. E. Trusheim, I. Aharonovich, Quantum nanophotonics with group IV defects in diamond, *Nature Communications* **2019**, *10*, 5625.
[26] M. W. Doherty, N. B. Manson, P. Delaney, F. Jelezko, J. Wrachtrup, L. C. L. Hollenberg, The nitrogen-vacancy colour centre in diamond, *Physics Reports* **2013**, *528*, 1.
[27] A. Lohrmann, B. C. Johnson, J. C. McCallum, S. Castelletto, A review on single photon sources in silicon carbide, *Reports on Progress in Physics* **2017**, *80*, 034502.
[28] S. Castelletto, Silicon carbide single-photon sources: challenges and prospects, *Materials for Quantum Technology* **2021**, *1*, 023001.
[29] Y. Zhou, Z. Wang, A. Rasmita, S. Kim, A. Berhane, Z. Bodrog, G. Adamo, A. Gali, I. Aharonovich, W.-b. Gao, Room temperature solid-state quantum emitters in the telecom range, *Science Advances* **2018**, *4*, eaar3580.
[30] A. M. Berhane, K.-Y. Jeong, Z. Bodrog, S. Fiedler, T. Schröder, N. V. Triviño, T. Palacios, A. Gali, M. Toth, D. Englund, I. Aharonovich,

Bright Room-Temperature Single-Photon Emission from Defects in Gallium Nitride, *Advanced Materials* **2017**, *29*, 1605092.
[31] X. Ma, N. F. Hartmann, J. K. S. Baldwin, S. K. Doorn, H. Htoon, Room-temperature single-photon generation from solitary dopants of carbon nanotubes, *Nature Nanotechnology* **2015**, *10*, 671.
[32] X. He, H. Htoon, S. K. Doorn, W. H. P. Pernice, F. Pyatkov, R. Krupke, A. Jeantet, Y. Chassagneux, C. Voisin, Carbon nanotubes as emerging quantum-light sources, *Nature Materials* **2018**, *17*, 663.
[33] M. Turunen, M. Brotons-Gisbert, Y. Dai, Y. Wang, E. Scerri, C. Bonato, K. D. Jöns, Z. Sun, B. D. Gerardot, Quantum photonics with layered 2D materials, *Nature Reviews Physics* **2022**, *4*, 219.
[34] S. I. Azzam, K. Parto, G. Moody, Prospects and challenges of quantum emitters in 2D materials, *Applied Physics Letters* **2021**, *118*, 240502.
[35] M. Toth, I. Aharonovich, Single Photon Sources in Atomically Thin Materials, *Annual Review of Physical Chemistry* **2019**, *70*, 123.
[36] Y. Lin, J. W. Connell, Advances in 2D boron nitride nanostructures: nanosheets, nanoribbons, nanomeshes, and hybrids with graphene, *Nanoscale* **2012**, *4*, 6908.
[37] I. Aharonovich, J.-P. Tetienne, M. Toth, Quantum Emitters in Hexagonal Boron Nitride, *Nano Letters* **2022**, *22*, 9227.
[38] M. Kianinia, Z.-Q. Xu, M. Toth, I. Aharonovich, Quantum emitters in 2D materials: Emitter engineering, photophysics, and integration in photonic nanostructures, *Applied Physics Reviews* **2022**, *9*, 011306.
[39] A. B. D.-a.-j.-w.-i. Shaik, P. Palla, Optical quantum technologies with hexagonal boron nitride single photon sources, *Scientific Reports* **2021**, *11*, 12285.
[40] S. Vaidya, X. Gao, S. Dikshit, I. Aharonovich, T. Li, Quantum sensing and imaging with spin defects in hexagonal boron nitride, *Advances in Physics: X* **2023**, *8*, 2206049.
[41] J. Storteboom, P. Dolan, S. Castelletto, X. Li, M. Gu, Lifetime investigation of single nitrogen vacancy centres in nanodiamonds, *Optics Express* **2015**, *23*, 11327.
[42] N. Nikolay, N. Mendelson, E. Özelci, B. Sontheimer, F. Böhm, G. Kewes, M. Toth, I. Aharonovich, O. Benson, Direct measurement of quantum efficiency of single-photon emitters in hexagonal boron nitride, *Optica* **2019**, *6*, 1084.
[43] C. Wang, C. Kurtsiefer, H. Weinfurter, B. Burchard, Single photon emission from SiV centres in diamond produced by ion implantation, *Journal of Physics B: Atomic, Molecular and Optical Physics* **2006**, *39*, 37.

[44] M. Nguyen, N. Nikolay, C. Bradac, M. Kianinia, E. Ekimov, N. Mendelson, O. Benson, I. Aharonovich, Photodynamics and quantum efficiency of germanium vacancy color centers in diamond, *Advanced Photonics* **2019**, *1*, 066002.
[45] Y. Rah, Y. Jin, S. Kim, K. Yu, Optical analysis of the refractive index and birefringence of hexagonal boron nitride from the visible to near-infrared, *Optics Letters* **2019**, *44*, 3797.
[46] G. Grosso, H. Moon, B. Lienhard, S. Ali, D. K. Efetov, M. M. Furchi, P. Jarillo-Herrero, M. J. Ford, I. Aharonovich, D. Englund, Tunable and high-purity room temperature single-photon emission from atomic defects in hexagonal boron nitride, *Nature Communications* **2017**, *8*, 705.
[47] G. Noh, D. Choi, J.-H. Kim, D.-G. Im, Y.-H. Kim, H. Seo, J. Lee, Stark Tuning of Single-Photon Emitters in Hexagonal Boron Nitride, *Nano Letters* **2018**, *18*, 4710.
[48] N. V. Proscia, Z. Shotan, H. Jayakumar, P. Reddy, C. Cohen, M. Dollar, A. Alkauskas, M. Doherty, C. A. Meriles, V. M. Menon, Near-deterministic activation of room-temperature quantum emitters in hexagonal boron nitride, *Optica* **2018**, *5*, 1128.
[49] C. Li, Z.-Q. Xu, N. Mendelson, M. Kianinia, M. Toth, I. Aharonovich, Purification of single-photon emission from hBN using post-processing treatments, *Nanophotonics* **2019**, *8*, 2049.
[50] T. Vogl, G. Campbell, B. C. Buchler, Y. Lu, P. K. Lam, Fabrication and Deterministic Transfer of High-Quality Quantum Emitters in Hexagonal Boron Nitride, *ACS Photonics* **2018**, *5*, 2305.
[51] L. Gan, D. Zhang, R. Zhang, Q. Zhang, H. Sun, Y. Li, C.-Z. Ning, Large-Scale, High-Yield Laser Fabrication of Bright and Pure Single-Photon Emitters at Room Temperature in Hexagonal Boron Nitride, *ACS Nano* **2022**, *16*, 14254.
[52] T. Vogl, H. Knopf, M. Weissflog, P. K. Lam, F. Eilenberger, Sensitive single-photon test of extended quantum theory with two-dimensional hexagonal boron nitride, *Physical Review Research* **2021**, *3*, 013296.
[53] L. Orphal-Kobin, K. Unterguggenberger, T. Pregnolato, N. Kemf, M. Matalla, R.-S. Unger, I. Ostermay, G. Pieplow, T. Schröder, Optically Coherent Nitrogen-Vacancy Defect Centers in Diamond Nanostructures, *Physical Review X* **2023**, *13*, 011042.
[54] T. T. Tran, M. Kianinia, M. Nguyen, S. Kim, Z.-Q. Xu, A. Kubanek, M. Toth, I. Aharonovich, Resonant Excitation of Quantum Emitters in Hexagonal Boron Nitride, *ACS Photonics* **2018**, *5*, 295.
[55] A. Dietrich, M. Bürk, E. S. Steiger, L. Antoniuk, T. T. Tran, M. Nguyen, I. Aharonovich, F. Jelezko, A. Kubanek, Observation of Fourier

transform limited lines in hexagonal boron nitride, *Physical review B* **2018**, *98*, 081414.
[56] T. T. Tran, C. Bradac, A. S. Solntsev, M. Toth, I. Aharonovich, Suppression of spectral diffusion by anti-Stokes excitation of quantum emitters in hexagonal boron nitride, *Applied Physics Letters* **2019**, *115*, 071102.
[57] C. Fournier, K. Watanabe, T. Taniguchi, J. Barjon, S. Buil, J.-P. Hermier, A. Delteil, Investigating the fast spectral diffusion of a quantum emitter in hBN using resonant excitation and photon correlations, *Physical review B* **2023**, *107*, 195304.
[58] L. Sapienza, M. Davanço, A. Badolato, K. Srinivasan, Nanoscale optical positioning of single quantum dots for bright and pure single-photon emission, *Nature Communications* **2015**, *6*, 7833.
[59] X. He, N. F. Hartmann, X. Ma, Y. Kim, R. Ihly, J. L. Blackburn, W. Gao, J. Kono, Y. Yomogida, A. Hirano, T. Tanaka, H. Kataura, H. Htoon, S. K. Doorn, Tunable room-temperature single-photon emission at telecom wavelengths from sp3 defects in carbon nanotubes, *Nature Photonics* **2017**, *11*, 577.
[60] H. L. Stern, C. M. Gilardoni, Q. Gu, S. Eizagirre Barker, O. F. J. Powell, X. Deng, S. A. Fraser, L. Follet, C. Li, A. J. Ramsay, H. H. Tan, I. Aharonovich, M. Atatüre, A quantum coherent spin in hexagonal boron nitride at ambient conditions, *Nature Materials* **2024**, *23*, 1379.
[61] N. Mendelson, D. Chugh, J. R. Reimers, T. S. Cheng, A. Gottscholl, H. Long, C. J. Mellor, A. Zettl, V. Dyakonov, P. H. Beton, S. V. Novikov, C. Jagadish, H. H. Tan, M. J. Ford, M. Toth, C. Bradac, I. Aharonovich, Identifying carbon as the source of visible single-photon emission from hexagonal boron nitride, *Nature Materials* **2021**, *20*, 321.
[62] A. Gottscholl, M. Kianinia, V. Soltamov, S. Orlinskii, G. Mamin, C. Bradac, C. Kasper, K. Krambrock, A. Sperlich, M. Toth, I. Aharonovich, V. Dyakonov, Initialization and read-out of intrinsic spin defects in a van der Waals crystal at room temperature, *Nature Materials* **2020**, *19*, 540.
[63] T. T. Tran, C. Elbadawi, D. Totonjian, C. J. Lobo, G. Grosso, H. Moon, D. R. Englund, M. J. Ford, I. Aharonovich, M. Toth, Robust Multicolor Single Photon Emission from Point Defects in Hexagonal Boron Nitride, *ACS Nano* **2016**, *10*, 7331.
[64] R. Bourrellier, S. Meuret, A. Tararan, O. Stéphan, M. Kociak, L. H. G. Tizei, A. Zobelli, Bright UV Single Photon Emission at Point Defects in h-BN, *Nano Letters* **2016**, *16*, 4317.
[65] M. Mackoit-Sinkevičienė, M. Maciaszek, C. G. Van de Walle, A. Alkauskas, Carbon dimer defect as a source of the 4.1 eV luminescence in hexagonal boron nitride, *Applied Physics Letters* **2019**, *115*, 212101.

[66] H. Hamdi, G. Thiering, Z. Bodrog, V. Ivády, A. Gali, Stone–Wales defects in hexagonal boron nitride as ultraviolet emitters, *npj Computational Materials* **2020**, *6*, 178.
[67] S. Li, A. Pershin, G. Thiering, P. Udvarhelyi, A. Gali, Ultraviolet Quantum Emitters in Hexagonal Boron Nitride from Carbon Clusters, *The Journal of Physical Chemistry Letters* **2022**, *13*, 3150.
[68] I. Zhigulin, J. Horder, V. Ivády, S. J. U. White, A. Gale, C. Li, C. J. Lobo, M. Toth, I. Aharonovich, M. Kianinia, Stark Effect of Blue Quantum Emitters in Hexagonal Boron Nitride, *Physical Review Applied* **2023**, *19*, 044011.
[69] M. Maciaszek, L. Razinkovas, Blue Quantum Emitter in Hexagonal Boron Nitride and a Carbon Chain Tetramer: a First-Principles Study, *ACS Applied Nano Materials* **2024**, *7*, 18979.
[70] D. Kozawa, S. X. Li, T. Ichihara, A. G. Rajan, X. Gong, G. He, V. B. Koman, Y. Zeng, M. Kuehne, K. S. Silmore, D. Parviz, P. Liu, A. T. Liu, S. Faucher, Z. Yuan, J. Warner, D. Blankschtein, M. S. Strano, Discretized hexagonal boron nitride quantum emitters and their chemical interconversion, *Nanotechnology* **2023**, *34*, 115702.
[71] F. Hayee, L. Yu, J. L. Zhang, C. J. Ciccarino, M. Nguyen, A. F. Marshall, I. Aharonovich, J. Vučković, P. Narang, T. F. Heinz, J. A. Dionne, Revealing multiple classes of stable quantum emitters in hexagonal boron nitride with correlated optical and electron microscopy, *Nature Materials* **2020**, *19*, 534.
[72] X. Li, G. D. Shepard, A. Cupo, N. Camporeale, K. Shayan, Y. Luo, V. Meunier, S. Strauf, Nonmagnetic Quantum Emitters in Boron Nitride with Ultranarrow and Sideband-Free Emission Spectra, *ACS Nano* **2017**, *11*, 6652.
[73] M. S. Islam, R. K. Chowdhury, M. Barthelemy, L. Moczko, P. Hebraud, S. Berciaud, A. Barsella, F. Fras, Large-Scale Statistical Analysis of Defect Emission in hBN: Revealing Spectral Families and Influence of Flake Morphology, *ACS Nano* **2024**, *18*, 20980.
[74] M. E. Turiansky, A. Alkauskas, L. C. Bassett, C. G. Van de Walle, Dangling Bonds in Hexagonal Boron Nitride as Single-Photon Emitters, *Physical Review Letters* **2019**, *123*, 127401.
[75] Q. Tan, J.-M. Lai, X.-L. Liu, D. Guo, Y. Xue, X. Dou, B.-Q. Sun, H.-X. Deng, P.-H. Tan, I. Aharonovich, W. Gao, J. Zhang, Donor–Acceptor Pair Quantum Emitters in Hexagonal Boron Nitride, *Nano Letters* **2022**, *22*, 1331.
[76] C. Jara, T. Rauch, S. Botti, M. A. L. Marques, A. Norambuena, R. Coto, J. E. Castellanos-Águila, J. R. Maze, F. Munoz, First-Principles Identification of Single Photon Emitters Based on Carbon Clusters in

Hexagonal Boron Nitride, *The Journal of Physical Chemistry A* **2021**, *125*, 1325.
[77] S. A. Tawfik, S. Ali, M. Fronzi, M. Kianinia, T. T. Tran, C. Stampfl, I. Aharonovich, M. Toth, M. J. Ford, First-principles investigation of quantum emission from hBN defects, *Nanoscale* **2017**, *9*, 13575.
[78] Á. Ganyecz, R. Babar, Z. Benedek, I. Aharonovich, G. Barcza, V. Ivády, First-principles theory of the nitrogen interstitial in hBN: a plausible model for the blue emitter, *Nanoscale* **2024**, *16*, 4125.
[79] Q. T. Trinh, A. Banerjee, Y. Yang, S. H. Mushrif, Sub-Surface Boron-Doped Copper for Methane Activation and Coupling: First-Principles Investigation of the Structure, Activity, and Selectivity of the Catalyst, *The Journal of Physical Chemistry C* **2017**, *121*, 1099.
[80] Q. T. Trinh, K. Bhola, P. N. Amaniampong, F. Jérôme, S. H. Mushrif, Synergistic Application of XPS and DFT to Investigate Metal Oxide Surface Catalysis, *The Journal of Physical Chemistry C* **2018**, *122*, 22397.
[81] B. Chettri, P. K. Patra, N. N. Hieu, D. P. Rai, Hexagonal boron nitride (h-BN) nanosheet as a potential hydrogen adsorption material: A density functional theory (DFT) study, *Surfaces and Interfaces* **2021**, *24*, 101043.
[82] F. Ducry, D. Waldhoer, T. Knobloch, M. Csontos, N. Jimenez Olalla, J. Leuthold, T. Grasser, M. Luisier, An ab initio study on resistance switching in hexagonal boron nitride, *npj 2D Materials and Applications* **2022**, *6*, 58.
[83] J. R. Reimers, A. Sajid, R. Kobayashi, M. J. Ford, Understanding and Calibrating Density-Functional-Theory Calculations Describing the Energy and Spectroscopy of Defect Sites in Hexagonal Boron Nitride, *Journal of Chemical Theory and Computation* **2018**, *14*, 1602.
[84] M. Novotný, M. Dubecký, F. Karlický, Toward accurate modeling of structure and energetics of bulk hexagonal boron nitride, *Journal of Computational Chemistry* **2024**, *45*, 115.
[85] P. Huang, M. Grzeszczyk, K. Vaklinova, K. Watanabe, T. Taniguchi, K. S. Novoselov, M. Koperski, Carbon and vacancy centers in hexagonal boron nitride, *Physical review B* **2022**, *106*, 014107.
[86] R. W. Dorn, P. M. Heintz, I. Hung, K. Chen, J.-S. Oh, T.-H. Kim, L. Zhou, Z. Gan, W. Huang, A. J. Rossini, Atomic-Level Structure of Mesoporous Hexagonal Boron Nitride Determined by High-Resolution Solid-State Multinuclear Magnetic Resonance Spectroscopy and Density Functional Theory Calculations, *Chemistry of Materials* **2022**, *34*, 1649.
[87] M. A. Sakib, B. Triplett, W. Harris, N. Hussain, A. Senichev, M. Momenzadeh, J. Bocanegra, P. Vabishchevich, R. Wu, A. Boltasseva, V.

M. Shalaev, M. R. Shcherbakov, Purcell-Induced Bright Single Photon Emitters in Hexagonal Boron Nitride, *Nano Letters* **2024**, *24*, 12390.
[88] M. K. Prasad, O. A. Al-Ani, J. P. Goss, J. D. Mar, Charge transfer due to defects in hexagonal boron nitride/graphene heterostructures: An ab initio study, *Physical Review Materials* **2023**, *7*, 094003.
[89] F. Wu, A. Galatas, R. Sundararaman, D. Rocca, Y. Ping, First-principles engineering of charged defects for two-dimensional quantum technologies, *Physical Review Materials* **2017**, *1*, 071001.
[90] O. Golami, K. Sharman, R. Ghobadi, S. C. Wein, H. Zadeh-Haghighi, C. Gomes da Rocha, D. R. Salahub, C. Simon, $Ab initio$ and group theoretical study of properties of a carbon trimer defect in hexagonal boron nitride, *Physical review B* **2022**, *105*, 184101.
[91] K. Li, T. J. Smart, Y. Ping, Carbon trimer as a 2 eV single-photon emitter candidate in hexagonal boron nitride: A first-principles study, *Physical Review Materials* **2022**, *6*, L042201.
[92] S. Li, A. Pershin, P. Li, A. Gali, Exceptionally strong coupling of defect emission in hexagonal boron nitride to stacking sequences, *npj 2D Materials and Applications* **2024**, *8*, 16.
[93] V. Ivády, G. Barcza, G. Thiering, S. Li, H. Hamdi, J.-P. Chou, Ö. Legeza, A. Gali, Ab initio theory of the negatively charged boron vacancy qubit in hexagonal boron nitride, *npj Computational Materials* **2020**, *6*, 41.
[94] C. Cholsuk, A. Zand, A. Çakan, T. Vogl, The hBN Defects Database: A Theoretical Compilation of Color Centers in Hexagonal Boron Nitride, *The Journal of Physical Chemistry C* **2024**, *128*, 12716.
[95] Y. Shen, S. Zhu, Machine learning mechanical properties of defect-engineered hexagonal boron nitride, *Computational Materials Science* **2023**, *220*, 112030.
[96] F. L. Thiemann, P. Rowe, E. A. Müller, A. Michaelides, Machine Learning Potential for Hexagonal Boron Nitride Applied to Thermally and Mechanically Induced Rippling, *The Journal of Physical Chemistry C* **2020**, *124*, 22278.
[97] R. Pederson, B. Kalita, K. Burke, Machine learning and density functional theory, *Nature Reviews Physics* **2022**, *4*, 357.
[98] B. Huang, G. F. von Rudorff, O. A. von Lilienfeld, The central role of density functional theory in the AI age, *Science* **2023**, *381*, 170.
[99] N. Alem, R. Erni, C. Kisielowski, M. D. Rossell, W. Gannett, A. Zettl, Atomically thin hexagonal boron nitride probed by ultrahigh-resolution transmission electron microscopy, *Physical review B* **2009**, *80*, 155425.

[100] C. Jin, F. Lin, K. Suenaga, S. Iijima, Fabrication of a Freestanding Boron Nitride Single Layer and Its Defect Assignments, *Physical Review Letters* **2009**, *102*, 195505.
[101] J. C. Meyer, A. Chuvilin, G. Algara-Siller, J. Biskupek, U. Kaiser, Selective Sputtering and Atomic Resolution Imaging of Atomically Thin Boron Nitride Membranes, *Nano Letters* **2009**, *9*, 2683.
[102] G. H. Ryu, H. J. Park, J. Ryou, J. Park, J. Lee, G. Kim, H. S. Shin, C. W. Bielawski, R. S. Ruoff, S. Hong, Z. Lee, Atomic-scale dynamics of triangular hole growth in monolayer hexagonal boron nitride under electron irradiation, *Nanoscale* **2015**, *7*, 10600.
[103] J. H. Warner, M. H. Rümmeli, A. Bachmatiuk, B. Büchner, Atomic Resolution Imaging and Topography of Boron Nitride Sheets Produced by Chemical Exfoliation, *ACS Nano* **2010**, *4*, 1299.
[104] T. A. Bui, G. T. Leuthner, J. Madsen, M. R. A. Monazam, A. I. Chirita, A. Postl, C. Mangler, J. Kotakoski, T. Susi, Creation of Single Vacancies in hBN with Electron Irradiation, *Small* **2023**, *19*, 2301926.
[105] H. Park, Y. Wen, S. X. Li, W. Choi, G.-D. Lee, M. Strano, J. H. Warner, Atomically Precise Control of Carbon Insertion into hBN Monolayer Point Vacancies using a Focused Electron Beam Guide, *Small* **2021**, *17*, 2100693.
[106] S. Singla, P. Joshi, G. I. López-Morales, S. Sarkar, S. Sarkar, J. Flick, B. Chakraborty, Probing Correlation of Optical Emission and Defect Sites in Hexagonal Boron Nitride by High-Resolution STEM-EELS, *Nano Letters* **2024**, *24*, 9212.
[107] Y. Shi, C. Hamsen, X. Jia, K. K. Kim, A. Reina, M. Hofmann, A. L. Hsu, K. Zhang, H. Li, Z.-Y. Juang, M. S. Dresselhaus, L.-J. Li, J. Kong, Synthesis of Few-Layer Hexagonal Boron Nitride Thin Film by Chemical Vapor Deposition, *Nano Letters* **2010**, *10*, 4134.
[108] L. Song, L. Ci, H. Lu, P. B. Sorokin, C. Jin, J. Ni, A. G. Kvashnin, D. G. Kvashnin, J. Lou, B. I. Yakobson, P. M. Ajayan, Large Scale Growth and Characterization of Atomic Hexagonal Boron Nitride Layers, *Nano Letters* **2010**, *10*, 3209.
[109] K. K. Kim, A. Hsu, X. Jia, S. M. Kim, Y. Shi, M. Hofmann, D. Nezich, J. F. Rodriguez-Nieva, M. Dresselhaus, T. Palacios, J. Kong, Synthesis of Monolayer Hexagonal Boron Nitride on Cu Foil Using Chemical Vapor Deposition, *Nano Letters* **2012**, *12*, 161.
[110] J. S. Lee, S. H. Choi, S. J. Yun, Y. I. Kim, S. Boandoh, J.-H. Park, B. G. Shin, H. Ko, S. H. Lee, Y.-M. Kim, Y. H. Lee, K. K. Kim, S. M. Kim, Wafer-scale single-crystal hexagonal boron nitride film via self-collimated grain formation, *Science* **2018**, *362*, 817.
[111] T.-A. Chen, C.-P. Chuu, C.-C. Tseng, C.-K. Wen, H. S. P. Wong, S. Pan, R. Li, T.-A. Chao, W.-C. Chueh, Y. Zhang, Q. Fu, B. I. Yakobson,

W.-H. Chang, L.-J. Li, Wafer-scale single-crystal hexagonal boron nitride monolayers on Cu (111), *Nature* **2020**, *579*, 219.
[112] N. Mendelson, Z.-Q. Xu, T. T. Tran, M. Kianinia, J. Scott, C. Bradac, I. Aharonovich, M. Toth, Engineering and Tuning of Quantum Emitters in Few-Layer Hexagonal Boron Nitride, *ACS Nano* **2019**, *13*, 3132.
[113] I. H. Abidi, N. Mendelson, T. T. Tran, A. Tyagi, M. Zhuang, L.-T. Weng, B. Özyilmaz, I. Aharonovich, M. Toth, Z. Luo, Selective Defect Formation in Hexagonal Boron Nitride, *Advanced Optical Materials* **2019**, *7*, 1900397.
[114] C. Li, N. Mendelson, R. Ritika, Y. Chen, Z.-Q. Xu, M. Toth, I. Aharonovich, Scalable and Deterministic Fabrication of Quantum Emitter Arrays from Hexagonal Boron Nitride, *Nano Letters* **2021**, *21*, 3626.
[115] Y. Chen, X. Xu, C. Li, A. Bendavid, M. T. Westerhausen, C. Bradac, M. Toth, I. Aharonovich, T. T. Tran, Bottom-Up Synthesis of Hexagonal Boron Nitride Nanoparticles with Intensity-Stabilized Quantum Emitters, *Small* **2021**, *17*, 2008062.
[116] N. M. H. Duong, E. Glushkov, A. Chernev, V. Navikas, J. Comtet, M. A. P. Nguyen, M. Toth, A. Radenovic, T. T. Tran, I. Aharonovich, Facile Production of Hexagonal Boron Nitride Nanoparticles by Cryogenic Exfoliation, *Nano Letters* **2019**, *19*, 5417.
[117] E. Burcu, *Powder Preparation, Properties and Industrial Applications of Hexagonal Boron Nitride*, in *Sintering Applications*, (Ed: E. Burcu), IntechOpen, Rijeka, Croatia **2013**, Ch. 2.
[118] T. Taniguchi, K. Watanabe, Synthesis of high-purity boron nitride single crystals under high pressure by using Ba–BN solvent, *Journal of Crystal Growth* **2007**, *303*, 525.
[119] L. Schué, I. Stenger, F. Fossard, A. Loiseau, J. Barjon, Characterization methods dedicated to nanometer-thick hBN layers, *2D Materials* **2017**, *4*, 015028.
[120] Y. Li, V. Garnier, P. Steyer, C. Journet, B. Toury, Millimeter-Scale Hexagonal Boron Nitride Single Crystals for Nanosheet Generation, *ACS Applied Nano Materials* **2020**, *3*, 1508.
[121] T. B. Hoffman, B. Clubine, Y. Zhang, K. Snow, J. H. Edgar, Optimization of Ni–Cr flux growth for hexagonal boron nitride single crystals, *Journal of Crystal Growth* **2014**, *393*, 114.
[122] S. Liu, R. He, L. Xue, J. Li, B. Liu, J. H. Edgar, Single Crystal Growth of Millimeter-Sized Monoisotopic Hexagonal Boron Nitride, *Chemistry of Materials* **2018**, *30*, 6222.
[123] N. Zhang, N. Yang, W. Wang, X. Zhong, X. Chen, Growth of hexagonal boron nitride crystals at atmospheric pressure from CuCr flux, *Journal of Crystal Growth* **2021**, *562*, 126074.

[124] S. Liu, R. He, Z. Ye, X. Du, J. Lin, H. Jiang, B. Liu, J. H. Edgar, Large-Scale Growth of High-Quality Hexagonal Boron Nitride Crystals at Atmospheric Pressure from an Fe–Cr Flux, *Crystal Growth & Design* **2017**, *17*, 4932.
[125] J. Li, C. Elias, G. Ye, D. Evans, S. Liu, R. He, G. Cassabois, B. Gil, P. Valvin, B. Liu, J. H. Edgar, Single crystal growth of monoisotopic hexagonal boron nitride from a Fe–Cr flux, *Journal of Materials Chemistry C* **2020**, *8*, 9931.
[126] C. Maestre, P. Steyer, B. Toury, C. Journet, V. Garnier, Hexagonal Boron Nitride Crystal Growth in the Li3BN2-BN System, *Chemistry of Materials* **2024**, *36*, 9848.
[127] L. J. Martínez, T. Pelini, V. Waselowski, J. R. Maze, B. Gil, G. Cassabois, V. Jacques, Efficient single photon emission from a high-purity hexagonal boron nitride crystal, *Physical review B* **2016**, *94*, 121405.
[128] Y. Chen, M. T. Westerhausen, C. Li, S. White, C. Bradac, A. Bendavid, M. Toth, I. Aharonovich, T. T. Tran, Solvent-Exfoliated Hexagonal Boron Nitride Nanoflakes for Quantum Emitters, *ACS Applied Nano Materials* **2021**, *4*, 10449.
[129] K. S. Novoselov, A. K. Geim, S. V. Morozov, D. Jiang, Y. Zhang, S. V. Dubonos, I. V. Grigorieva, A. A. Firsov, Electric Field Effect in Atomically Thin Carbon Films, *Science* **2004**, *306*, 666.
[130] G. Clark, J. R. Schaibley, J. Ross, T. Taniguchi, K. Watanabe, J. R. Hendrickson, S. Mou, W. Yao, X. Xu, Single Defect Light-Emitting Diode in a van der Waals Heterostructure, *Nano Letters* **2016**, *16*, 3944.
[131] S. J. U. White, T. Yang, N. Dontschuk, C. Li, Z.-Q. Xu, M. Kianinia, A. Stacey, M. Toth, I. Aharonovich, Electrical control of quantum emitters in a Van der Waals heterostructure, *Light: Science & Applications* **2022**, *11*, 186.
[132] H. Akbari, S. Biswas, P. K. Jha, J. Wong, B. Vest, H. A. Atwater, Lifetime-Limited and Tunable Quantum Light Emission in h-BN via Electric Field Modulation, *Nano Letters* **2022**, *22*, 7798.
[133] Y. Yu, I. C. Seo, M. Luo, K. Lu, B. Son, J. K. Tan, D. Nam, Tunable single-photon emitters in 2D materials, *Nanophotonics* **2024**, *13*, 3615.
[134] T. T. Tran, C. Zachreson, A. M. Berhane, K. Bray, R. G. Sandstrom, L. H. Li, T. Taniguchi, K. Watanabe, I. Aharonovich, M. Toth, Quantum Emission from Defects in Single-Crystalline Hexagonal Boron Nitride, *Physical Review Applied* **2016**, *5*, 034005.
[135] Y. Chen, C. Li, S. White, M. Nonahal, Z. Q. Xu, K. Watanabe, T. Taniguchi, M. Toth, T. T. Tran, I. Aharonovich, Generation of High-Density Quantum Emitters in High-Quality, Exfoliated Hexagonal Boron Nitride, *ACS Applied Materials & Interfaces* **2021**, *13*, 47283.

[136] Z.-Q. Xu, C. Elbadawi, T. T. Tran, M. Kianinia, X. Li, D. Liu, T. B. Hoffman, M. Nguyen, S. Kim, J. H. Edgar, X. Wu, L. Song, S. Ali, M. Ford, M. Toth, I. Aharonovich, Single photon emission from plasma treated 2D hexagonal boron nitride, *Nanoscale* **2018**, *10*, 7957.
[137] C. Elbadawi, T. T. Tran, M. Kolíbal, T. Šikola, J. Scott, Q. Cai, L. H. Li, T. Taniguchi, K. Watanabe, M. Toth, I. Aharonovich, C. Lobo, Electron beam directed etching of hexagonal boron nitride, *Nanoscale* **2016**, *8*, 16182.
[138] S. Choi, T. T. Tran, C. Elbadawi, C. Lobo, X. Wang, S. Juodkazis, G. Seniutinas, M. Toth, I. Aharonovich, Engineering and Localization of Quantum Emitters in Large Hexagonal Boron Nitride Layers, *ACS Applied Materials & Interfaces* **2016**, *8*, 29642.
[139] A. Kumar, Ç. Samaner, C. Cholsuk, T. Matthes, S. Paçal, Y. Oyun, A. Zand, R. J. Chapman, G. Saerens, R. Grange, S. Suwanna, S. Ateş, T. Vogl, Polarization Dynamics of Solid-State Quantum Emitters, *ACS Nano* **2024**, *18*, 5270.
[140] C. Fournier, A. Plaud, S. Roux, A. Pierret, M. Rosticher, K. Watanabe, T. Taniguchi, S. Buil, X. Quelin, J. Barjon, J. P. Hermier, A. Delteil, Position-controlled quantum emitters with reproducible emission wavelength in hexagonal boron nitride, *Nature Communications* **2021**, *12*, 3779.
[141] A. Gale, C. Li, Y. Chen, K. Watanabe, T. Taniguchi, I. Aharonovich, M. Toth, Site-Specific Fabrication of Blue Quantum Emitters in Hexagonal Boron Nitride, *ACS Photonics* **2022**, *9*, 2170.
[142] Y. Chen, A. Gale, K. Yamamura, J. Horder, A. Condos, K. Watanabe, T. Taniguchi, M. Toth, I. Aharonovich, Annealing of blue quantum emitters in carbon-doped hexagonal boron nitride, *Applied Physics Letters* **2023**, *123*, 041902.
[143] C. Fournier, S. Roux, K. Watanabe, T. Taniguchi, S. Buil, J. Barjon, J.-P. Hermier, A. Delteil, Two-Photon Interference from a Quantum Emitter in Hexagonal Boron Nitride, *Physical Review Applied* **2023**, *19*, L041003.
[144] J. Ziegler, R. Klaiss, A. Blaikie, D. Miller, V. R. Horowitz, B. J. Alemán, Deterministic Quantum Emitter Formation in Hexagonal Boron Nitride via Controlled Edge Creation, *Nano Letters* **2019**, *19*, 2121.
[145] M. Hennessey, B. Whitefield, A. Gale, M. Kianinia, J. A. Scott, I. Aharonovich, M. Toth, Framework for Engineering of Spin Defects in Hexagonal Boron Nitride by Focused Ion Beams, *Advanced Quantum Technologies* **2024**, 2300459.
[146] X. Xu, Z. O. Martin, D. Sychev, A. S. Lagutchev, Y. P. Chen, T. Taniguchi, K. Watanabe, V. M. Shalaev, A. Boltasseva, Creating

Quantum Emitters in Hexagonal Boron Nitride Deterministically on Chip-Compatible Substrates, *Nano Letters* **2021**, *21*, 8182.
[147] M. Koperski, K. Pakuła, K. Nogajewski, A. K. Dąbrowska, M. Tokarczyk, T. Pelini, J. Binder, T. Fąs, J. Suffczyński, R. Stępniewski, A. Wysmołek, M. Potemski, Towards practical applications of quantum emitters in boron nitride, *Scientific Reports* **2021**, *11*, 15506.
[148] J. E. Fröch, C. Li, Y. Chen, M. Toth, M. Kianinia, S. Kim, I. Aharonovich, Purcell Enhancement of a Cavity-Coupled Emitter in Hexagonal Boron Nitride, *Small* **2022**, *18*, 2104805.
[149] S. Kim, J. E. Fröch, J. Christian, M. Straw, J. Bishop, D. Totonjian, K. Watanabe, T. Taniguchi, M. Toth, I. Aharonovich, Photonic crystal cavities from hexagonal boron nitride, *Nature Communications* **2018**, *9*, 2623.
[150] L. Sortino, A. Gale, L. Kühner, C. Li, J. Biechteler, F. J. Wendisch, M. Kianinia, H. Ren, M. Toth, S. A. Maier, I. Aharonovich, A. Tittl, Optically addressable spin defects coupled to bound states in the continuum metasurfaces, *Nature Communications* **2024**, *15*, 2008.
[151] C. Li, J. E. Fröch, M. Nonahal, T. N. Tran, M. Toth, S. Kim, I. Aharonovich, Integration of hBN Quantum Emitters in Monolithically Fabricated Waveguides, *ACS Photonics* **2021**, *8*, 2966.
[152] M. Nonahal, C. Li, H. Ren, L. Spencer, M. Kianinia, M. Toth, I. Aharonovich, Engineering Quantum Nanophotonic Components from Hexagonal Boron Nitride, *Laser & Photonics Reviews* **2023**, *17*, 2300019.
[153] D. Gérard, M. Rosticher, K. Watanabe, T. Taniguchi, J. Barjon, S. Buil, J.-P. Hermier, A. Delteil, Top-down integration of an hBN quantum emitter in a monolithic photonic waveguide, *Applied Physics Letters* **2023**, *122*, 264001.
[154] L. Spencer, J. Horder, S. Kim, M. Toth, I. Aharonovich, Monolithic Integration of Single Quantum Emitters in hBN Bullseye Cavities, *ACS Photonics* **2023**, *10*, 4417.
[155] X. Xu, A. B. Solanki, D. Sychev, X. Gao, S. Peana, A. S. Baburin, K. Pagadala, Z. O. Martin, S. N. Chowdhury, Y. P. Chen, T. Taniguchi, K. Watanabe, I. A. Rodionov, A. V. Kildishev, T. Li, P. Upadhyaya, A. Boltasseva, V. M. Shalaev, Greatly Enhanced Emission from Spin Defects in Hexagonal Boron Nitride Enabled by a Low-Loss Plasmonic Nanocavity, *Nano Letters* **2023**, *23*, 25.
[156] T. T. Tran, D. Wang, Z.-Q. Xu, A. Yang, M. Toth, T. W. Odom, I. Aharonovich, Deterministic Coupling of Quantum Emitters in 2D Materials to Plasmonic Nanocavity Arrays, *Nano Letters* **2017**, *17*, 2634.
[157] M. Nguyen, S. Kim, T. T. Tran, Z.-Q. Xu, M. Kianinia, M. Toth, I. Aharonovich, Nanoassembly of quantum emitters in hexagonal boron nitride and gold nanospheres, *Nanoscale* **2018**, *10*, 2267.

[158] S. Kim, N. M. H. Duong, M. Nguyen, T.-J. Lu, M. Kianinia, N. Mendelson, A. Solntsev, C. Bradac, D. R. Englund, I. Aharonovich, Integrated on Chip Platform with Quantum Emitters in Layered Materials, *Advanced Optical Materials* **2019**, *7*, 1901132.
[159] C. Li, J. Jang, T. Badloe, T. Yang, J. Kim, J. Kim, M. Nguyen, S. A. Maier, J. Rho, H. Ren, I. Aharonovich, Arbitrarily structured quantum emission with a multifunctional metalens, *eLight* **2023**, *3*, 19.
[160] T. T. H. Do, M. Nonahal, C. Li, V. Valuckas, H. H. Tan, A. I. Kuznetsov, H. S. Nguyen, I. Aharonovich, S. T. Ha, Room-temperature strong coupling in a single-photon emitter-metasurface system, *Nature Communications* **2024**, *15*, 2281.
[161] K. Parto, S. I. Azzam, N. Lewis, S. D. Patel, S. Umezawa, K. Watanabe, T. Taniguchi, G. Moody, Cavity-Enhanced 2D Material Quantum Emitters Deterministically Integrated with Silicon Nitride Microresonators, *Nano Letters* **2022**, *22*, 9748.
[162] J. E. Fröch, S. Kim, N. Mendelson, M. Kianinia, M. Toth, I. Aharonovich, Coupling Hexagonal Boron Nitride Quantum Emitters to Photonic Crystal Cavities, *ACS Nano* **2020**, *14*, 7085.
[163] T. Vogl, R. Lecamwasam, B. C. Buchler, Y. Lu, P. K. Lam, Compact Cavity-Enhanced Single-Photon Generation with Hexagonal Boron Nitride, *ACS Photonics* **2019**, *6*, 1955.
[164] Y. Chen, T. N. Tran, N. M. H. Duong, C. Li, M. Toth, C. Bradac, I. Aharonovich, A. Solntsev, T. T. Tran, Optical Thermometry with Quantum Emitters in Hexagonal Boron Nitride, *ACS Applied Materials & Interfaces* **2020**, *12*, 25464.
[165] A. J. Healey, S. C. Scholten, T. Yang, J. A. Scott, G. J. Abrahams, I. O. Robertson, X. F. Hou, Y. F. Guo, S. Rahman, Y. Lu, M. Kianinia, I. Aharonovich, J. P. Tetienne, Quantum microscopy with van der Waals heterostructures, *Nature Physics* **2023**, *19*, 87.
[166] X. Lyu, Q. Tan, L. Wu, C. Zhang, Z. Zhang, Z. Mu, J. Zúñiga-Pérez, H. Cai, W. Gao, Strain Quantum Sensing with Spin Defects in Hexagonal Boron Nitride, *Nano Letters* **2022**, *22*, 6553.
[167] A. Gottscholl, M. Diez, V. Soltamov, C. Kasper, D. Krauße, A. Sperlich, M. Kianinia, C. Bradac, I. Aharonovich, V. Dyakonov, Spin defects in hBN as promising temperature, pressure and magnetic field quantum sensors, *Nature Communications* **2021**, *12*, 4480.
[168] N. Ronceray, Y. You, E. Glushkov, M. Lihter, B. Rehl, T.-H. Chen, G.-H. Nam, F. Borza, K. Watanabe, T. Taniguchi, S. Roke, A. Keerthi, J. Comtet, B. Radha, A. Radenovic, Liquid-activated quantum emission from pristine hexagonal boron nitride for nanofluidic sensing, *Nature Materials* **2023**, *22*, 1236.

[169] A. Al-Juboori, H. Z. J. Zeng, M. A. P. Nguyen, X. Ai, A. Laucht, A. Solntsev, M. Toth, R. Malaney, I. Aharonovich, Quantum Key Distribution Using a Quantum Emitter in Hexagonal Boron Nitride, *Advanced Quantum Technologies* **2023**, *6*, 2300038.
[170] Ç. Samaner, S. Paçal, G. Mutlu, K. Uyanık, S. Ateş, Free-Space Quantum Key Distribution with Single Photons from Defects in Hexagonal Boron Nitride, *Advanced Quantum Technologies* **2022**, *5*, 2200059.
[171] D. Scognamiglio, A. Gale, A. Al-Juboori, M. Toth, I. Aharonovich, On-demand quantum light sources for underwater communications, *Materials for Quantum Technology* **2024**, *4*, 025402.
[172] R. M. Pope, E. S. Fry, Absorption spectrum (380–700 nm) of pure water. II. Integrating cavity measurements, *Applied Optics* **1997**, *36*, 8710.
[173] M. Abasifard, C. Cholsuk, R. G. Pousa, A. Kumar, A. Zand, T. Riel, D. K. L. Oi, T. Vogl, The ideal wavelength for daylight free-space quantum key distribution, *APL Quantum* **2024**, *1*, 016113.
[174] N. Ahmadi, S. Schwertfeger, P. Werner, L. Wiese, J. Lester, E. Da Ros, J. Krause, S. Ritter, M. Abasifard, C. Cholsuk, R. G. Krämer, S. Atzeni, M. Gündoğan, S. Sachidananda, D. Pardo, S. Nolte, A. Lohrmann, A. Ling, J. Bartholomäus, G. Corrielli, M. Krutzik, T. Vogl, QUICK3 - Design of a Satellite-Based Quantum Light Source for Quantum Communication and Extended Physical Theory Tests in Space, *Advanced Quantum Technologies* **2024**, *7*, 2300343.
[175] C. Cholsuk, A. Çakan, S. Suwanna, T. Vogl, Identifying Electronic Transitions of Defects in Hexagonal Boron Nitride for Quantum Memories, *Advanced Optical Materials* **2024**, *12*, 2302760.
[176] T. Vogl, K. Sripathy, A. Sharma, P. Reddy, J. Sullivan, J. R. Machacek, L. Zhang, F. Karouta, B. C. Buchler, M. W. Doherty, Y. Lu, P. K. Lam, Radiation tolerance of two-dimensional material-based devices for space applications, *Nature Communications* **2019**, *10*, 1202.
[177] N. Mendelson, M. Doherty, M. Toth, I. Aharonovich, T. T. Tran, Strain-Induced Modification of the Optical Characteristics of Quantum Emitters in Hexagonal Boron Nitride, *Advanced Materials* **2020**, *32*, 1908316.
[178] M. Kianinia, B. Regan, S. A. Tawfik, T. T. Tran, M. J. Ford, I. Aharonovich, M. Toth, Robust Solid-State Quantum System Operating at 800 K, *ACS Photonics* **2017**, *4*, 768.
[179] M. Yu, J. Lee, K. Watanabe, T. Taniguchi, J. Lee, Electrically Pumped h-BN Single-Photon Emission in van der Waals Heterostructure, *ACS Nano* **2025**, *19*, 504.

[180] G. Park, I. Zhigulin, H. Jung, J. Horder, K. Yamamura, Y. Han, H. Cho, H.-W. Jeong, K. Watanabe, T. Taniguchi, M. Oh, G.-H. Lee, M.-H. Jo, I. Aharonovich, J. Kim, Narrowband Electroluminescence from Color Centers in Hexagonal Boron Nitride, *Nano Letters* **2024**, *24*, 15268.
[181] L. J. Rogers, K. D. Jahnke, T. Teraji, L. Marseglia, C. Müller, B. Naydenov, H. Schauffert, C. Kranz, J. Isoya, L. P. McGuinness, F. Jelezko, Multiple intrinsically identical single-photon emitters in the solid state, *Nature Communications* **2014**, *5*, 4739.
[182] S. Lu, P. Shen, H. Zhang, G. Liu, B. Guo, Y. Cai, H. Chen, F. Xu, T. Zheng, F. Xu, X. Chen, D. Cai, J. Kang, Towards n-type conductivity in hexagonal boron nitride, *Nature Communications* **2022**, *13*, 3109.
[183] M. Atatüre, D. Englund, N. Vamivakas, S.-Y. Lee, J. Wrachtrup, Material platforms for spin-based photonic quantum technologies, *Nature Reviews Materials* **2018**, *3*, 38.
[184] S.-H. Wei, B. Jing, X.-Y. Zhang, J.-Y. Liao, C.-Z. Yuan, B.-Y. Fan, C. Lyu, D.-L. Zhou, Y. Wang, G.-W. Deng, H.-Z. Song, D. Oblak, G.-C. Guo, Q. Zhou, Towards Real-World Quantum Networks: A Review, *Laser & Photonics Reviews* **2022**, *16*, 2100219.
[185] R. Uppu, L. Midolo, X. Zhou, J. Carolan, P. Lodahl, Quantum-dot-based deterministic photon–emitter interfaces for scalable photonic quantum technology, *Nature Nanotechnology* **2021**, *16*, 1308.
[186] A. L. Exarhos, D. A. Hopper, R. R. Grote, A. Alkauskas, L. C. Bassett, Optical Signatures of Quantum Emitters in Suspended Hexagonal Boron Nitride, *ACS Nano* **2017**, *11*, 3328.
[187] N. R. Jungwirth, G. D. Fuchs, Optical Absorption and Emission Mechanisms of Single Defects in Hexagonal Boron Nitride, *Physical Review Letters* **2017**, *119*, 057401.
[188] J. C. Stewart, Y. Fan, J. S. H. Danial, A. Goetz, A. S. Prasad, O. J. Burton, J. A. Alexander-Webber, S. F. Lee, S. M. Skoff, V. Babenko, S. Hofmann, Quantum Emitter Localization in Layer-Engineered Hexagonal Boron Nitride, *ACS Nano* **2021**, *15*, 13591.
[189] M. Koperski, K. Nogajewski, M. Potemski, Single photon emitters in boron nitride: More than a supplementary material, *Optics Communications* **2018**, *411*, 158.
[190] Z. Shotan, H. Jayakumar, C. R. Considine, M. Mackoit, H. Fedder, J. Wrachtrup, A. Alkauskas, M. W. Doherty, V. M. Menon, C. A. Meriles, Photoinduced Modification of Single-Photon Emitters in Hexagonal Boron Nitride, *ACS Photonics* **2016**, *3*, 2490.
[191] L. Fleury, J. M. Segura, G. Zumofen, B. Hecht, U. P. Wild, Nonclassical Photon Statistics in Single-Molecule Fluorescence at Room Temperature, *Physical Review Letters* **2000**, *84*, 1148.

[192] M. Fischer, A. Sajid, J. Iles-Smith, A. Hötger, D. I. Miakota, M. K. Svendsen, C. Kastl, S. Canulescu, S. Xiao, M. Wubs, K. S. Thygesen, A. W. Holleitner, N. Stenger, Combining experiments on luminescent centres in hexagonal boron nitride with the polaron model and ab initio methods towards the identification of their microscopic origin, *Nanoscale* **2023**, *15*, 14215.
[193] X. Sun, Q. Li, J. Huang, J. Jian, P. Lu, X. Zhang, J. L. MacManus-Driscoll, H. Wang, Strain and property tuning of the 3D framed epitaxial nanocomposite thin films via interlayer thickness variation, *Journal of Applied Physics* **2019**, *125*, 082530.